PEOPLE'S DEMOCRATIC REPUBLIC OF ALGERIA

Ministry of High Education and Scientific Research

University of BLIDA1

Institute of Aeronautics and Space Studies

Navigation department

A thesis submitted for the Master degree in CNS/ATM

Theme:

Study and comparison of attitude observers presented in the special orthogonal group SO (3)

Presented by

ABDELKEBIR AKRAM

RAHIM ABDELKADER

Under the supervision of

Mm. BENCHEIKH SALIHA

2019/2020

Acknowledgements

This thesis marks the final of our study in Aeronautical Engineering. The process of conducting research and writing thesis has long been a challenging one, but we are grateful to receive a lot of support from many people.

Firstly, our thanks and appreciation to our thesis advisor Dr. "SALIHA BENCHEIKH". We are in debt to her for all her teachings, her advices especially for giving us support throughout the duration of this work.

We are grateful as well to all teachers and the community of Institute of Aeronautics and Space Studies, they were always humble and we appreciate their help, their guidance, their contribution, their helpful comments and their recommendations during the 5 years of studies.

Finally, a big thanks also to all those people whose names are not listed here for their assistance and help.

THANK YOU

Dedication 1

First of all, thanks to Allah to give me all the opportunities and the courage in this life.

I would like to acknowledge those who supported me during the completion of this thesis. Most importantly, I would like to thank my parents especially my mother for her love and kindness, all my brothers and sisters for their unlimited support, invaluable encouragements and unconditional love.

All of you push me to be a better person every day. I'm very grateful to have your support.

Special thanks to my dear friends and colleagues for their support and sincere friendship specially my little brother "BOUKHATEM MOHAMED EL-AMINE".

I would also specially thank my work partner in this thesis "ABDELKEBIR AKRAM", and all of my other colleagues and friends at Institute of Aeronautics and Space Studies for their help and fellowship.

Also, a deepest thank to the Dr. DEHOUCHE SIHAM and the Ph. D student "ABDALLAH TOUAIBIA" for their support and advices.

Finally, thanks to everyone who helped and supported me during my life and my studies, I am really grateful to you.

"RAHIM ABDELKADER"

Dedication 2

First, I would like to thank our God for providing me the ability and the strength that was needed to complete this work.

To whom I owe what I am,

To my dear parents and all the ABDELKEBIR family, no dedication can be fairly enough to express what you deserve for all the sacrifices you have done for me since my birth, your prayers have been of great help to me to carry out my studies and this journey would not have been possible without you.

Special thanks will be given to my dear partner and friend "RAHIM ABDLKADER" for his hard work and support during the making of this study.

I would like to thank my college family my friends: Dhiyae, Farouk, Djamel, Lotfi and many others for being there for me throughout my entire college experience making it way easier and more fun.

"ABDELKEBIR AKRAM"

Abstract

In this thesis, we treated four attitude nonlinear observers, where the attitude is represented by an orthogonal matrix belonging to the special orthogonal group SO(3).

First, we studied two versions of nonlinear complementary filter recently developed by Soulaimane Berkane, where the gains depend on the state of the system which give an amelioration of robustness for the perturbations of gyroscopic measures.

Then, we studied also another two nonlinear observers namely, the invariant and the cascaded, developed by Minh-Duc Hua, which use INS/GPS measurements.

Finally, we compared between the four to know which one of them gives a good accuracy at estimating the attitude using MATLAB for simulate the results.

ملخص

في هذه الأطروحة، درسنا أربعة ملاحظين غير خطيين، حيث يتم تمثيل السلوك بمصفوفة متعامدة تنتمي إلى المجموعة المتعامدة الخاصة SO(3).

أولاً ، درسنا نسختين من المرشح التكميلي غير الخطي الذي طوره سليمان بركان مؤخرًا ، حيث تتمتع هذه المرشحات بأرباح تعتمد على حالة النظام التي تعطي تحسينًا في المتانة لاضطرابات القياسات الجيروسكوبية.

بعد ذلك ، درسنا أيضًا ملاحظين غير خطيين آخرين وهما: الثابت والمتسلسل اللذان يستخدمان قياسات INS/GPS ، التي طورها Minh-Duc Hua.

أخيرًا ، قارنا بين الملاحظين الأربعة لمعرفة الجيد لتقدير السلوك باستخدام MATLAB في محاكاة النتائج.

Résumé

Dans cette thèse, nous avons traité quatre observateurs d'attitude, où l'attitude est représentée par une matrice orthogonale appartenant au groupe orthogonal spécial SO(3).

Premièrement, nous avons étudié deux versions de filtre complémentaire non linéaire récemment développé par Soulaimane Berkane, où ces filtres ont des gains dépendants de l'état du système et qui donnent une amélioration de la robustesse aux perturbations des mesures gyroscopiques.

Ensuite, nous avons également étudié deux autres observateurs non linéaires à savoir, l'invariant et l'en cascade qui utilisent des mesures INS/GPS, développées par Minh-Duc Hua.

Enfin, nous avons fait une comparaison entre les quatre observateurs pour connaître le bon pour l'estimation de l'attitude en utilisant MATLAB pour simuler les résultats.

Table of contents

Chapter IV Simulations and interpretations

List of Figures

List of Symbols

e: Earth Centered-Earth Fixed frame.

i: Earth Centered Inertial frame.

n: Navigation frame.

b: Body frame.

φ: Roll angle.

θ: Pitch angle.

ψ: Yaw angle.

q: Quaternion.

g: The acceleration due to gravity.

ω: The angular velocity measured by gyroscopes.

Ω: Skew-symmetric matrix of the angular velocity.

f: The specific force measured by accelerometers.

$SO(3)$: Special Orthogonal group.

$\mathbb{R}_+$: The set of nonnegative real numbers.

$\mathbb{R}^n$: Real n dimensional vector.

$\mathbb{R}^{n\times m}$: Real $n \times m$ dimensional matrix.

$\det(.)$: Determinant of the component.

$\mathrm{Tr}(.)$: Trace of the component.

I_n: Identity matrix with dimension n-by- n.

List of Abbreviations

AGAS: Almost Global Asymptotic Stability.

DCM: Direction Cosine Matrix.

ECEF: Earth Centered-Earth fixed.

ECI: Earth centered Inertial frame.

EKF: Extended Kalman Filter.

ENU: East-North-Up.

FOAM: Fast Optimal Attitude Matrix.

FOG: Fiber Optic Gyroscope.

GPS: Global Positioning System.

IMU: Inertial Measurements Unit.

INS: Inertial Navigation System.

NED: North-East-Down.

PPS: Precise Positioning Service.

QUEST: QUaternion ESTimator.

RLGs: Ring laser gyroscopes.

SAW: Surface Acoustic Wave.

SPS: Standard Positioning Service.

SVD: Singular Value Decomposition.

UAVs: unmanned airborne vehicles.

UKF: Unscented Kalman Filter

USAF: The United States Air Force.

General introduction

The theory of attitude estimation holds an increasingly important place in different fields such as aerospace, robotics, motion capture and automatic for both linear and nonlinear systems, the problem of attitude estimation of linear systems was completely solved in the years 1960−1970, but the case of nonlinear systems, which concerns most physical systems, remains a widely open and very active research subject. After that the attitude estimation problems were extended to uncertain, then chaotic systems that constitute a class of nonlinear systems with very complex behavior.

When it is not possible to directly measure or estimate the attitude of a system, for physical or financial reasons, an auxiliary dynamic system, called an observer, is used, which is responsible for estimating the attitude of the system, based on two phases, namely a phase of synthesis or design, which consists in choosing the dynamics of the observer using the available information, namely the dynamic model of the system studied, its inputs and its measured outputs, and a phase of analyzing the convergence of the state estimated by the observer and the real state of system.

The attitude can be estimated by several methods developed since the 1970s, like the dynamic methods which use the measurements of INS sensors (accelerometers which provide the linear acceleration, and the gyroscopes which provide the angular velocities), with the Kalman's filters or the nonlinear observers, and sometimes with the use of a complementary GPS (Global Positioning System) information, and in this case, it's called INS/GPS fusion.

For the physical and the financial reasons, the problem of choosing the sensors is solved thanks to the appearance of MEMS (Micro Electro-Mechanical Systems) technology which has led to the design of reduced size sensors (accelerometers, gyroscopes) which having also a low energy consumption.

For robust attitude estimation, we proposed the study of four state observers, and we structured this thesis in four chapters introduced as follows

The first chapter, is a general introduction and notions about the attitude, coordinate frames, and Attitude parameterization, then an overview on state observers defining the design of a state observer, then we mention some state observers for linear systems and nonlinear systems.

The second chapter, is an overview about attitude estimators, we mentioned sensors used, and the different approaches to determine the attitude based on inertial sensors and based on fusion IMU/GPS

The third chapter, is our main goal, we studied her the four attitude observers, the first is “smooth nonlinear complementary filter” proposed by Mr. Mahony, the second one is “nonsmooth nonlinear complementary filter” proposed by Mr. Berkane which is a Mahony’s filter modified, the third and the fourth observers are “The invariant observer” and “The cascaded observer” proposed by Mr. Minh-Duc Hua, the study was about the convergence of the state estimated by each observer to the real state of system using the available information from IMU/GPS fusion.

The last chapter, contains a simulation under MATLAB will be done in order to examine the performance of these observers and comparing between the convergence results.

Finally, a general conclusion about all what we mentioned in this thesis. And we close this work by a bibliographical reference.

Chapter I

Concepts of attitude and state observers

I.1 Introduction

The attitude is an important information in several high precision applications, including navigation of autonomous aerial vehicles, like unmanned airborne vehicles (UAVs), and mobile robotics. For such applications, a high precision navigation system requires expensive and light weight IMU sensors, that have long term bias stability to measure this attitude. But, such kind of navigation systems are not desirable because their cost constraint. In addition, there is no sensor to provide attitude directly. Therefore, to be able to have information about the attitude and obviously all system state variables at any time, the development of a robust state estimator called “observer” is the interest of researchers.

In this chapter, the coordinate frames and the most useful attitude parameterizations are given. After that, a synthesis of conventional observers, defined for linear and nonlinear systems, is made to introduce the attitude observers proposed in chapter I.

I.2 Attitude concept

The attitude is the relative orientation of body-frame with respect to inertial-frame. It can be estimated using accelerometer and gyroscope measurements.

However, accelerometer and gyro measurements are referenced to inertial space, but velocity, position, and orientation of rigid body are needed in a system referenced to the Earth. Consequently, mathematical symbols, coordinate systems, and coordinate transformations are basic elements of the navigation system. We will then be ready to define the coordinate systems and coordinate transformations in the first of this section following by the expressions of attitude parameterization.

I.2.1 Coordinate frames

In order to discuss the attitude and the quantities measured by the accelerometer and gyroscope, a number of coordinate frames need to be introduced.

There are many reference frames some of them are defined as follows.

I.2.1.1 Earth centered Inertial

The Earth centered Inertial frame (ECI)**,** denoted by the symbol “i”, is a stationary frame. The IMU measures linear acceleration and angular velocity with respect to this frame. Its origin is located at the center of the earth, and its axes are aligned with respect to the stars. The frame “i” is illustrated in **Figure I.1**, and is defined as:

- Origin is the Earth's center of mass, (the geo-center of Earth).
- X_{ECI} is a Vernal equinox axis at J2000 (where equatorial & ecliptic plane intersect).
- Z_{ECI} is Earth rotation axis at Epoch J2000 (near the pole star).
- Y_{ECI} is the axis defined as the RHR orthogonal to X_{ECI} and Z_{ECI}

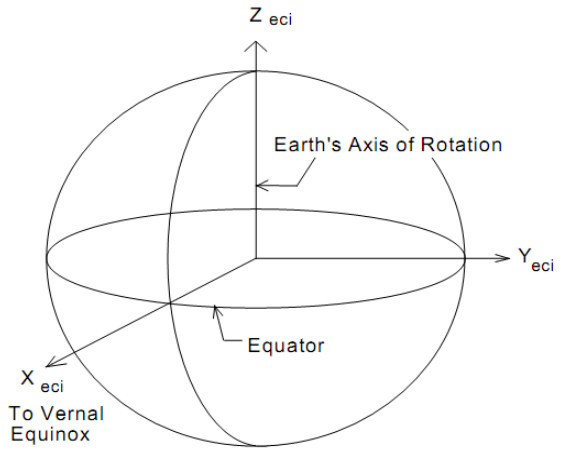

Figure I.1 ECI axes

I.2.1.2 Earth Centered-Earth Fixed

Earth Centered-Earth fixed (ECEF) is a very familiar Cartesian coordinate reference frame $[x, y, z]$ for the Earth, denoted by the symbol "e". It is defined as

- Origin is at the Earth's center of mass.
- x-axis extends through the intersection of the prime meridian GREENWICH and the equator.
- z-axis extends through the true north and south poles (coincident with the Earth's spin axis).
- y-axis completes the RH coordinate system, passing through the equator and +90deg East longitude, near the Maldives islands in the Indian Ocean.

The ECEF frame is illustrated in the **Figure I.2**. This reference frame rotates with the surface of the EARTH.

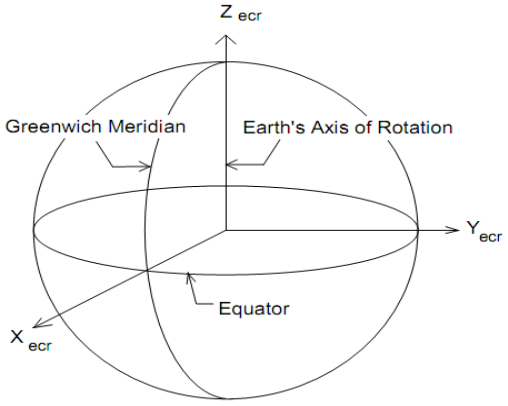

Figure I.2 ECEF axes

I.2.1.3 Body frame

Body frame, denoted by the symbol “b”, is the coordinate frame of the moving IMU. Its origin is located in the center of the accelerometer triad, and it is aligned to the casing. All the inertial measurements are resolved in this frame. The x-axis is Roll (φ); the y-axis is the Pitch (θ) and the z-axis is the Yaw or heading (ψ). The b-frame is illustrated in the **Figure I.3**.

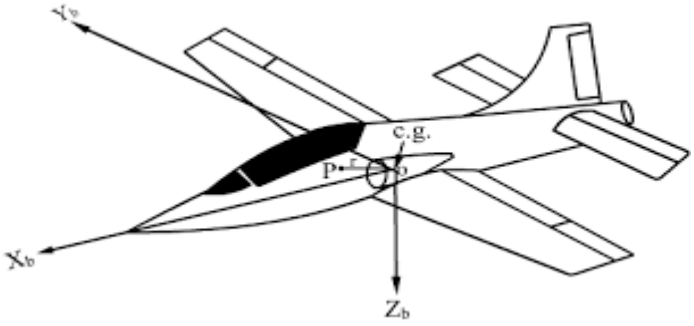

Figure I.3 Body frame (b)

I.2.1.4 Navigation frame

The navigation frame, denoted by the symbol “n”, is a local geographic frame in which we want to navigate. In other words, we are interested in the position and orientation of the b-frame with respect to this frame.

The n-frame has two configurations: East-North-Up (ENU) configuration and North-East-Down (NED) configuration. The last configuration is to be defined here.

The North-East-Down frame (NED) is a local frame, implemented in the field of inertial navigation, defined relative to the Earth’s reference ellipsoid (WGS 84), usually as the tangent plane to the ellipsoid. Its origin is at the location of the navigation system. The NED frame is illustrated in **Figure I.4**.

- X- axis points towards true North.
- Y- axis points towards East.
- Z- axis points downwards normal to the Earth’s surface.

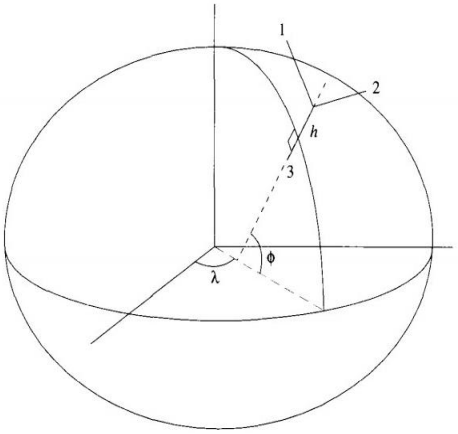

Figure I.4 Local NED frame.

I.2.2 Attitude parameterization

Defining the rotational orientation of a rigid body requires a minimum of three parameters. However, many attitude representations utilize more than three parameters. While there are numerous attitude representations that can be used to define the orientation of a system, some of the more common representations include direction cosine matrix (DCM), Euler angles, and unit quaternion.

I.2.2.1 Direction Cosine Matrix (DCM)

A direction cosine matrix is a transformation matrix, which is composed of the direction cosine values between the initial coordinate system and the target coordinate system.

Let A be the initial coordinate system, and B be the target coordinate system of a transformation. The base vectors of A are given by Xa, Y_a and Z_a, and X_b, Y_b, Z_b are the base vectors of system B. The direction cosine matrix which transforms a vector from system A to system B shall be called $\mathrm{C_a^b}$ and is defined by

$$C_a^b = \begin{bmatrix} \cos(\theta_{x,x}) & \cos(\theta_{x,y}) & \cos(\theta_{x,z}) \\ \cos(\theta_{y,x}) & \cos(\theta_{y,y}) & \cos(\theta_{y,z}) \\ \cos(\theta_{z,x}) & \cos(\theta_{z,y}) & \cos(\theta_{z,z}) \end{bmatrix} \quad \text{(I.1)}$$

$\mathrm{C_a^b}$ is an orthonormal matrix because the base vectors of A and B are orthogonal unit vectors. Therefore, the transpose of a DCM is the same as the DCM representing the

inverse transformation. For all transformation matrices, the transpose is equal to the inverse of the matrix

$$[C_a^b]^T[C_a^b] = I \quad so \quad [C_a^b]^{-1} = [C_a^b]^T = [C_b^a] \tag{I.2}$$

$$\text{and} \qquad \text{Det } [\mathrm{C}_{\mathrm{a}}^{\mathrm{b}}] = 1 \tag{I.3}$$

Let r^x be the position vector referenced in the x-frame. The transformation from the frame A to the frame B can be accomplished as follows

$$r^b = \mathrm{C}_{\mathrm{a}}^{\mathrm{b}} \; r^a \tag{I.4}$$

The Transformation from a frame to another can be accomplished through an intermediate frame or frames. Let C be another frame, the base vectors are given by Xc, Y_C and Z_C. The transformation from the frame B to the frame C is then given by

$$r^C = \mathrm{C}_{\mathrm{b}}^{\mathrm{C}} \; \mathrm{C}_{\mathrm{a}}^{\mathrm{b}} \; r^a \tag{I.5}$$

I.2.2.2 Euler angles

The orientation of a rigid body with respect to an inertial coordinate system can be described by three successive transformations about the body fixed axis. The three angles used for the successive transformation are the Euler angles. Usually they are used for graphical display of the spacecraft orientation, since they are relatively easy to interpret. Anybody axis can be used for the first transformation. The second rotation must be performed by any of the two axes not taken for the first transformation. The final transformation is about any axes not employed by the second transformation. Therefore 12 different transformation sequences (sets of Euler angles) exist for this scheme to describe the attitude of a rigid body. The transformation matrix, C_n^b, for the transformation sequences is obtained by the multiplication of three elementary transformation matrices C_1, C_2 and C_3 as

$$C_1 = \begin{bmatrix} cos\,\psi & sin\,\psi & 0 \\ -sin\,\psi & cos\,\psi & 0 \\ 0 & 0 & 1 \end{bmatrix} \quad C_2 = \begin{bmatrix} cos\,\theta & 0 & -sin\,\theta \\ 0 & 1 & 0 \\ sin\,\theta & 0 & cos\,\theta \end{bmatrix} \quad C_3 = \begin{bmatrix} 1 & 0 & 0 \\ 0 & cos\,\varphi & sin\,\varphi \\ 0 & -sin\,\varphi & cos\,\varphi \end{bmatrix} \tag{I.6}$$

$$C_n^b = C_1C_2C_3 = \begin{bmatrix} cos\,\theta\,cos\,\psi & cos\,\theta\,sin\,\psi & -sin\,\theta \\ -cos\,\varphi\,sin\,\psi + sin\,\varphi\,sin\,\theta\,cos\,\psi & cos\,\varphi\,cos\,\psi + sin\,\varphi\,sin\,\theta\,sin\,\psi & sin\,\varphi\,cos\,\theta \\ sin\,\varphi\,sin\,\psi + cos\,\varphi\,cos\,\theta\,cos\,\psi & -sin\,\varphi\,cos\,\psi + cos\,\varphi\,sin\,\theta\,sin\,\psi & cos\,\varphi\,cos\,\theta \end{bmatrix}$$

with

Roll angle (φ): represent the rotations around x-axis.
Pitch angle (θ): represent the rotations around the y-axis.
Yaw angle (ψ): represent the rotations around the axis z-axis.

This relation is not only to express the rotation matrix according to the Euler angles, the reverse is also possible and is defined as

$$\varphi = arctg\left(\frac{C_n^b(2,3)}{C_n^b(3,3)}\right) \qquad \theta = arcsin\left(-C_n^b(1,3)\right) \qquad \psi = arctg\left(\frac{C_n^b(1,2)}{C_n^b(1,1)}\right) \tag{I.7}$$

The transpose of the transformation matrix can be obtained using

$$[C_b^n] = C_1(-\Psi)C_2(-\theta)C_3(-\varphi) = [C_n^b]^T \tag{I.8}$$

I.2.2.3 Quaternion

The representation of relative orientation using Euler angles is easy to develop and to visualize, but computationally intense. Also, a singularity problem occurs when describing attitude kinematics in terms of Euler angles, and therefore, it is not an effective method for spacecraft attitude dynamics. The widely used quaternion representation is based on Euler's rotational theorem, which states that the relative orientation of two coordinate systems can be described by only one rotation about a fixed axis $\vec{u}$, and one angle α.

A Quaternion is a (4×1) vector, which elements consists of a scalar part α and a vector part $\vec{u}$. The scalar part is the first element of the matrix. Any rotation can be represented by the quaternion $q = (\alpha, \vec{u})$

$$q = \alpha + u_x\vec{\imath} + u_y\vec{\jmath} + u_z\vec{k} \tag{I.9}$$

Let q and p be two quaternions having elements {a, b, c, d} and {e, f, g, h} respectively. Then quaternion multiplication is defined as follows

$$q \cdot p = \begin{pmatrix} a & -b & -c & -d \\ b & a & -d & c \\ c & d & a & -b \\ d & -c & b & a \end{pmatrix} \begin{pmatrix} e \\ f \\ g \\ h \end{pmatrix} \tag{I.10}$$

The rotation matrix can be expressed according to the elements of the unitary quaternion using the following mathematical relation

$$C_B^L = \begin{bmatrix} a^2 + b^2 - c^2 - d^2 & 2(bc - ad) & 2(ac + bd) \\ 2(bc + ad) & a^2 - b^2 + c^2 - d^2 & 2(cd - ab) \\ 2(bd - ac) & 2(ab + cd) & a^2 - b^2 - c^2 + d^2 \end{bmatrix} \quad \text{(I.11)}$$

The reverse is also possible and is defined as

$$q_B^L = \begin{bmatrix} \frac{1}{2}\sqrt{1 + C_{11} + C_{22} + C_{33}} \\ (C_{32} - C_{23})/4a \\ (C_{13} - C_{31})/4a \\ (C_{21} - C_{12})/4a \end{bmatrix} \quad \text{(I.12)}$$

The Euler angles can also be determined directly from the elements of the unitary quaternion such as

$$\begin{aligned} \varphi &= tan^{-1}\left(\frac{2(c\,d - ab)}{1 - 2(b^2 + c^2)}\right) \\ \theta &= sin^{-1}(-2(bd + ac)) \\ \psi &= tan^{-1}\left(\frac{2(bc - a\,d)}{1 - 2(c^2 + d^2)}\right) \end{aligned} \quad \text{(I.13)}$$

I.3 Overview on state observers

Availability of all state variables for direct measurement is rarely verified in practice. In most cases there is a real need for a reliable estimation of the unmeasured variables, especially when used for the synthesis of control laws or for process monitoring. Indeed, the state of a system may correspond to a physical quantity that cannot always be measured directly. The development of a command law or the determination of a failure of a component of a system often require access to the value of one or more of its states. For this, it is necessary to design an auxiliary system, called “observer”, which is in charge for reconstructing the non-measurable states by exploiting the available information to know the dynamic model of the system, its measured outputs and possibly its inputs.

I.3.1 Observer definition

A state observer is an auxiliary dynamical system that mirrors the behavior of a physical system, and it is driven by input and output measurements of the physical system in order to provide an estimate of internal states of the physical system. So, the primary consideration in the design of an observer is that the estimate of the states should be close to the actual value of the system states. On the other hand, the functional observation problem centers on the construction of an auxiliary dynamical system, known as the functional observer, in order to estimate a linear function or functions of the system states. Obviously, a functional observer is a general form of the state observer because when the linear functions are chosen then the problem reduces to the problem of state observation.

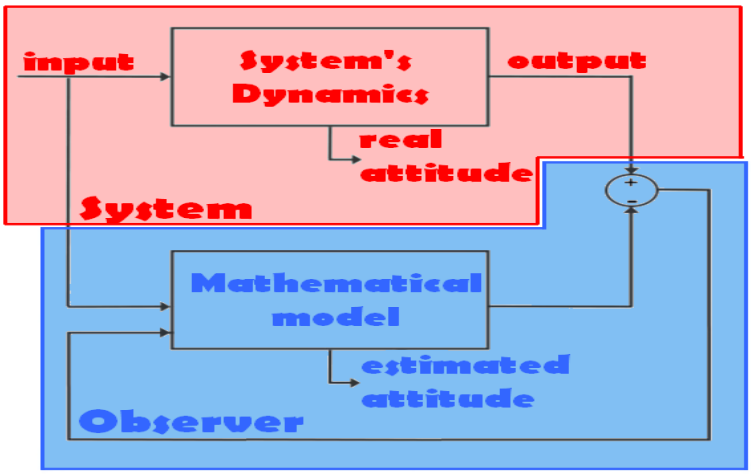

Figure I.5 Design of a state observer

I.3.2 Observers for linear systems

A simple and optimal solution to the problem of estimating the state of linear systems was proposed by Luenberger [2] in the deterministic framework, and by Kalman [3] in the stochastic framework. In both cases, the dynamic model of the linear system defined by

$$\begin{cases} \dot{x}(t) = Ax(t) + Bu(t) + Mw(t) \\ y(t) = Cx(t) + v(t) \end{cases} \quad \text{(I.14)}$$

where $x(t) \in R^n$, $u(t) \in R^m$ and $y(t) \in R^p$ are the state vector, the control input vector and the measurement output vector, respectively. A, B, C and M are constant matrices of the corresponding dimensions. w and v are independent white gaussian noises of size n and p, respectively having characteristics bellow

$$\begin{cases} E[w] = 0 \\ E[w \cdot w^t] = Q \end{cases} \qquad \begin{cases} E[v] = 0 \\ E[v \cdot v^T] = R \end{cases} \quad \text{(I.15)}$$

where Q and R describe the noise covariance matrices of state and measurements.

I.3.2.1 Luenberger observer

The deterministic observer of Luenberger makes it possible to reconstruct the state of an observable system from the measurement of inputs and outputs. It is used in state feedback commands when all or part of the state vector cannot be measured.

Luenberger's theory of observation is essentially based on pole placement techniques in the deterministic case, i.e. noise w and v are zero.

$$\begin{cases} \dot{x}(t) = Ax(t) + Bu(t) \\ y(t) = Cx(t) \end{cases} \quad \text{(I.16)}$$

Luenberger proposes the following observer for the system (I.16)

$$\begin{cases} \dot{\hat{x}}(t) = A\hat{x}(t) + Bu(t) + L\big(y(t) - \hat{y}(t)\big) \\ \hat{y}(t) = C\hat{x}(t) \end{cases} \quad \text{(I.17)}$$

The observer state estimation error is defined as follows

$$e(t) = x(t) - \hat{x}(t) \quad \text{(I.18)}$$

By taking the derivative of (I.17) and substituting (I.16) and (I.17), the error dynamics can be obtained as follows

$$\begin{aligned}\dot{e}(t) &= \dot{x}(t) - \dot{\hat{x}}(t) \\ &= \big(Ax(t) + Bu(t)\big) - \Big(A\hat{x}(t) + Bu(t) + L\big(y(t) - \hat{y}(t)\big)\Big) \\ &= \big(Ax(t) + Bu(t)\big) - \Big(A\hat{x}(t) + Bu(t) + L\big(Cx(t) - C\hat{x}(t)\big)\Big) \\ &= (A - LC)x(t) - (A - LC)\hat{x}(t)\end{aligned} \tag{I.19}$$

Incorporating the definition in (I.18), this collapses to the following differential equation

$$\dot{e}(t) = (A - LC)e(t) \tag{I.20}$$

This differential equation can be readily solved. The solution being an exponential function of the form

$$e(t) = e^{(A-LC)t}e(t_0) \tag{I.21}$$

For the estimation error to approach zero, the eigenvalues of $(A - LC)$ must have negative real parts, or equivalently $(A - LC)$ must be Hurwitz.

Since the system is time-invariant, the system parameters A and C are constant. A large liberty is left to the choice of eigenvalues, but in practice we choose a dynamic of error faster than that of the process. However, they cannot be taken infinitely large for two main reasons: one can use only achievable gains and the increase in the bandwidth of the reconstructed no longer allows to neglect the noise that becomes principal in high frequencies. The matrix L must therefore be chosen to satisfy those conditions via the method of pole positioning.

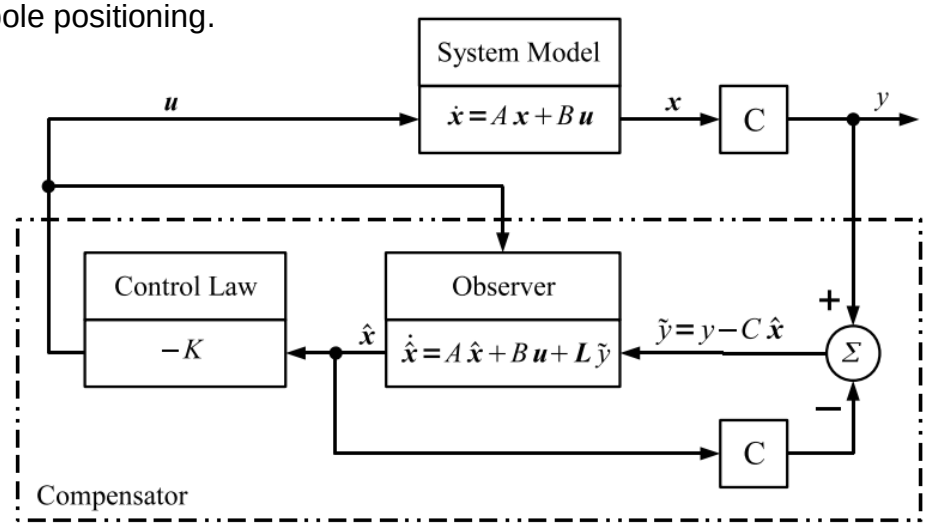

Figure I.6 Schematic of a full-order state observer.

I.3.2.2 Kalman observer

Kalman's theory of observation requires the resolution of a Riccati's equation. Kalman, uses the statistical properties of noise and presents the following observer structure

$$\dot{\hat{x}}(t) = A\hat{x}(t) + Bu(t) + K\big(y(t) - C\hat{x}(t)\big) \tag{I.22}$$

Minimizing the matrix's covariance of estimation error

$$E[e(t)e(t)^T] = P \tag{I.23}$$

Then, the expression of the observer's gain is obtained by

$$K = PC^T R^{-1} \tag{I.24}$$

Where P is solution for Riccati's equation

$$AP + PA - PC^T R^{-1} CP + MQM^T = 0 \tag{I.25}$$

Under specific conditions [4], we can show that the matrix P tends towards a limit and that the filter is stable, which allow to conserve gain (K) value [5].

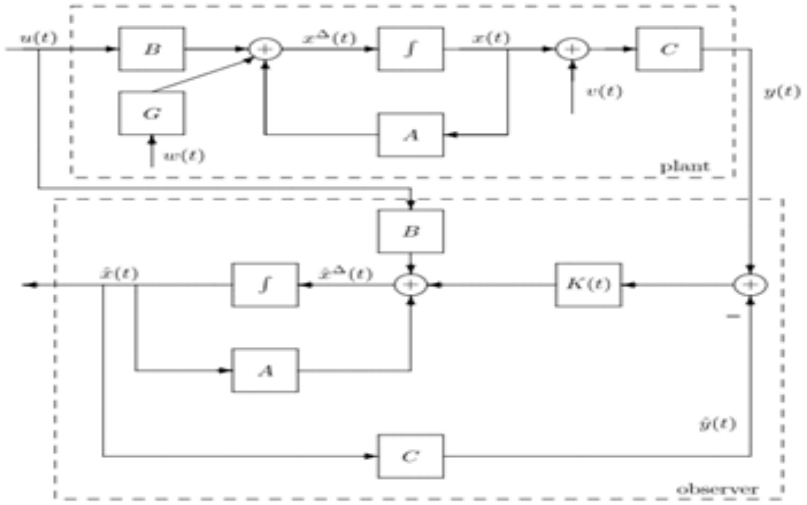

Figure I.7 Kalman filter design.

I.3.2.3 Observer with unknown input

Observer theory with unknown input is applicable to linear systems (I.16). Only this time, the unknown inputs are involved in the system model

$$\begin{cases} \dot{x}(t) = Ax(t) + Bu(t) + Ed(t) \\ y(t) = Cx(t) \end{cases} \quad \text{(I.26)}$$

Where $d(t) \in R^q$ unknown input and E matrix of corresponding dimensions.

For the system (I.26), an observer is said to have unknown input if the estimation error tends to zero in the presence of unknown inputs. Its structure is given by

$$\begin{cases} \dot{z}(t) = Fz(t) + TBu(t) + Ky(t) \\ \hat{\dot{x}}(t) = z(t) + Hy(t) \end{cases} \quad \text{(I.27)}$$

Where $z(t) \in R^n$ is the observer's state vector and $\hat{x}(t) \in R^n$ is the system's estimated state vector, the matrices F, T, K and H that will be determined to stabilize the observer and decouple the unknown inputs. By posing $K = K_1 + K_2$, the derivative of the estimation error relative to time will be given by

$$\begin{aligned} &\dot{e}(t) = \dot{x}(t) - \hat{\dot{x}}(t) \\ &\dot{e}(t) = (A - HCA - K_1C)e(t) - [F(A - HCA - K_1C)]z(t) - [T - (I - HC)]Bu(t) - \\ &(I - HC)Ed(t) - [K_2 - (A - HCA - K_1C)H]y(t) \end{aligned} \quad \text{(I.28)}$$

Thus, the conditions for decoupling the unknown input are

$$\begin{aligned} &F = A - HCA - K_1C \qquad K = K_1 + K_2 \\ &T = I - HC \qquad (HC - I)E = 0 \\ &K_2 = FH \end{aligned}$$

If these conditions are satisfied, then the dynamic error will be

$$\dot{e}(t) = Fe(t) \quad \text{(I.29)}$$

In order to ensure that the estimation error asymptotically tends to zero, the eigenvalues of F must be real negative. The necessary and sufficient conditions for the existence of such an observer for a system described by equation (I.28) are [5].

$$\begin{aligned} &Rang(CE) = Rang(E) \\ &(C, A_l)\ est\ stable, A_l = A - AE[(CE)^T CE]^{-1}(CE)^T CA \end{aligned}$$

The first condition means that the number of rows linearly independent of the matrix C must not be less than the number of columns linearly independent of the matrix, that is, the number of independent measurements must be greater than or equal to the number of unknown inputs to be decoupled.

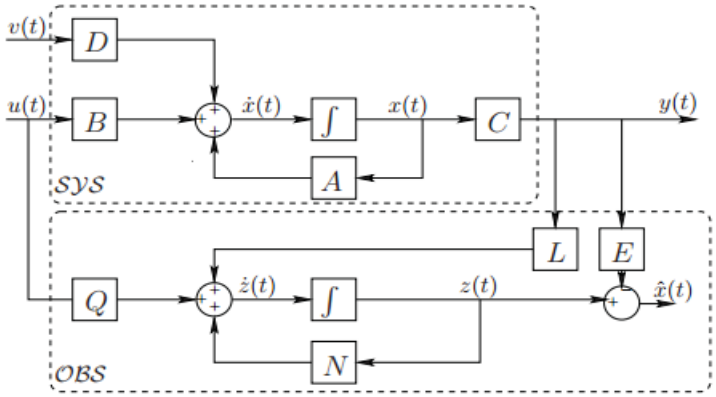

Figure I.8 Structural diagram of OUI.

I.3.3 Observers for nonlinear systems

The field of state estimation of non-linear systems is still largely open. Although, as we shall see, many methods have been developed to design non-linear observers, the problem remains unresolved in many cases. This is an active domain of research, as knowledge of the state of a system is required in multiple applications. Most physical systems are nonlinear. Sometimes a linearization approximation helps to find a satisfactory solution to the estimation problem. However, this method cannot always be applied, the class of non-linear systems concerned is quite small. Therefore, it is necessary to design specific solutions for non-linear systems.

Since its introduction by Than in 1973, the observer for a nonlinear system has been a topic of interest of recent publications. Over the past 15 years, a variety of methods has been developed for constructing observers for some nonlinear systems.

The dynamic model of the nonlinear system defined by

$$\begin{cases} \dot{x}(t) = f\big(x(t), u(t)\big) + Mw(t) \\ y(t) = h\big(x(t), u(t)\big) + v(t) \end{cases} \tag{I.30}$$

Where x(t) ∈ R^n, u(t) ∈ R^m and y(t) ∈ R^p are the state vector, the control input vector and the measurement output vector, respectively. w and v are independent white gaussian noises of size n and p, respective characterized by

$$\begin{cases} E[w] = 0 \\ E[w \cdot w^t] = Q \end{cases} \qquad \begin{cases} E[v] = 0 \\ E[v \cdot v^T] = R \end{cases} \tag{I.31}$$

I.3.3.1 Extended Luenberger observer

The ELO is relatively simple and light-weight computationally. In its simplest form, it uses a constant feedback gain matrix that is computed at design time from the steady-state solution of a Ricatti equation, and therefore avoids the real-time covariance update and computation of the system Jacobian that is necessary for the EKF.

To review the basics of the Extended Luenberger Observer, consider the nonlinear system

$$\begin{cases} \dot{x} = f(x, u, d) \\ y = h(x) \\ z = g(x) \end{cases} \tag{I.32}$$

Where x ∈ R^n is the state, u(t) ∈ R^m is the control input, d ∈ R^q is a disturbance measurement, y ∈ R^r is the measured output, and z ∈ R^p is the performance output.

The Extended Luenberger Observer takes the form:

$$\begin{aligned} \dot{\hat{x}} &= f(\hat{x}, u, d) + K(y - \hat{y}) \\ \hat{y} &= h(\hat{x}) \\ \hat{z} &= g(\hat{x}) \end{aligned} \tag{I.33}$$

Where $\hat{x}$ ∈ R^n is the state estimate, $\hat{z}$ ∈ R^p is the performance output estimate, and K is the observer gain, with the vector $K(y - \hat{y})$, which is called output injection, added to the state equations.

The state estimate error $\tilde{x} = x - \hat{x}$ is then governed by the system

$$\begin{aligned} \dot{\tilde{x}} &= f(x, u, d) - f(\hat{x}, u, d) - K(y - \hat{y}) \\ \tilde{y} &= h(x) - h(\hat{x}) \\ \tilde{z} &= g(x) - g(\hat{x}) \end{aligned} \tag{I.34}$$

We linearize (I.34) about an equilibrium $\bar{x}$ in a neighborhood of x, defining

$$F = \frac{\partial f}{\partial x}\Big|_{x=\bar{x}} \quad H = \frac{\partial h}{\partial x}\Big|_{x=\bar{x}} \text{, and} \quad G = \frac{\partial g}{\partial x}\Big|_{x=\bar{x}} \tag{I.35}$$

So that the linearized error dynamics, neglecting higher-order terms, are

$$\begin{aligned} \dot{\tilde{x}} &= (F - KH)\tilde{x} \\ \tilde{y} &= H\tilde{x} \\ \tilde{z} &= G\tilde{x} \end{aligned} \tag{I.36}$$

There exists an observer gain K to make the origin of (I.36) locally exponentially stable if the pair (F; H) is detectable. In fact, more generally we can consider nonlinear changes of state coordinates $z = \Phi(\mathrm{x}, \mathrm{u}, \mathrm{d})$ nonlinear changes of the output coordinates $\xi = \Gamma(y)$ and nonlinear output injection K(y).

By solving the steady-state Algebraic Riccati Equation

$$0 = AP + PA^T - PH^T R^{-1} HP + \Phi^T Q \Phi \tag{I.37}$$

From which the observer gain is $K = (R^{-1}HP)^T$ (I.38)

I.3.3.2 Extended Kalman Filter

The extended Kalman filter is for estimating the state of a nonlinear system. Its design is based on the generalization of the filter linear Kalman (I.22) using classical techniques of linearization of dynamics nonlinear. Thus, the matrices A and C are replaced by the Jacobian matrices f and h, evaluated in $x(t)$. The system studied is linearized at each moment along estimated trajectories. We have

$$\begin{aligned} A(t) &= \frac{\partial f}{\partial x}\big(\hat{x}(t), u(t)\big) \\ C(t) &= \frac{\partial h}{\partial x}\big(\hat{x}(t), u(t)\big) \end{aligned} \tag{I.39}$$

The dynamic of the extended Kalman filter takes the form

$$\dot{\hat{x}}(t) = f\big(\hat{x}(t), u(t)\big) + K(t)\Big(y(t) - h\big(\hat{x}(t), u(t)\big)\Big) \tag{I.40}$$

The expression (I.24) of the gain $K(t)$ becomes

$$K(t) = P(t)C^T(t)R^{-1} \tag{I.41}$$

And Riccati equation (I.25) is also modified

$$\dot{P}(t) = A(t)P(t) + P(t)A^T(t) - P(t)C^T(t)R^{-1}C(t)P(t) + MQM^T \tag{I.42}$$

It can be underlined that these are only local results, namely that global convergence cannot be guaranteed without additional hypotheses. In addition, the synthesis of this filter uses an approximation of Taylor in the first order, therefore the functions f and h must be derivable, which is not the case for all nonlinear systems. On the other hand, it can be assumed that by using higher order terms of Taylor's development, performance is improved.

I.3.3.3 High-gain observers

The so-called "high gain" techniques can be applied without transforming the initial system. In this case, the observer's design is done directly from the structure of the system for the class of nonlinear systems described by the following model

$$\begin{cases} \dot{x}(t) = Ax(t) + f(x(t), u(t)) \\ y(t) = Cx(t) \end{cases} \tag{I.43}$$

The dynamics of the state consist of an uncontrolled linear part and a controlled non-linear part, checking in general the condition of Lipschitz in relation to x. A function f is called k-Lipschitzienne if there exists k > 0 such as

$$\|f(x) - f(y)\| \leq k\|x - y\| \tag{I.44}$$

The "high gain" observer has the following structure

$$\dot{x}(t) = A\hat{x}(t) + f(\hat{x}, u) + L(y - C\hat{x}) \tag{I.45}$$

The name "high gain" comes from the structure of the observer: when the nonlinear function f has a great Lipschitz constant, the slightest error between the real state and the estimated state will reverberate and grow. Therefore, the observer's gain L in (I.45) must be important to compensate for this error amplification.

The dynamics of the estimation error e = x - x̂ is deduced from (I.43) and (I.45) as

$$\dot{e}(t) = (A - LC)e(t) + f(x, u) - f(\hat{x}, u) \tag{I.46}$$

The result is as follows

$$k < \frac{\lambda_{min}(Q)}{2\lambda_{max}(P)} \tag{I.47}$$

Where “k” is the Lipschitz constant of “f”, and “P”, “Q” are two positive symmetrical matrices respectively, and solutions of the Riccati’s equation

$$(A - LC)^T P + P(A - LC) = -Q \tag{I.48}$$

Then (I.45) is an asymptotic observer of the nonlinear system (I.43).

The “Thau” method is not constructive, it gives no indication on the choice of a gain satisfying the condition (I.47).

This is a verification technique, which guarantees asymptotic convergence from the estimated state x̂ to the real state x, when the gain L has already been chosen.

If there is a small ε > 0 such as the Riccati equation

$$AP + PA^T + P\left(k^2 I - \frac{1}{\varepsilon} C^T C\right) P + I + \varepsilon I = 0 \tag{I.49}$$

Admits a symmetrical solution defined positive P, then just choose

$$L = \frac{1}{2\varepsilon} P C^T \tag{I.50}$$

To ensure the asymptotic convergence of the observer (I.45).

These "high gain" techniques are widely used in the literature. These are mainly verification techniques, which make it possible to establish sufficient conditions for convergence from the estimated state to the actual state. The non-linear observer structure is a Luenberger structure extended to the nonlinear case. The error increase of (I.46) uses Lipschitz’s condition, which is hardly optimal. These conditions are therefore more often conservative.

I.3.3.4 Sliding mode observers

The principle of the sliding mode observers SMO consists in constraining, using discontinuous functions, the dynamics of system's order n to converge towards a variety s of dimension (n-p) called sliding surface (p being the dimension of the measurement vector). The attractiveness and invariance of this surface are ensured by the sliding condition.

In the case of SMO, the dynamics concerned are those of observation errors

$$\tilde{x} = x - \hat{x} \tag{I.51}$$

From their initial values x̃(0), these errors must converge towards the equilibrium values on which errors between the output of the real system and the output of the observer $\tilde{y} = y - \hat{y}$ become zero.

The sliding mode observer is defined with the following structure

$$\dot{\hat{x}} = f(\hat{x}, u) + \Lambda\Gamma_s \tag{I.52}$$

Where $x \in R^n$ is the state, $u \in R^m$ is the control input, Λ is the matrix with corrective terms of gains of the observer, and Γ_s is a vector with $\Gamma_s = [sign(\tilde{y}_1), \dots, sign(\tilde{y}_p)]^T$.

The Sliding surface is defined by

$$s = \tilde{y} = y - \hat{y} \cong 0 \tag{I.53}$$

And the dynamic errors

$$\dot{\tilde{x}} = \dot{x} - \dot{\hat{x}} = \Delta f - \Lambda\Gamma_s \tag{I.54}$$

With $\Delta f = f(x, u) - f(\hat{x}, u)$

The sliding surface, allowing the synthesis of a sliding mode observer, and it must satisfy the condition of attractiveness $s\dot{s} = 0$ which is ensured if the Lyapunov function $v(s) = \frac{1}{2}s^T s$ satisfies $\dot{v}(s) < 0$ when $s \neq 0$, and the invariance condition is satisfied using the corrective terms of gains Λ.

The correction term used is proportional to the discontinuous sign function applied to the output error. The study of stability and convergence for such observers is based on the use of Lyapunov functions.

I.3.3.5 Observers with variable structure

Observers with variable structure are another family of observers. In all the methods seen above, the dynamic model of the studied system was assumed to be perfectly known. Here, it is a question of developing a certain robustness vis-à-vis parametric uncertainty. The method used to build these observers is based on the theory of slippery modes. The class of systems studied is described by

$$\begin{cases} \dot{x}(t) = Ax(t) + f(x(t), u(t)) \\ y(t) = Cx(t) \end{cases} \quad \text{(I.55)}$$

The function f represents the nonlinearities and uncertainties of the system. The following hypotheses are made about the system (I.55):

(i) The pair (C, A) is detectable, so there is a K matrix such that the matrix (A-KC) is stable.

(ii) The function f is of the form

$$f\big(x(t), u(t)\big) = P^{-1}C^{T}h(x(t), u(t)) \quad \text{(I.56)}$$

Where P is a positive symmetrical matrix, solution of the Lyapunov equation (P exists according to hypothesis (i))

$$(1 - KC)^{T}P + P(A - KC) = -Q \quad \text{(I.57)}$$

And the function h is unknown but stubborn

$$\|h(x(t), u(t)\| \leq \rho\big(u(t)\big) \quad \text{(I.58)}$$

It should be noted that nonlinearity does not occur in the observer structure proposed by [6]

$$\dot{\hat{x}}(t) = A\hat{x}(t) + K\big(y(t) - C\hat{x}(t)\big) + k\big(\hat{x}(t), u(t), y(t)\big) \quad \text{(I.59)}$$

With

$$k(\hat{x}(t),u(t),y(t)) = \begin{cases} \frac{P^{-1}C^T(y(t)-C\hat{x}(t))}{\|y(t)-C\hat{x}(t)\|}\rho(u(t)) \;\; if \;\; (x(t)-\hat{x}(t)) \neq 0 \\ 0 \;\; if \;\; (x(t)-\hat{x}(t)) = 0 \end{cases} \quad \text{(I.60)}$$

The term $\kappa(\hat{x}(t),u(t),y(t))$ in (I.60) can be considered a variable gain, which becomes infinite when the estimation error is small. It is demonstrated in [7] that the observer (I.59) is an exponential observer of the system (I.55).

It should be noted that the exact knowledge of the system is not necessary, it is enough to know an increase ρ(u) on nonlinearities or uncertainties. On the other hand, hypothesis (ii) imposes a structural constraint on f, which can be difficult to verify in the presence of model uncertainties.

The discontinuity of the κ function (I.60) is another disadvantage of this method: a high frequency oscillatory regime may appear in the dynamics of the estimation error.

I.4 Conclusion

In this chapter we first underlined the notation of attitude, which is the orientation of a frame fixed in the body relative to a fixed reference frame, and we introduced some of the more common representations and reference frames that can be used in the next chapters.

In the second section of this chapter the notion of state observers was underlined, in the case of linear and nonlinear systems. This is a domain of research where there are still many unresolved problems, due to no general methodology for the construction of observers.

The construction of observers decomposes into synthesis, and design to choose the dynamics of the observer and a phase of analysis of the convergence of the observed state to the real state of the system. The observer design for nonlinear systems is based on the generalization of linear system observers, using classical linearization techniques for nonlinear dynamic. Some of observers discussed in this chapter are the basis of the attitude observers, which will be studied in the next chapter.

Chapter II

Overview of attitude estimators

II.1 Introduction

Attitude estimation, or orientation, has over time become an important scientific issue. Determining the attitude of a rigid body is the subject of numerous studies in different fields, such as aerospace (for the control of satellites), robotics (air, sea and land), motion capture (for medicine or the animation of avatars for video games), ecophysiology (for the study of behavioral responses of animals).

The first attitude estimation methods in the 1970s were developed to find a solution to the Wahba problem. This is to solve an optimization problem to find the rotation matrix based on the knowledge of at least two vectors, expressed in a mobile frame of reference linked to the body and whose projections in a fixed frame (of reference) are known.

A good estimation of the vehicle's attitude is very important. In the present work we focus on the problem of attitude estimation based on measurements provided by a GPS and an IMU embarked on the vehicle. The vehicle's position and linear velocity are directly measured by the GPS, but the reconstruction of its attitude poses difficulties.

We use sensors to get information about our vehicle's attitude, which are used to measure a property from which the navigation system computes its outputs; examples include accelerometers, gyroscopes, and radio navigation receivers.

The output of a navigation system is known as the navigation solution. It comprises the position and velocity of the navigating object. Some navigation systems also provide some or all of the attitude (including heading), acceleration, and angular rate. Similarly, the position solution is just the position of the object.

II.2 Sensors used for attitude determination

The ability of the ancient Egyptian surveyors to orient some of their monuments to the meridian with accuracy has long perplexed modern societies. Although generally their temples were not well placed, the pyramids, and especially the Great Pyramid, were oriented almost precisely to True Geographical North.

To account for this, various methods have been proposed which range from pure chance to a precise star measuring system. However, the means used for orienting the pyramids was actually based on the movements of the sun. Many ancient cultures have made use of the sun's movements by measuring its shadows with an instrument called a gnomon, a pole placed vertically on the ground.

Ancient pictographs show the Egyptians, too, made use of this instrument. With the gnomon and a notched device called a bay (once considered to be a means for sighting distant stars), they were able to read the shadows with precision.

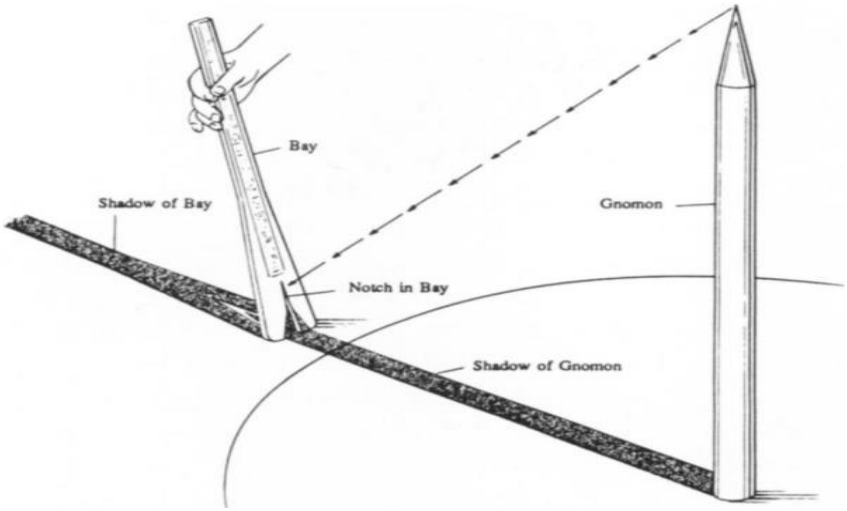

Figure II.1 Manner of defining tip of shadow by using a BAY.

Another method to find true north by building a circular wall higher than a man whose top is an absolute plane. This wall would form an artificial horizon to an observer standing in its center. This observer, while sighting over a pole or through the slit of a bay, would direct another to mark the position of a star as it rose above the wall, and again, when the star set. True north may be obtained, he claims, with a line taken between the bisection of these two points and the center pole [39].

II.2.1 Compass

A compass is a navigational instrument for determining direction relative to the Earth's magnetic poles. It consists of a magnetized pointer (usually marked on the North end) free to align itself with Earth's magnetic field. The compass greatly improved the safety and efficiency of travel, especially ocean travel. A compass can be used to calculate heading, used with a sextant to calculate latitude, and with a marine chronometer to calculate longitude.

It thus provides a much improved navigational capability that has only been recently supplanted by modern devices such as the Global Positioning System (GPS). A compass is any magnetically sensitive device capable of indicating the direction of the magnetic north of a planet's magnetosphere. The face of the compass generally highlights the cardinal points of north, south, east and west. Often, compasses are built as a standalone sealed instrument with a magnetized bar or needle turning freely upon a pivot, or moving in a fluid, thus able to point in a northerly and southerly direction.

The compass was invented in ancient China , and was used for navigation by the 11th century. The dry compass was invented in medieval Europe around 1300. This was supplanted in the early 20th century by the liquid-filled magnetic compass.

II.2.2 Sun sensor and Stars trackers

There are many devices used today on modern spacecraft to accurately determine their position. Magnetometers can be used in conjunction with the Earth’s magnetic field. Sun sensors can be used for attitude determination, but the sun must be visible to the spacecraft. The problem is that the sun sensor and magnetometers can only achieve an accuracy of 0.1 degree [12]. A solution to the accuracy problem is using a star tracker.

Star trackers are the most accurate device in use for determining a spacecraft’s position. The star tracker is essentially a camera for the sole purpose of observing star patterns as observed on the celestial sphere [13]. The star tracker is attached to the satellite onboard computer as part of the ADCS (Attitude Determination and Control Subsystem) [13] The star tracker operates automatically, getting images of star patterns

within its Field of Vision (FOV). The stars observed by the camera can then be identified and the orientation of the spacecraft can be calculated.

II.2.3 Magnetometer

Magnetometers are instruments used for measuring the strength and direction of magnetic fields. They are used extensively in aircraft navigation, marine navigation, and oilfield borehole applications. The magnetometers are used to determine the vehicle heading, where heading is defined as the angle formed between the longitudinal axis of the vehicle projected onto the horizontal plane and magnetic north. In most applications, normally a pair of magnetometers are mounted perpendicular to each other or a triad of magnetometers is mounted orthogonally.

A cluster of three magnetometers with the sensor axes mounted orthogonal and aligned with the body axes measures the three components vector

$$m^b = R_n^b m^n \tag{II.1}$$

Where $m^n = [\, m_N \quad m_E \quad m_D \,]$, represent the magnitude and direction of the Earth's magnetic field. The magnetic field is different around the globe and in fact time-varying as well.

II.2.3.1 Magnetometer error model

Assuming small scale-factor errors and small misalignment errors, the magnetometer output can be modeled as [14]

$$m_{imu}^b \approx R_n^b m^n + b_{mag}^b + w_{mag} \tag{II.2}$$

Where b_{mag}^b is the local magnetic disturbance, and w_{mag} is bounded unmodeled errors and measurement noise. The local magnetic disturbance is modeled as a slowly time-varying disturbance.

$$\dot{b}_{mag}^b = w_{bmag} \tag{II.3}$$

Where w_{bmag} is Gaussian white noise.

II.2.4 Inertial sensors

Inertial measurement unit (IMU) combines multiple accelerometers and gyroscopes. Three accelerometers and tree gyroscopes together can make IMU with six degrees of freedom. Accelerometers measure final forces and gyroscopes measure the angular rate of the IMU body with respect to inertial space in body axes. These sensors are mounted in orthogonal sensitive axes. It also includes temperature sensor, calibration store, clock, power supplies and IMU processor [15, 16, and 17].

II.2.4.1 Gyroscopes

Gyroscopes are devices that sense angular rate with respect to inertial space. There are a lot of gyroscope types [8] the main types of gyroscope are outlined below.

Conventional gyroscope consists of a spinning wheel mounted on two gimbals which allow it to rotate in all three axes, as show in **Figure II.2**. An effect of the conservation of angular momentum is that the spinning wheel will resist changes in orientation. Hence when a mechanical gyroscope is subjected to a rotation the wheel will remain at a constant global orientation and the angles between adjacent gimbals will change. To measure the orientation of the device the angles between adjacent gimbals can be read using angle pick-offs. Note that a conventional gyroscope measures orientation. In contrast nearly all modern gyroscopes are rate-gyros, which measure angular velocity.

The main disadvantage of mechanical gyroscopes is that they contain moving parts. Moving parts cause friction, which in turn causes the output to drift over time. To minimize friction high-precision bearings and special lubricants are used, adding to the cost of the device. Mechanical gyroscopes also require a few minutes to warm up, which is not ideal in many situations.

A fiber optic gyroscope (FOG) uses the interference of light to measure angular velocity. A FOG consists of a large coil of optical fiber. To measure rotation two light beams are fired into the coil in opposite directions. If the sensor is undergoing a rotation then the beam travelling in the direction of rotation will experience a longer path to the other end of the fiber than the beam travelling against the rotation, this is known as the Sagnac effect.

When the beams exit the fiber, they are combined. The phase shift introduced due to the Sagnac effect causes the beams to interfere, resulting in a combined beam whose intensity depends on the angular velocity. It is therefore possible to measure the angular velocity by measuring the intensity of the combined beam.

Ring laser gyroscopes (RLGs) are also based on the Sagnac effect. The difference between a FOG and RLG is that in a RLG laser beams are directed around a closed path using mirrors rather than optical fiber.

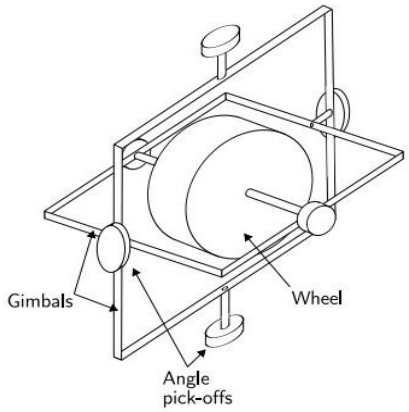

Figure II.2 Conventional mechanical gyroscope [8].

II.2.4.2 Accelerometers

An accelerometer can be broadly classified as a mechanical or solid state or MEMS device [8]. (**Figure II.3**) shows a simple accelerometer. A proof mass is free to move with respect to the accelerometer case along the accelerometer's sensitive axis, restrained by springs. A pickoff measures the position of the mass with respect to the case. When an accelerating force along the sensitive axis is applied to the case, the proof mass will initially continue at its previous velocity, so the case will move with respect to the mass, compressing one spring and stretching the other. This alters the forces the springs transmit. Consequently, the case will move with respect to the mass until the acceleration of the mass due to the asymmetric forces exerted by the springs matches the acceleration of the case due to the externally applied force. The resultant position of the mass with respect to the case is proportional to the applied acceleration. By measuring this with a pickoff, an acceleration measurement is obtained [9].

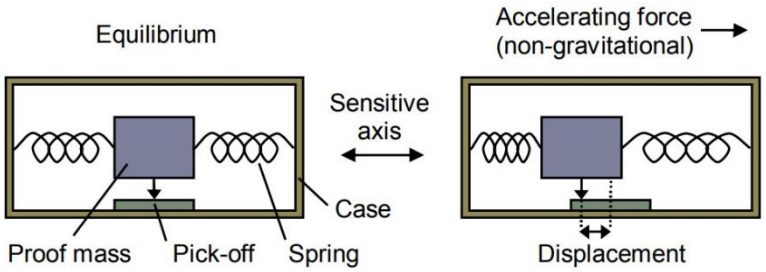

Figure II.3 A simple mechanical accelerometer [9].

An important exception is gravitational acceleration. This acts on the proof mass directly, not via the springs, and applies the same acceleration to all components of the accelerometer, so there is no relative motion of the mass with respect to the case.

An accelerometer measures the specific force of the accelerometer case with respect to inertial space, which does not accelerate or rotate with respect to the rest of the universe. An IMU containing a triad of accelerometers with mutually-orthogonal sensitive axes measures the specific force vector, f_{ib}^{b} , where the subscript “i”,”b” denotes measurement of the origin of the IMU body frame, “b”, with respect to an inertial frame, “i”, and the superscript b denotes that the components of the vector are resolved along the axes of the IMU body frame, which normally coincide with the sensitive axes of the constituent sensors .The specific force may be expressed in terms of the inertially referenced acceleration, a_{ib}^{b}, and the gravitational acceleration , γ_{ib}^{b}, using [9]

$$f_{ib}^{b} = a_{ib}^{b} - \gamma_{ib}^{b} \tag{II.4}$$

However, it is often more convenient to express the specific force in terms of the Earth referenced acceleration,a_{eb}^{b} . Thus

$$f_{ib}^{b} = a_{eb}^{b} - g_{b}^{b} \tag{II.5}$$

Where g_{b}^{b} is the acceleration due to gravity, the sum of the gravitational acceleration and the outward centrifugal acceleration due to the Earth’s rotation.

Solid-state accelerometers can be broken into various sub-groups, including surface acoustic wave, vibratory, silicon and quartz devices. An example of a solid-state accelerometer is the surface acoustic wave (SAW) accelerometer. A SAW accelerometer consists of a cantilever beam which is resonated at a particular

frequency, A mass is attached to one end of the beam which is free to move. The other end is rigidly attached to the case. When an acceleration is applied along the input axis the beam bends. This causes the frequency of the surface acoustic wave to change proportionally to the applied strain. By measuring this change in frequency, the acceleration can be determined.

Micro-machined silicon accelerometers use the same principles as mechanical and solid-state sensors. There are two main classes of MEMS accelerometer. The first class consists of mechanical accelerometers (devices which measure the displacement of a supported mass) manufactured using MEMS techniques. The second class consists of devices which measure the change in frequency of a vibrating element caused by a change of tension, as in SAW accelerometers.

II.2.4.3 Inertial sensors errors:

All types of accelerometer and gyro exhibit biases, scale factor and cross-coupling errors, and random noise to a certain extent. Higher-order errors and angular rate specific force cross-sensitivity may also occur, depending on the sensor type. Each of these errors is discussed in turn [18].

II.2.4.3.a Biases:

The bias is a constant error exhibited by all accelerometers and gyros. It is independent of the underlying specific force and angular rate. In most cases, the bias is the dominant term in the overall error of an inertial instrument.

The accelerometer and gyro biases of an IMU, following sensor calibration and compensation, are denoted by the vectors b_a and b_g respectively. It is sometimes convenient to split the biases into static,b_{as} and b_{gs} , and dynamic,b_{ad} and b_{gd} [9], where

$$b_a = b_{as} + b_{ad} \tag{II.6}$$

$$b_g = b_{gs} + b_{gd} \tag{II.7}$$

Where The static component comprises the run-to-run variation of each instrument bias plus the residual fixed bias remaining after sensor calibration. It is constant throughout an IMU operating period, but varies from run to run, the dynamic component, also known as the in-run bias variation or bias instability, varies over periods of the order

of a minute and also incorporates the residual temperature-dependent bias remaining after sensor calibration. The dynamic bias is typically about 10% of the static bias.

II.2.4.3.b Scale Factor

The scale factor error is the departure of the input-output gradient of the instrument from unity following unit conversion by the IMU. The accelerometer output error due to the scale factor error is proportional to the true specific force along the sensitive axis, while the gyro output error due to the scale factor error is proportional to the true angular rate about the sensitive axis. The accelerometer and gyro scale factor errors of an IMU are denoted by the vectors $s_a$and s_g respectively.

II.2.4.3.c Cross-Coupling Errors

In all types of IMUs arise from the misalignment of the sensitive axes of the inertial sensors with respect to the orthogonal axes of the body frame due to manufacturing limitations. These make each accelerometer sensitive to the specific force along the axes orthogonal to its sensitive axis and each gyro sensitive to the angular rate about the axes orthogonal to its sensitive axis. The axes misalignment also produces additional scale factor errors, but these are typically two to four orders of magnitude smaller than the cross-coupling errors.

The scale factor and cross-coupling errors for a nominally orthogonal accelerometer and gyro triad may be expressed as the following matrices [9]

$$M_a = \begin{bmatrix} s_{a,x} & m_{a,xy} & m_{a,xz} \\ m_{a,yx} & s_{a,y} & m_{a,yz} \\ m_{a,zx} & m_{a,zy} & s_{a,z} \end{bmatrix} \quad \text{(II.8)}$$

$$M_g = \begin{bmatrix} s_{g,x} & m_{g,xy} & m_{g,xz} \\ m_{g,yx} & s_{g,y} & m_{g,yz} \\ m_{g,zx} & m_{g,zy} & s_{g,z} \end{bmatrix} \quad \text{(II.9)}$$

Where: $m_{a,xy}$ is used to denote the cross-coupling coefficient of x-axis specific force sensed by the y-axis accelerometer. $m_{g,xy}$ is used to denote the cross-coupling coefficient of x-axis angular rate sensed by the y-axis accelerometer.

II.2.4.3.d Random noise

All inertial sensors exhibit random noise from a number of sources. Electrical noise limits the resolution of inertial sensors. particularly MEMS sensors, where the signal is very weak. Pendulous accelerometers exhibit noise due to mechanical instabilities. Vibratory gyros can exhibit high-frequency resonances. In addition, vibration from RLG dither motors and spinning-mass gyros can induce accelerometer noise.

The accelerometer and gyro random noise are sometimes described as random walks, which can be a cause of confusion. Random noise on the specific force measurements is integrated to produce a random-walk error on the inertial velocity solution. Similarly, random noise on the angular rate measurements is integrated to produce an attitude random-walk error. The standard deviation of a random-walk process is proportional to the square root of the integration time. The same random walk errors are obtained by summing the random noise on integrated specific force and attitude increment IMU outputs. The random noise on each IMU sample is denoted by the vectors $w_a$and w_g for the accelerometers and gyros, respectively.

II.2.4.3.e Error Models

The following equations show how the main error sources contribute to the accelerometer and gyro outputs [9]

$$\tilde{f}_{ib}^{b} = b_a + (I_3 + M_a) f_{ib}^{b} + w_a \tag{II.10}$$

$$\tilde{\omega}_{ib}^{b} = b_a + (I_3 + M_a) \omega_{ib}^{b} + G_g f_{ib}^{b} + w_a \tag{II.11}$$

Where

$\tilde{f}_{ib}^{b}$ is the IMU-output specific force vector, $\tilde{\omega}_{ib}^{b}$ is the IMU-output angular rate vector, f_{ib}^{b} and ω_{ib}^{b} are the true counterparts, and I_3 is the identity matrix.

II.2.5 Global Positioning System (GPS)

The Global Positioning System (GPS) is a space-based radionavigation system which is managed for the Government of the United States by the U.S. Air Force (USAF).

The system operator GPS was originally developed as a military force enhancement system and will continue to play this role. However, GPS has also demonstrated a significant potential to benefit the civil community in an increasingly large variety of applications.

In an effort to make this beneficial service available to the greatest number of users while ensuring that the national security interests of the United States are observed, two GPS services are provided.

The Precise Positioning Service (PPS) is available primarily to the military of the United States and its allies for users properly equipped with PPS receivers. The Standard Positioning Service (SPS) is designed to provide a less accurate positioning capability than PPS for civil and all other users throughout the world.

II.2.5.1 Basic GPS concept

The position of a certain point in space can be found from distances measured from this point to some known positions in space. Let us use some examples to illustrate this point. In **Figure II.4**, the user position is on the *x*-axis; this is a one-dimensional case. If the satellite position S_1 and the distance to the satellite x_1 are both known, the user position can be at two places, either to the left or right of S_1. In order to determine the user position, the distance to another satellite with known position must be measured. In this figure, the positions of S_2 and x_2 uniquely determine the user position *U*.

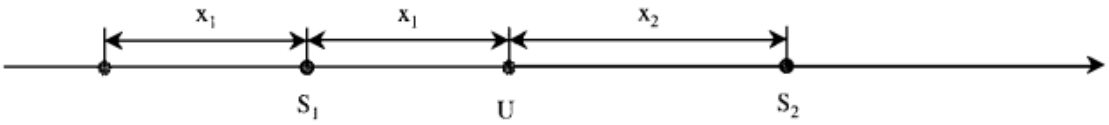

Figure II.4 One-dimensional user position.

Figure II.5 shows a two-dimensional case. In order to determine the user position, three satellites and three distances are required. The trace of a point with constant

distance to a fixed point is a circle in the two-dimensional case. Two satellites and two distances give two possible solutions because two circles intersect at two points. A third circle is needed to uniquely determine the user position. For similar reasons one might decide that in a three-dimensional case four satellites and four distances are needed. The equal-distance trace to a fixed point is a sphere in a three-dimensional case. Two spheres intersect to make a circle. This circle intersects another sphere to produce two points. In order to determine which point is the user position, one more satellite is needed.

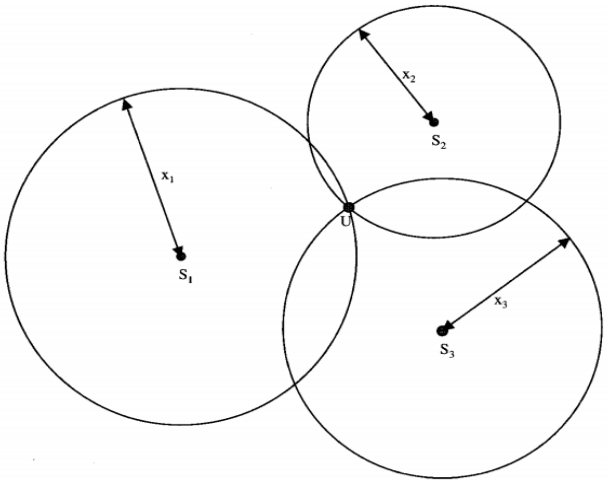

Figure II.5 Two-dimensional user position.

II.2.5.2 GPS measurements

In GPS, the position of the satellite is known from the ephemeris data transmitted by the satellite. One can measure the distance from the receiver to the satellite. Therefore, the position of the receiver can be determined.

In the above discussion, the distance measured from the user to the satellite is assumed to be very accurate and there is no bias error. However, the distance measured between the receiver and the satellite has a constant unknown bias, because the user clock usually is different from the GPS clock. In order to resolve this bias error one more satellite is required. Therefore, in order to find the user position five satellites are needed.

If one uses four satellites and the measured distance with bias error to measure a user position, two possible solutions can be obtained.

Theoretically, one cannot determine the user position. However, one of the solutions is close to the earth's surface and the other one is in space. Since the user position is usually close to the surface of the earth, it can be uniquely determined. Therefore, the general statement is that four satellites can be used to determine a user position, even though the distance measured has a bias error. In the following discussion four satellites are considered the minimum number required in finding the user position.

II.2.5.3 Basic equations for finding user position

In this section the basic equations for determining the user position will be presented. Assume that the distance measured is accurate and under this condition three satellites are sufficient. In **Figure II.6**, there are three known points at locations r_1 or $(\mathrm{x}_1, \mathrm{y}_1, \mathrm{z}_1)$, r_2 or $(\mathrm{x}_2\ \mathrm{y}_2, \mathrm{z}_2)$, and r_3 or $(\mathrm{x}_3, \mathrm{y}_3, \mathrm{z}_3)$, and an unknown point at $\mathrm{r}_\mathrm{u}$or $(\mathrm{x}_\mathrm{u}, \mathrm{y}_\mathrm{u}, \mathrm{z}_\mathrm{u})$.

If the distances between the three known points to the unknown point can be measured as ρ_1, ρ_2, and ρ_3, these distances can be written as:

$$\rho_1 = \sqrt{(x_1 - x_u)^2 + (y_1 - y_u)^2 + (z_1 - z_u)^2}$$

$$\rho_2 = \sqrt{(x_2 - x_u)^2 + (y_2 - y_u)^2 + (z_2 - z_u)^2} \qquad \text{(II.12)}$$

$$\rho_2 = \sqrt{(x_3 - x_u)^2 + (y_3 - y_u)^2 + (z_3 - z_u)^2}$$

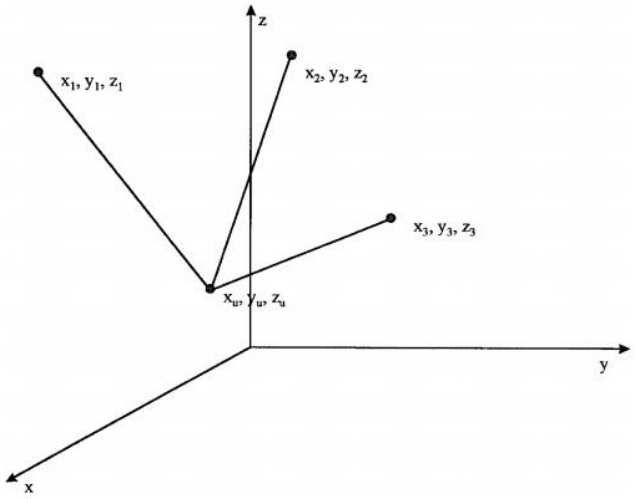

Figure II.6 Use three known position to find one unknown position.

In GPS operation, the positions of the satellites are given. This information can be obtained from the data transmitted from the satellites. The distances from the user (the unknown position) to the satellites must be measured simultaneously at a certain time instance. Each satellite transmits a signal with a time reference associated with it. By measuring the time of the signal traveling from the satellite to the user the distance between the user and the satellite can be found.

II.2.5.4 Measurement of pseudo range

Every satellite sends a signal at a certain time t_{si}. The receiver will receive the signal at a later time t_u. The distance between a user and the satellite, "i" is

$$\rho_{iT} = c(t_u - t_{si}) \tag{II.13}$$

Where c is the speed of light, ρ_{iT} is often referred to as the true value of pseudo range from user to satellite i, t_{si} is referred to as the true time of transmission from satellite i, t_u is the true time of reception.

From a practical point of view, it is difficult, if not impossible, to obtain the correct time from the satellite or the user. The actual satellite clock time $t'_{si}$and actual user clock time t'_u are related to the true time as

$$t'_{si} = t_{si} + \Delta b_i \tag{II.14}$$

$$t'_u = t_u + b_{ut}$$

Where Δb_i is the satellite clock error, b_{ut} is the user clock bias error, besides the clock error, there are other factors affecting the pseudo range measurement. The measured pseudo range ρ_i can be written as [11]

$$\rho_i = \rho_{iT} + \Delta D_i - c(\Delta b_i - b_{ut}) + c(\Delta T_i + \Delta I_i + v_i + \Delta v_i) \tag{II.15}$$

Where ΔD_i is the satellite position error effect on range, ΔT_i is the tropospheric delay error, ΔI_i is the ionospheric delay error, v_i is the receiver measurement noise error, Δv_i is the relativistic time correction.

As a result, Equation (II.12) must be modified as

$$\rho_1 = \sqrt{(x_1 - x_u)^2 + (y_1 - y_u)^2 + (z_1 - z_u)^2} + b_u$$

$$\rho_2 = \sqrt{(x_2 - x_u)^2 + (y_2 - y_u)^2 + (z_2 - z_u)^2} + b_u \quad \text{(II.16)}$$

$$\rho_3 = \sqrt{(x_3 - x_u)^2 + (y_3 - y_u)^2 + (z_3 - z_u)^2} + b_u$$

$$\rho_4 = \sqrt{(x_4 - x_u)^2 + (y_4 - y_u)^2 + (z_4 - z_u)^2} + b_u$$

Where b_u is the user clock bias error expressed in distance, which is related to the quantity b_{ut} by $b_u = c \times b_{ut}$ In Equation (II.16), four equations are needed to solve for four unknowns x_u, y_u, z_u, and b_u. Thus, in a GPS receiver, a minimum of four satellites is required to solve for the user position.

II.2.5.5 Solution of user position from pseudo ranges

It is difficult to solve for the four unknowns in Equation (II.16), because they are nonlinear simultaneous equations. One common way to solve the problem is to linearize them. The above equations can be written in a simplified form as

$$\rho_i = \sqrt{(x_i - x_u)^2 + (y_i - y_u)^2 + (z_i - z_u)^2} + b_u \quad \text{(II.17)}$$

Where *i* = 1, 2, 3, and 4, and x_u, y_u z_u, and b_u are the unknowns. The pseudo range ρ_i and the positions of the satellites x_i, y_i, z_i are known.

Differentiate this equation, and the result is (II.18)

$$\delta\rho_i = \frac{(x_i - x_u)\delta x_u + (y_i - y_u)\delta y_u + (z_i - z_u)\delta z_u}{\sqrt{(x_i - x_u)^2 + (y_i - y_u)^2 + (z_i - z_u)^2}} + \delta b_u$$

$$\delta\rho_i = \frac{(x_i - x_u)\delta x_u + (y_i - y_u)\delta y_u + (z_i - z_u)\delta z_u}{\rho_i - b_u} + \delta b_u$$

In this equation, δx_u, δy_u, δz_u, and δb_ucan be considered as the only unknowns. The quantities x_u, y_u z_u, and b_u are treated as known values because one can assume some initial values for these quantities. From these initial values a new set of δx_u, δy_u, δz_u,and δb_ucan be calculated.

With δx_u, δy_u, δz_u,and δb_u as unknowns, the above equation becomes a set of linear equations. This procedure is often referred to as linearization. The above equation can be written in matrix form as

$$\begin{bmatrix}\delta\rho_1\\ \delta\rho_2\\ \delta\rho_3\\ \delta\rho_4\end{bmatrix}=\begin{bmatrix}\alpha_{11} & \alpha_{12} & \alpha_{13} & 1\\ \alpha_{21} & \alpha_{22} & \alpha_{23} & 1\\ \alpha_{31} & \alpha_{32} & \alpha_{33} & 1\\ \alpha_{41} & \alpha_{42} & \alpha_{43} & 1\end{bmatrix}\begin{bmatrix}\delta x_u\\ \delta y_u\\ \delta z_u\\ \delta b_u\end{bmatrix} \quad \text{(II.19)}$$

Where

$$\alpha_{i1}=\frac{x_i-x_u}{\rho_i-b_u} \qquad \alpha_{i2}=\frac{y_i-y_u}{\rho_i-b_u} \qquad \alpha_{i3}=\frac{z_i-z_u}{\rho_i-b_u} \quad \text{(II.20)}$$

The solution of Equation (II.19) is

$$\begin{bmatrix}\delta x_u\\ \delta y_u\\ \delta z_u\\ \delta b_u\end{bmatrix}=\begin{bmatrix}\alpha_{11} & \alpha_{12} & \alpha_{13} & 1\\ \alpha_{21} & \alpha_{22} & \alpha_{23} & 1\\ \alpha_{31} & \alpha_{32} & \alpha_{33} & 1\\ \alpha_{41} & \alpha_{42} & \alpha_{43} & 1\end{bmatrix}^{-1}\begin{bmatrix}\delta\rho_1\\ \delta\rho_2\\ \delta\rho_3\\ \delta\rho_4\end{bmatrix} \quad \text{(II.21)}$$

This equation obviously does not provide the needed solutions directly; however, the desired solutions can be obtained from it. In order to find the desired position solution, this equation must be used repetitively in an iterative way. A quantity is often used to determine whether the desired result is reached and this quantity can be defined as

$$\delta v=\sqrt{{\delta x_u}^2+{\delta y_u}^2+{\delta z_u}^2+{\delta b_u}^2} \quad \text{(II.22)}$$

When this value is less than a certain predetermined threshold, the iteration will stop. Sometimes, the clock bias b_u is not included in Equation (II.22).

II.2.5.6 User position in spherical coordinate system

The user position calculated from the above discussion is in a Cartesian coordinate system. It is usually desirable to convert to a spherical system and label the position in latitude, longitude, and altitude as the every-day maps use these notations.

The latitude of the earth is from -90 to 90 degrees with the equator at 0 degree. The longitude is from -180 to 180 degrees with the Greenwich meridian at 0 degree. The

altitude is the height above the earth's surface. If the earth is a perfect sphere, the user position can be found easily as shown in **Figure II.7**. From this figure.

The distance from the center of the earth to the user is

$$r = \sqrt{{x_u}^2 + {y_u}^2 + {z_u}^2} \tag{II.23}$$

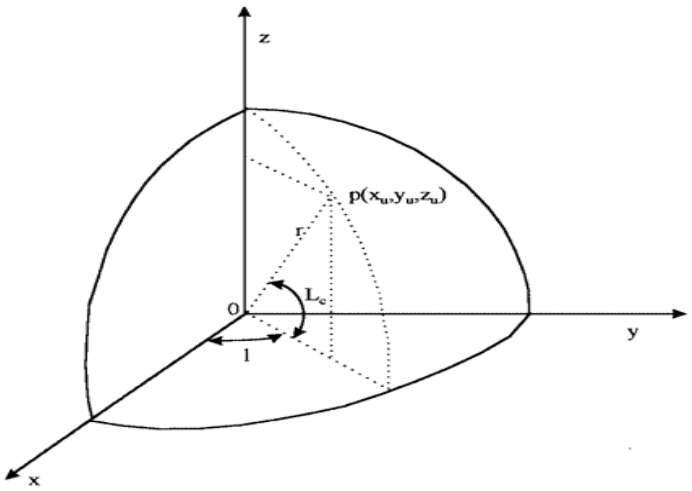

Figure II.7 An octet of an ideal spherical earth.

The latitude L_c is: $$L_c = \tan^{-1}\left(\frac{z_u}{\sqrt{x_u^2+{y_u}^2}}\right) \tag{II.24}$$

The longitude l is: $$l = \tan^{-1}\left(\frac{y_u}{x_u}\right) \tag{II.25}$$

The altitude h is: $$h = r - r_e \tag{II.26}$$

II.2.5.7 GPS errors

Ranging errors are typically grouped into six classes **Figure II.8**

- Ionosphere: Errors in corrections of pseudorange measurements caused by ionospheric effects (free electrons in the ionosphere).

- Troposphere: Errors in corrections of pseudorange measurements caused by tropospheric effects; temperature, pressure, and humidity contribute to variations in the speed of light.

- Multipath: Errors caused by reflected signals entering the receiver antenna.

- Ephemeris: Ephemeris data errors in transmitted parameters in navigation messages for satellites' true positions.

- Satellite Clock: Clock errors in the transmitted clock data for GPS.

- Receiver Errors: Errors in the receiver's measurement of range caused by thermal noise, software accuracy, and interchannel biases.

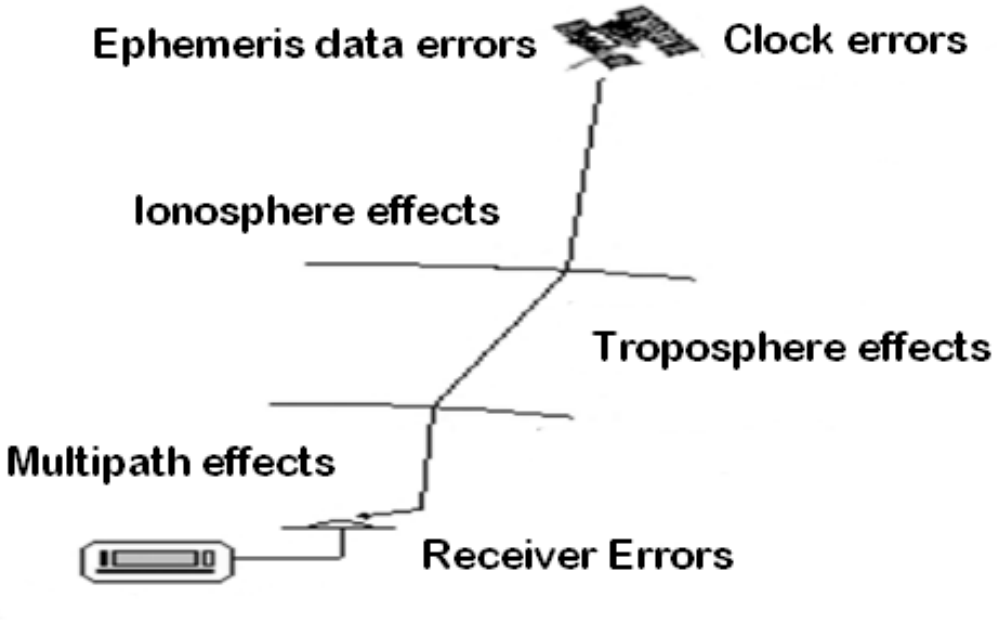

Figure II.8 GPS errors.

II.3 Different approaches to attitude estimation

A rigid body moving inside the earth satisfies the following equation $\dot{R} = R[\omega]_{\times}$.

The solution of this equation is not really reliable in long term applications because of gyroscopic drifts and measurement noise. Then, the attitude can be reconstructed using estimation algorithms merging measurements from several sensors. And several solutions to the attitude estimation problem have been developed in the literature.

Depending on the number of sensors used, there are two main categories of approaches: approaches using measurements (observations) from inertial sensors (accelerometers, magnetometers, gyroscopes) and approaches using a complementary measurement source such as GPS in addition to inertial sensor measurements.

II.3.1 Attitude estimation based on inertial sensors

There are two types of estimators.

II.3.1.1 Static Attitude estimators

Static Attitude estimation is probably the oldest systematic trend of estimating the attitude of a flying vehicle with an acceptable accuracy. This class of attitude estimation techniques takes advantage of the body vector observations to numerically determine the attitude without necessarily considering its kinematics. In this way, the attitude is merely regarded as a matrix (or quaternion) that transforms a vector $x \in R^3$ in one frame to a vector $y \in R^3$ in another frame and as a result, can be obtained by mathematical optimization techniques. Therefore, the information of the original system's dynamics is disregarded and attitude is found on an optimization basis.

The method, also known as deterministic solution, is characterized by finding the attitude estimate in a single point in time when observations of some known vectors in the inertial frame are available in the body frame. It has a simple estimation process with relatively small computational cost. However, this comes with a lower accuracy than the other methods that rely on additional information of the system dynamics.

Although the earliest deterministic solution techniques relied only on body vector measurements and literally put the system equations aside, the emergence of recursive techniques that considered system dynamics for propagation of states in late 1990s provided more reliable methods with remarkable resemblance to the Kalman filter

Major development of these methods, also known as batch attitude determination algorithms, started with the early optimization methods proposed to solve the Wahba's problem [19]. In this problem, with the assumption that two sets of simultaneously observed unit vectors $\hat{V}_1$,..., $\hat{V}_\mathrm{N}$ and $\widehat{W}_1$,..., $\widehat{W}_\mathrm{N}$ are respectively known in the inertial frame (i.e., the reference coordinate system) and the body frame, orthogonal matrix R, representing the rotation matrix, is numerically found by minimizing the loss function.

$$\mathrm{L(R)} = \frac{1}{2}\sum_1^\mathrm{n} \mathrm{a_i} \left|\widehat{W}_\mathrm{i} - R\hat{V}_\mathrm{i}\right|^2 \tag{II.27}$$

Where $\mathrm{a_i}$, $i = 1, \dots, N$ are non-negative weights and N is the number of measurements. By normalizing these weights to have $\sum_1^\mathrm{n} \mathrm{a_i} = 1$, it is straightforward to show that

$$\mathrm{L(R)} = 1 - \sum_1^\mathrm{n} \mathrm{a_i}\, \widehat{W}_\mathrm{i}^{\,T} R\, \hat{V}_\mathrm{i} = 1 - tr(RB^T) \tag{II.28}$$

Where tr denotes the trace operator and matrix B is defined as

$$B = \sum_1^\mathrm{n} \mathrm{a_i}\, \widehat{W}_\mathrm{i}\, \hat{V}_\mathrm{i}^{\,T} \tag{II.29}$$

Equation (II.2) reduces the problem to finding the appropriate matrix R that maximizes the term tr (RB^T). It should be noted that Wahba's problem addresses the attitude determination in a closed-form reconstruction manner. For generalizations of this problem readers are referred to [20] and [21].

Earlier solutions to the Wahba's least squares problem included a method using polar decomposition of the matrix B proposed in [22], and other algorithms in [23], [24], and [25]. Introduction of the Q-method [26], along with these algorithms divided the efforts of finding the optimal matrix R_{opt} into two classes of solutions where the first class directly computes matrix R_{opt} and the second tries to find the optimal quaternion associated with the orientation matrix. Structural differences in numerous proposed

algorithms belonging to each class result in different computational costs and execution times.

II.3.1.1.a Triad

The earliest attitude reconstruction method, known as TRIAD [27], was designed to work with only two non-collinear unit reference vectors $\hat{V}_1$, $\hat{V}_2$ in inertial frame and their corresponding unit observation vectors $\hat{W}_1$, $\hat{W}_2$ in body frame to construct a new orthonormal reference with bases $(\hat{r}_1, \hat{r}_2, \hat{r}_3)$ and observation vectors $(\hat{b}_1, \hat{b}_2, \hat{b}_3)$.

$$\hat{r}_1 = \hat{V}_1 \qquad \hat{r}_2 = (\hat{V}_1 \times \hat{V}_2)/|\hat{V}_1 \times \hat{V}_2| \qquad \hat{r}_3 = (\hat{V}_1 \times (\hat{V}_1 \times \hat{V}_2))/|\hat{V}_1 \times \hat{V}_2| \quad \text{(II.30)}$$

$$\hat{b}_1 = \hat{W}_1 \qquad \hat{b}_2 = (\hat{W}_1 \times \hat{W}_2)/|\hat{W}_1 \times \hat{W}_2| \quad \hat{b}_3 = (\hat{W}_1 \times (\hat{W}_1 \times \hat{W}_2))/|\hat{W}_1 \times \hat{W}_2| \quad \text{(II.31)}$$

From which the attitude matrix can be simply found by

$$R = \sum_1^{\mathrm{n}} \hat{b}_{\mathrm{i}} \hat{r}_{\mathrm{i}}^T \quad \text{(II.32)}$$

Although this method seems to be very simple, in practice it suffers from the fact that parts of measurements are discarded. Therefore, the optimal attitude reconstruction methods were given more attention since they do not eliminate any parts of the observed vectors.

II.3.1.1.b SVD and FOAM

A descendant of the method proposed in [22], Singular Value Decomposition (SVD) method is a point-by-point algorithm to determine the optimal attitude matrix in the Wahba problem framework [28]. In this approach, similar to the other deterministic techniques, only sensor measurements are used and information about the system model is disregarded. The method consists of a direct “singular value” decomposition [29] of the matrix B that gives

$$\mathrm{B} = \mathrm{U}\,\mathrm{S}\,V^T \quad \text{(II.33)}$$

Where U and V are orthogonal matrices and S is a singular value diagonal matrix of the form

$$\mathrm{S} = \mathrm{diag}(s_1, s_2, s_3) \quad \text{(II.34)}$$

With the singular values $s_i, i = 1,2,3$, obeying the inequalities $s_1 > s_2 > s_3 > 0$.

Proper orthogonal matrices of U_+ and V_+ along with the diagonal matrix S' are defined as

$$\mathrm{U}_+ = \mathrm{U}[\mathrm{diag}(1,1,\det \mathrm{U})] \tag{II.35}$$

$$\mathrm{V}_+ = \mathrm{V}[\mathrm{diag}(1,1,\det \mathrm{V})] \tag{II.36}$$

$$\mathrm{S}' = \mathrm{diag}(\mathrm{s}_1, \mathrm{s}_2, \mathrm{s}_3(\det \mathrm{U})(\det \mathrm{V})) \tag{II.37}$$

Where det denotes the determinant of a matrix and (det U) (det V) = ±1. Then, the matrix B is decomposed into the following form

$$B = \mathrm{U}_+ \mathrm{S}' V_+^T \tag{II.38}$$

And the optimal matrix R_{opt} , which minimizes the cost function (II.27), is found to be

$$R_{opt} = \mathrm{U}_+ \mathrm{V}_+ = U[diag\big(1,1,(\det U)(\det V)\big)]\, V^T \tag{II.39}$$

Another version of this method, known as Fast Optimal Attitude Matrix (FOAM), Markley uses the properties of the matrix B to rewrite the optimal rotation matrix (II.39) as

$$\mathrm{R_{opt}} = [(\mathrm{k} + \|\mathrm{B}\|^2)\mathrm{B} + \lambda\, \mathrm{adj}\, \mathrm{B^T} - \mathrm{B}\, \mathrm{B^T B}]/\xi \tag{II.40}$$

Where adj denotes the adjoint matrix and

$$\|\mathrm{B}\|^2 = \mathrm{s_1}^2 + \mathrm{s_2}^2 + \mathrm{s_3}^2 \tag{II.41}$$

And the scalar coefficients $\mathrm{k}, \lambda\, and\, \xi$ are defined as

$$\mathrm{k} = \mathrm{s_2 s_3} + \mathrm{s_3 s_2} + \mathrm{s_1 s_2}$$

$$\lambda = \mathrm{s_1} + \mathrm{s_2} + \mathrm{s_3} \tag{II.42}$$

$$\xi = (\mathrm{s_2} + \mathrm{s_3})(\mathrm{s_3} + \mathrm{s_1})(\mathrm{s_1} + \mathrm{s_2})$$

Since the values of these coefficients depend on the SVD, FOAM takes advantage of an iterative computation strategy to avoid finding (s_1, s_2, s_3) and instead, directly computing the three scalar coefficients. The coefficients $\mathrm{k}\, and\, \xi$ can be expressed in term of $\lambda \,\mathrm{and}\, \mathrm{B}$ as

$$\dot{k} = \frac{1}{2}(\lambda^2 - \|B\|^2)$$

$$\xi = \dot{k}\lambda - \det B \tag{II.43}$$

Using (II.14) and the fact that $\lambda = \mathrm{tr}(R_{opt}\, B^T)$, λ can be found by solving the following equation

$$(\lambda^2 - \|B\|^2)^2 - 8\lambda \det B - 4\|\mathrm{adj}\, B\|^2 = 0 \tag{II.44}$$

Once this equation is recursively solved to find λ, all the other scalar coefficients can be computed. These will determine the optimal rotation matrix from (II.40).

In comparison to other methods. the FOAM algorithm is significantly higher in speed and is shown to be the most robust algorithm among the other deterministic attitude estimation methods. It also does not have problems in dealing with the special case of a 180 degrees rotation [30], [31]. The SVD and FOAM do not adopt quaternion parameterization and work entirely with a rotation matrix. This enables them to work without the requirement of computing eigenvalues and eigenvectors and save some computational time.

II.3.1.1.c Q-Method

Since the four components quaternion representation and the rotation matrix are related to each other by simple relations, it can be shown that a search for an optimal matrix R_{opt} in Wahba's problem leads to the computation of an optimal quaternion corresponding to that rotation matrix [26]. The method, known in literature as the Q-method, simplifies the previous optimization techniques by using the 4 × 1 quaternion vector instead of 3 × 3 rotation matrix.

Given the observation pairs of ($\hat{V}_i$, $\hat{W}_i$) and the positive coefficients a_i, let us define the following 3 × 3 matrix, 3 × 1 vector Z and scalar σ

$$S = B + B^T = \sum_1^n a_i\, \hat{W}_i \hat{V}_i^T + \hat{V}_i \hat{W}_i^T \tag{II.45}$$

$$Z = \sum_1^n a_i\, \hat{W}_i \times \hat{V}_i \tag{II.46}$$

$$\sigma = \mathrm{tr}(b) = \sum_1^n a_i\, \hat{V}_i^T\, \hat{W}_i \tag{II.47}$$

Defining the 4 × 4 symmetric matrix K as

$$\mathrm{K} = \begin{bmatrix} \mathrm{S} - \sigma I_3 & \mathrm{z} \\ \mathrm{z}^{\mathrm{T}} & \sigma \end{bmatrix} \tag{II.48}$$

Results in (II.27) to be written into the quadratic quaternion function

$$1 - L(R) = g(\mathrm{Q}) = \mathrm{Q}^{\mathrm{T}} K\, \mathrm{Q} \tag{II.49}$$

It is then clear that the minimization of L(R) is equivalent to finding the maximum value of the function g(Q). It is also easy to show that the optimal quaternion that maximizes (II.49) is the eigenvector associated with the largest positive eigenvalue of the matrix K. In other words

$$\mathrm{K}\mathrm{Q}_{\mathrm{opt}} = \lambda_{\max}\mathrm{Q}_{\mathrm{opt}} \tag{II.50}$$

Substituting (II.50) into (II.49) and applying the quaternion norm constraint gives the following expression for the optimized loss function

$$\mathrm{L}(\mathrm{R}_{\mathrm{opt}}) = 1 - \lambda_{\max} \tag{II.51}$$

II.3.1.1.d Least Squares

Consider the following nonlinear system

$$\dot{\mathrm{x}} = \mathrm{f}(\mathrm{x}, \mathrm{t}) + \mathrm{B}\, \mathrm{u}(\mathrm{t}) \tag{II.52}$$

$$\mathrm{y} = \mathrm{H}\mathrm{x} + \mathrm{v} \tag{II.53}$$

Now define ϵ_y as the difference between the noisy measurements and the vector $\mathrm{H}\hat{\mathrm{x}}$.

$$\epsilon_{\mathrm{y}} = \mathrm{y} - \mathrm{H}\hat{\mathrm{x}} \tag{II.54}$$

Where: $\hat{\mathrm{x}}$ represents the state estimates. ϵ_y is called the measurement residual. The most probable value of the vector x is the vector $\hat{\mathrm{x}}$ that minimizes the sum of squares between the observed values y and the vector $\mathrm{H}\hat{\mathrm{x}}$.So we will try to compute the $\hat{\mathrm{x}}$ that minimizes the cost function $\mathrm{J} = \epsilon_y^T\, \epsilon_y$

The algorithm of LS is written in the following [13]

$$K_k = P_{k-1}H_k^T[H_k P_{k-1} H_k^T + R]^{-1} \tag{II.55}$$

$$\hat{X}_k = \hat{X}_{k-1} + K_{k+1}[Y_{k+1} - H_k\hat{X}_{k-1}] \quad \text{(II.56)}$$

$$P_k = [I - K_kH_k]P_{k-1}[I - K_kH_k]^T + K_kRK_k^T \quad \text{(II.57)}$$

II.3.1.2 Dynamics estimators

To improve the quality of attitude estimation, several research works have been based on adding gyroscopic measurements through the rotation equation. These measurements provide information on the dynamics of the vehicle and correct any erroneous information mainly coming from the accelerometer. Such approaches, called "dynamic approaches".

Several alternative solutions have been proposed in the last decades. The surveys of nonlinear attitude estimation methods based on vector measurements (*i.e.,* vector observations), which contain a large number of literature citations, are useful sources to start a research on the topic. The paper [20] by one of the pioneers in the domain is also interesting. The author provides many interesting stories about the history of attitude estimation, and especially the QUEST (*i.e.,* QUaternion ESTimator) that he gave birth to and which has become one of the most widely-used spacecraft attitude estimation algorithms.

Recently and because of the nonlinearities associated with the problem of attitude estimation, approaches from the theory of nonlinear automation have given rise to nonlinear attitude observers. One of the first works in this direction is that of Salcudean [40] where a nonlinear observer is proposed for the estimation of angular velocities of a rigid body.

Recently, other nonlinear approaches have focused on the estimation of the rotation matrix $C \in SO(3)$ [37]. The works developed in [36], [35] are very remarkable and their originality is due to the fact that they exploit the group of $SO(3)$ rotation matrices and the Lie algebra associated with it. This approach was developed in order to estimate the attitude and the bias present in the measurements of gyros.

Although for nonlinear observers of the rotation matrix, it is shown that the attitude error converges to zero asymptotically globally. The advantage of nonlinear approaches

over the extended Kalman filter is that they guarantee global convergence, provided through analysis based on Lyapunov theory.

A- Kalman Filter algorithm

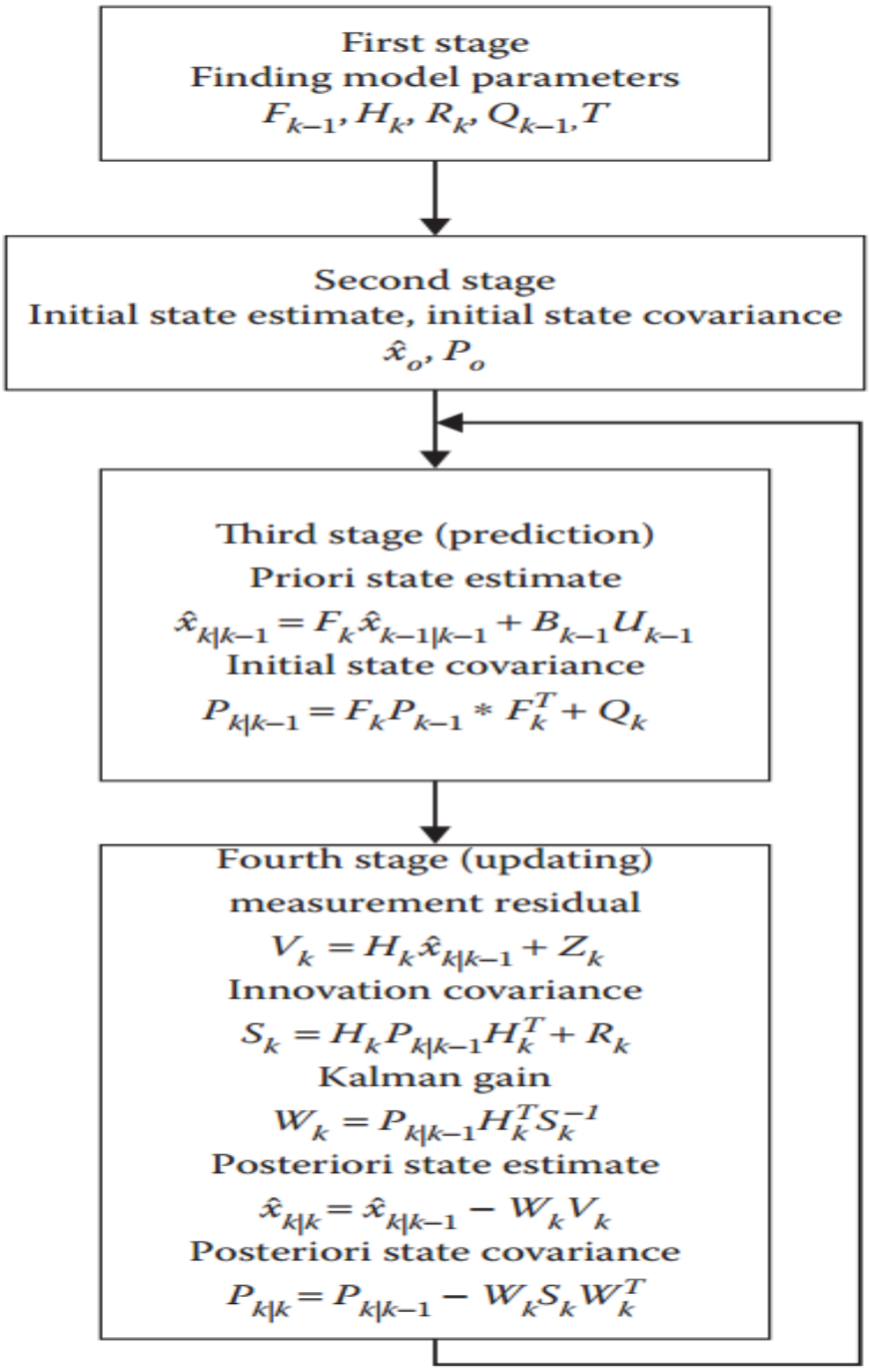

Figure II.9 Kalman filter algorithm.

B- Quaternion-based EKF

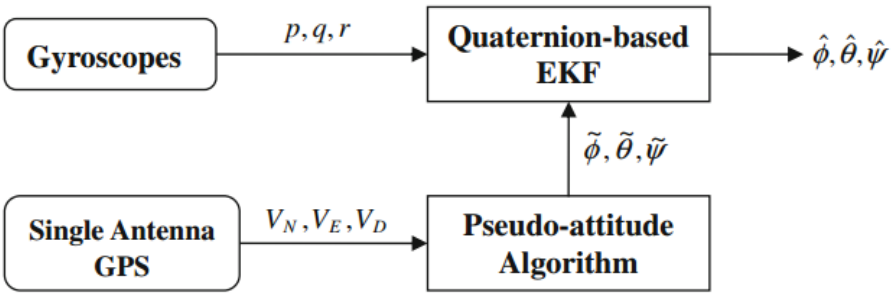

Figure II.10 The process of the fusion algorithm.

The quaternion was selected to present the states in the EKF rather than the Euler angles because it is free of singularities.

The quaternion, which represents a rotation about a specific axis, is defined in terms of four parameters in a column vector as follows

$$q = [q_0 \quad q_1 \quad q_2 \quad q_3]^T \tag{II.58}$$

With

$$\|q\| = \sqrt{{q_0}^2 + {q_1}^2 + {q_2}^2 + {q_3}^2} = 1 \tag{II.59}$$

The Euler angles can be derived as

$$\begin{aligned} \tan\emptyset &= \frac{2(q_0 q_1 + q_2 q_3)}{{q_0}^2 - {q_1}^2 - {q_2}^2 + {q_3}^2} \\ sin\theta &= 2(q_0 q_2 - q_3 q_1) \\ \tan\psi &= \frac{2(q_0 q_3 + q_1 q_2)}{{q_0}^2 + {q_1}^2 - {q_2}^2 - {q_3}^2} \end{aligned} \tag{II.60}$$

Since the drift of gyroscope results in accumulating error, some compensation for the drift is needed to give reliable estimations in the EKF. In this way, the accumulating error of gyroscope could be made to converge to zero. The state vector is given by

$$x = \begin{bmatrix} q \\ b \end{bmatrix} \tag{II.61}$$

Where q is the quaternion vector and b is the vector that contains the estimated bias of each gyroscope in the body coordinate frame. The drift of the gyroscope can be modeled as a random walk, so the dynamic equation of b is simply $\dot{b}$. The nonlinear

state transition and observation models in the EKF are represented as $f(x,\omega)$ and $h(x)$, respectively, and given by

$$f(x,\omega)=\frac{1}{2}\left[\begin{bmatrix}-q_1 & -q_2 & -q_3\\ q_0 & -q_3 & q_2\\ q_3 & q_0 & -q_1\\ -q_2 & q_1 & q_0\end{bmatrix}\begin{bmatrix}p\\ q\\ r\end{bmatrix}\right] \quad \text{(II.62)}$$
$$0_{3\times 1}$$

$$h(x)=\begin{bmatrix}\tan^{-1}\left(\frac{2(q_0q_1+q_2q_3)}{{q_0}^2-{q_1}^2-{q_2}^2+{q_3}^2}\right)\\ \sin^{-1}\big(2(q_0q_2-q_3q_1)\big)\\ \tan^{-1}\left(\frac{2(q_0q_3+q_1q_2)}{{q_0}^2+{q_1}^2-{q_2}^2-{q_3}^2}\right)\end{bmatrix} \quad \text{(II.63)}$$

In this study, the vector $h(x)$ is also the transformation from the quaternion to Euler angle representation. The process of the proposed sensor fusion algorithm is shown in **Figure II.10.** The inputs are the angular rates measured by the gyroscopes and the velocity with respect to ground in NED coordinates acquired from the GPS receiver, and the outputs are the estimated roll angle, pitch angle, and yaw angle, computed from the quaternion estimated in the EKF.

C- The Unscented Kalman Filter

The unscented Kalman filter (UKF) is an extension of the Kalman filter that reduces the linearization errors of the EKF. The use of the UKF can provide significant improvement over the EKF.

We have an n-state discrete time nonlinear system given by

$$x_{k+1}=f(x_k,u_k,t_k)+w_k \quad \text{(II.64)}$$
$$y_k=h(x_k,t_k)+v_k \quad \text{(II.65)}$$
$$w_k\sim(0,Q_k)$$
$$v_k\sim(0,R_k)$$

The UKF is initialized as follows

$$\hat{x}_0^+ = E(x_0) \tag{II.66}$$

$$P_0^+ = E[(x_0 - \hat{x}_0^+)(x_0 - \hat{x}_0^+)^T] \tag{II.67}$$

The following time update equations are used to propagate the state estimate and covariance from one measurement time to the next.

To propagate from time step $(k-1)$ to k, first choose sigma points $x_{k-1}^{(i)}$, with appropriate changes since the current best guess for the mean and covariance of x_k are $\hat{x}_{k-1}^+$, and P_{k-1}^+.

$$\hat{x}_{k-1}^{(i)} = \hat{x}_{k-1}^+ + \tilde{x}^{(i)} \quad i = 1, \dots, 2n$$

$$\tilde{x}^{(i)} = \left(\sqrt{nP_{k-1}^+}\right)_i^T \quad i = 1, \dots, n$$

$$\tilde{x}^{(n+i)} = -\left(\sqrt{nP_{k-1}^+}\right)_i^T \quad i = 1, \dots, n \tag{II.68}$$

Use the known nonlinear system equation $f(.)$ to transform the sigma points into $\hat{x}_k^{(i)}$ vectors, with appropriate changes since our nonlinear transformation is $f(.)$ rather than $h(.)$.

$$\hat{x}_k^{(i)} = f(\hat{x}_{k-1}^{(i)}, u_k, t_k) \tag{II.69}$$

Combine the $\hat{x}_k^{(i)}$ vectors to obtain the a priori state estimate at time k.

$$\hat{x}_k^- = \frac{1}{2n}\sum_{i=1}^{2n} \hat{x}_k^{(i)} \tag{II.70}$$

Estimate the a priori error covariance. However, we should add Q_{k-1} to the end of the equation to take the process noise into account

$$P_k^- = \frac{1}{2n}\sum_{i=1}^{2n}(\hat{x}_k^{(i)} - \hat{x}_k^-)(\hat{x}_k^{(i)} - \hat{x}_k^-)^T + Q_{k-1} \tag{II.71}$$

Now that the time update equations are done, we implement the measurement update equations.

Choose sigma points $x_{k-1}^{(i)}$, with appropriate changes since the current best guess for the mean and covariance of x_k are $\hat{x}_k^-$, and P_k^-.

$$\hat{x}_k^{(i)} = \hat{x}_k^+ + \tilde{x}^{(i)} \quad i = 1, \dots, 2n$$

$$\tilde{x}^{(i)} = \left(\sqrt{nP_k^+}\right)_i^T \quad i = 1, \dots, n$$

$$\tilde{x}^{(n+i)} = -\left(\sqrt{nP_k^+}\right)_i^T \quad i = 1, \dots, n \tag{II.72}$$

Use the known nonlinear measurement equation $h(.)$ to transform the sigma points into $\hat{y}_k^{(i)}$ vectors (predicted measurements).

$$\hat{y}_k^{(i)} = h(\hat{x}_k^{(i)}, t_k) \tag{II.73}$$

Combine the $\hat{y}_k^{(i)}$ vectors to obtain the predicted measurement at time k.

$$\hat{y}_k = \frac{1}{2n}\sum_{i=1}^{2n} \hat{y}_k^{(i)} \tag{II.74}$$

Estimate the covariance of the predicted measurement. However, we should add R_k to the end of the equation to take the measurement noise into account.

$$P_y = \frac{1}{2n}\sum_{i=1}^{2n}(\hat{y}_k^{(i)} - \hat{y}_k)(\hat{y}_k^{(i)} - \hat{y}_k)^T + R_k \tag{II.75}$$

Estimate the cross covariance between $\hat{x}_k^-$ and $\hat{y}_k$.

$$P_{xy} = \frac{1}{2n}\sum_{i=1}^{2n}(\hat{x}_k^{(i)} - \hat{x}_k^-)(\hat{y}_k^{(i)} - \hat{y}_k)^T \tag{II.76}$$

The measurement update of the state estimate can be performed using the normal Kalman filter equations.

$$K_k = P_{xy}P_y^{-1} \tag{II.77}$$

$$\hat{x}_k^+ = \hat{x}_k^- + K_k(y_k - \hat{y}_k) \tag{II.78}$$

$$P_k^+ = P_k^- - K_k P_y K_k^T \tag{II.79}$$

D- Nonlinear Complementary Filter [38]

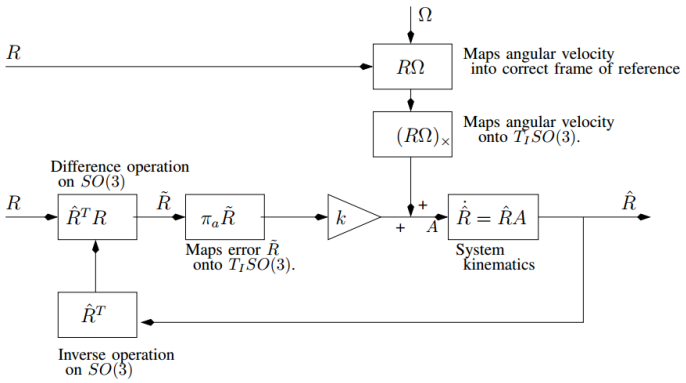

Figure II.11 Block diagram of the complementary filter.

the kinematics of the true system are given by

$$\dot{R} = R\Omega_{\times} = (R\Omega)_{\times}R \tag{II.80}$$

The dynamics of the filter $\hat{R}$ are required to evolve on $SO(3)$ and should have a form similar to the kinematics of R

$$\dot{\hat{R}} = (R\Omega + \hat{R}\omega(\hat{R}, R))_{\times}\hat{R}$$
$$\dot{\hat{R}} = \left((R\Omega)_{\times} + k_{est}\hat{R}\pi_a(\tilde{R})\hat{R}^T\right)\hat{R} \quad for\ \hat{R}(0) = \hat{R}_0 \tag{II.81}$$

where $\omega(\hat{R}, R)$ is a correction term that is zero when $\hat{R} = R$. And the kinematics of $\tilde{R}$ are given by

$$\dot{\tilde{R}} = \hat{R}^T(R\Omega + \hat{R}\omega)_{\times}^T R + \hat{R}^T(R\Omega)_{\times}R$$
$$\dot{\tilde{R}} = \omega_{\times}^T\tilde{R} = -\omega_{\times}\tilde{R} \tag{II.82}$$

Deriving the Lyapunov function E_t

$$\dot{E}_t = -\frac{1}{2}tr(\dot{\tilde{R}}) \tag{II.83}$$

Then

$$\dot{E}_t = -2k_{est}\cos^2\left(\frac{\theta}{2}\right)E_t \tag{II.84}$$

And for any initial condition $\hat{R}_0$ such that

$$\theta_0 = \frac{1}{\sqrt{2}}\left\|\log\left(\tilde{R}_0\right)\right\| < \pi \quad \text{(II.85)}$$

Then $E_t \rightarrow 0$ and $\hat{R}(t) \rightarrow R(t)$ exponentially.

Implementing a complementary filter on SO(3)

Given the theoretical form of the filter it is important to consider how such a filter may be implemented. In practice, the various inputs to the filter are replaced by measurements and filtered estimates of the states; There are three key inputs

- The reference rotation R that generates the error term $\hat{R}^T R$. Based on an understanding of complementary filter design it is natural to use the estimate R_y to generate the error term.

- A direct measurement of the angular velocity $\Omega_y \approx \Omega$ is available and used to drive the feedforward term in the filter.

- Finally, an estimate of the rotation R must be used to map the body-fixed-frame velocity back into the inertial frame.

Nonlinear observers

The algorithms are mentioned in **I.3.3**

II.3.2 Attitude estimation based on IMU/GPS fusion

II.3.2.1 Integration Architectures

Architecture 1 (Uncoupled Mode)

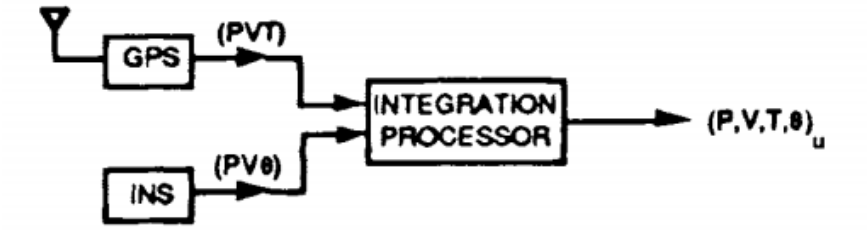

Figure II.12. uncoupled mode.

Figure II.12 illustrates the configuration in which GPS and an INS produce independent navigation solutions with no influence of one on the other. The integrated navigation solution is mechanized by an external integration processor that may be as simple as a selector or as complex as a multimode Kalman filter. All data busses are "simplex" (unidirectional).

The characterization of **Figure II.12** as an "uncoupled" mode is based on the independence of the GPS and INS navigation functions. Note that, in principle, the hardware could all be packaged in one physically integrated (embedded) unit; however, the functionality would still be that of uncoupled architecture. The potential benefits of integrating the navigation solutions from uncoupled GPS and inertial navigators are:

- It is the easiest, fastest, and potentially the cheapest approach when an INS and GPS are both available.

- It provides some tolerance to failures of subsystem components (except in the embedded configuration).

- Using an integration processor as simple as a selection algorithm can provide “en route” navigation at least as accurate as available from an INS.

Architecture 2 (Loosely Coupled Mode)

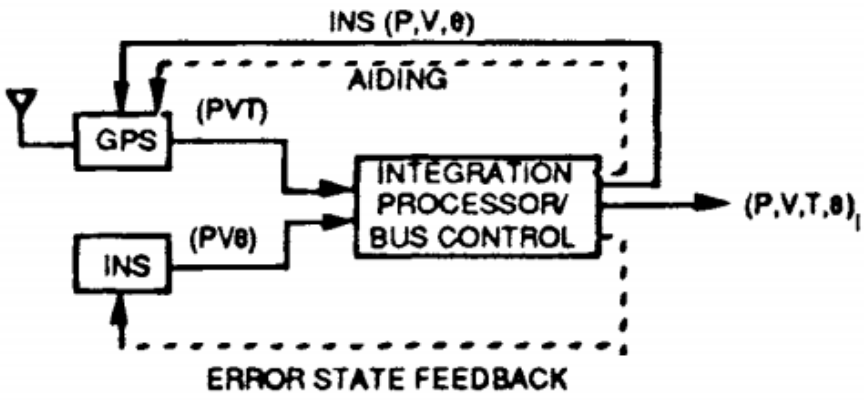

Figure II.13 Loosely coupled mode.

Figure II.13 illustrates a configuration in which there are several data paths between the integration processor and the GPS and the INS equipment. Among these, the provision of the system navigation solution to the GPS is the most important for getting the maximum benefit from the integration filter. The inertial aiding of GPS tracking loops is of next greatest benefit, and feedback of error states to the INS is of second-order benefit.

Reference navigation solution

GPS generally employs a Kalman filter mechanization to compute PVT updates based on current tracking loop measurements. when the system navigation solution is fed back to perform that propagation. In effect, the GPS measurements can now be used to correct the system navigation solution. Over short periods of time, that solution is very accurate because it incorporates INS data based on acceleration sensing. The filter can be tuned to have a longer time constant (filter memory), thereby increasing the effective averaging of each noisy GPS measurement.

Inertial aiding of GPS tracking loops

The availability of a GPS navigation solution can be increased significantly when inertial aiding is used to reduce the vehicle dynamics tracked by the UE code and carrier loops. In principle, this aiding could be applied directly from the INS to the GPS, but it is shown as an output of the integration processor in **Figure II.13** because of the following:

- GPS tracking loops must be aided by the projection of vehicle velocity along the line-of-sight (LOS) to each satellite being tracked. The conversion from inertial coordinates to GPS LOS coordinates is most appropriately done in the integration processor or in the GPS UE itself. In either case, INS velocity information is available within the processor hence aiding can be part of the data flow to the UE. This avoids the expense and risk of developing a custom interface from the INS to the GPS UE.

- Executing the coordinate transformation external to the INS retains flexibility in the selection of INS equipment and avoids the need to develop custom GPS/INS interfaces for each application. However, this raises a concern for "data latency" (i.e. feeding delayed data to the tracking loops).

Error-state feedback to the inertial navigation system

Most inertial navigation systems have the means to accept external inputs to reset their position and velocity solutions and to adjust the alignment of their stable platform. The adjustment may be executed by a mathematical correction in a "strap-down" inertial system, or it may be realized by torqueing a gimballed platform. In either case, the use of feedback can maintain inertial navigation errors at a level for which their dynamics are accurately modeled by the error state propagation equations embodied in the integration filter.

Architecture 3 (tightly Coupled Mode)

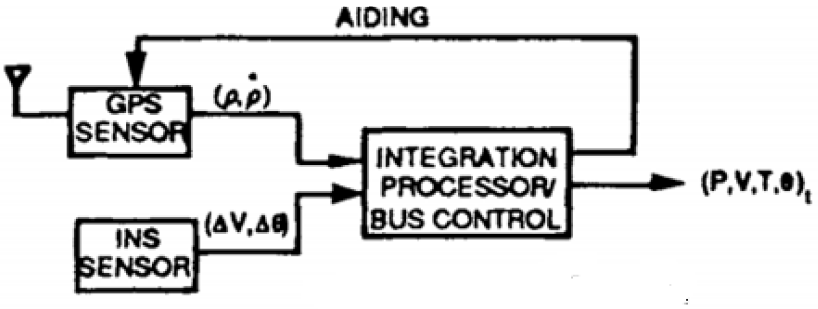

Figure II.14 Tightly coupled mode.

Figure II.14 illustrates the so-called tightly coupled integration mode. It differs from the loosely coupled mode in that both the GPS receiver and the inertial components are limited to their sensor functions. They are treated as sources of GPS code and carrier

measurements and inertial indications of acceleration (velocity change) and angular rate, respectively. These sensor outputs are then combined in one navigation processor that may mechanize an appropriately high-order integration filter [32-34].

In the tightly coupled mode, there is only one feedback from the navigation processor. Figure 3 illustrates the use of velocity aiding to the GPS tracking loops. Acceleration aiding could also be effectively used, but we are not aware of any particular mechanization using other than velocity aiding. The other paths used in loosely coupled architectures are not needed here because all computations involved in navigation processing are now internal to one processor. The concept of tightly coupled integration is often raised in connection with embedded GPS receivers. These are not necessarily synonymous. However, it is reasonable that we would choose to mechanize a tightly coupled integration algorithm if we had already taken the effort to design a GPS receiver that is physically and electrically integrated with an inertial sensor or with a powerful navigation processor.

II.3.2.2 Implementation of the integrated system with EKF

To implement the KF for the integrated navigation system, first we should build up the system model, i.e. to determine the state vector and derive the system dynamic equations as well as observation equations. Based on the system model.

State vector and system dynamic equations

The state vector contains the unknown parameters to be estimated in the Kalman filter. we choose 15 parameters for the state vector of the GPS/INS integrated navigation system. The parameters can be divided into two groups as

$$x = [x_1^T \quad x_2^T]^T \tag{II.86}$$

Where the first group contains three dimensional errors in position, velocity and orientation of the IMU

$$x_1 = [(\delta r^e)^T \quad (\delta v^e)^T \quad (\varepsilon^e)^T]^T = \left[\delta x_i, \delta y_i, \delta z_i, \delta v_x, \delta v_y, \delta v_z, \varepsilon_x, \varepsilon_y, \varepsilon_z\right]^T \tag{II.87}$$

And the second group is the sensors errors

$$x_2 = [d^T \quad b^T]^T \tag{II.88}$$

The position and velocity of the vehicle can be computed

$$\begin{aligned} x_i &= x_{i0} + \delta x_i, \quad v_x = v_{x0} + \delta v_x \\ y_i &= y_{i0} + \delta y_i, \quad v_y = v_{y0} + \delta v_y \\ z_i &= z_{i0} + \delta z_i, \quad v_z = v_{z0} + \delta v_z \end{aligned} \tag{II.89}$$

Where x_{i0}, y_{i0}, z_{i0} are coordinates, v_{x0}, v_{y0}, v_{z0} are velocities as delivered by IMU.

The IMU sensors errors in the second group contain two parts

The accelerometer's error $\delta a(t)$ consists of the constant (b) and random (W_A) parts:

$$\delta a(t) = b + W_A(t) \tag{II.90}$$

Where

b: is the accelerometer bias, which is modelled as random constant. This bias gets a random value within certain limit, usually specified as bias repeatability. This bias must be determined after each start of IMU.

$W_A(t)$: is random walk noise of the accelerometer.

Similarly, the error of the gyro can be described as

$$\delta\omega(t) = d + w_G(t) \tag{II.91}$$

Where

d: is the gyro drift. The same remark holds as for b.

$w_G(t)$: is random walk noise of the gyro.

The sensor errors are defined as

$$\begin{aligned} \widehat{\omega} &= \widetilde{\omega} + \delta\omega \\ \hat{a} &= \tilde{a} + \delta a \end{aligned} \tag{II.92}$$

The INS errors are modelled by a linear system described generally by the following dynamic state equation

$$\dot{x}(t) = F(t)x(t) + G(t)u(t) \tag{II.93}$$

And the measurement model is

$$z(t) = Hx(t) + v(t) \tag{II.94}$$

Where x is the state vector, F is the system dynamic matrix, G is input matrix, t is time, and u is a vector forcing function, whose elements are white noise. The discrete solution of Eq. (II.94) is

$$\boldsymbol{X}_k = \boldsymbol{\Phi}_{k,k-1}\,\boldsymbol{X}_{k-1} + \boldsymbol{W}_k \tag{II.95}$$

Where $\boldsymbol{\Phi}_{k,k-1}$ is the transition matrix from epoch k-1 to k and, $\boldsymbol{W}_k$ is the noise in the state vector. The Kalman filter can be applied iteratively based on this discrete solution.

The relationship between the transition matrix $\boldsymbol{\Phi}$ and dynamic matrix F can be expressed by

$$\boldsymbol{\Phi}_{k,k+1} = e^{F.\Delta t} \approx I + F_k\Delta t + \frac{1}{2}F_k^2\Delta t^2 + \frac{1}{3!}F_k^3\Delta t^3 + \frac{1}{4!}F_k^4\Delta t^4 + \ldots \tag{II.96}$$

It is the transition matrix between epochs k and k+1, where $\Delta t = \mathbf{t}_{k+1} - \mathbf{t}_k$ and

$$\boldsymbol{\Phi}_{k,k+1} = \int_k^{k+1} \boldsymbol{\Phi}_{k+1,\tau}\,G_\tau u_\tau d\tau \tag{II.97}$$

It is the driven response at epoch $k+1$ due to the presence of the white noise input during interval Δt.

Differenced GPS observation equations

In the case of differential or relative positioning, at least two GPS receivers measure pseudo-ranges to a set of common satellites simultaneously. Let two receivers on points A and B measure a satellite s and the point A is a known, reference point. The code and phase observation equations can be written as

$$P_A^s = P_A^s(t_A) - \dot{\rho}_A^s(t_A)\delta t_{\hat{t}A}$$

$$\lambda\varphi_A^s = \lambda\varphi_A^s - \dot{\rho}_A^s(t_A)\delta t_{\hat{t}A} \tag{II.98}$$

Where φ_A^s, P_A^s is the phase difference and pseudo-range by receiver A to satellite s; $t_A$is the nominal time of the signal reception measured by the clock of receiver A.

To reduce the atmospheric effects that are common to both stations, it is useful to form differenced equations. The single differences can be obtained by the difference equations of the two receivers towards one satellite

$$\lambda\varphi_{AB}^{s} = \lambda\varphi_{B}^{s} - \lambda\varphi_{A}^{s} = \rho_{AB}^{s} + c\delta t_{AB} + \lambda N_{AB}^{s}$$

$$P_{AB}^{s} = P_{B}^{s} - P_{A}^{s} = \rho_{AB}^{s} + c\delta t_{AB} \quad \text{(II.99)}$$

Where

$$\rho_{AB}^{s} = \rho_{B}^{s} - \rho_{A}^{s}$$

$$\delta t_{AB} = \delta t_{B} - \delta t_{A} \quad \text{(II.100)}$$

$$N_{AB}^{s} = N_{B}^{s} - N_{A}^{s}$$

In the similar way, it is possible to form double differences between two single differences. Let two receivers *A*, *B* observing simultaneously two satellites *s* and *t*. For each of the satellites a pair of single difference equation similar to (II.99) can be formed:

$$\lambda\varphi_{AB}^{s} = \rho_{AB}^{s} + c\delta t_{AB} + \lambda N_{AB}^{s}$$

$$\lambda\varphi_{AB}^{t} = \rho_{AB}^{t} + c\delta t_{AB} + \lambda N_{AB}^{t} \quad \text{(II.101)}$$

$$\rho_{AB}^{s} = \rho_{B}^{s} + c\delta t_{AB}$$

$$\rho_{AB}^{t} = \rho_{B}^{t} + c\delta t_{AB}$$

By subtracting code and phase equations, respectively, we get the following double difference equations

$$\lambda\varphi_{AB}^{st} = \lambda\varphi_{AB}^{t} - \lambda\varphi_{AB}^{s} = \rho_{AB}^{st} + \lambda N_{AB}^{t}$$

$$P_{AB}^{st} = P_{AB}^{t} - P_{AB}^{s} = \rho_{AB}^{st} \quad \text{(II.102)}$$

Where

$$\rho_{AB}^{st} = \rho_{AB}^{t} - \rho_{AB}^{s}$$

$$N_{AB}^{st} = N_{AB}^{t} - N_{AB}^{s} \quad \text{(II.103)}$$

We can see the receiver clock errors δt^{s} are eliminated, which is the most important feature of the double differences.

System observation equations

In practice, there is always an offset between the GPS antenna and the IMU as shown in **Figure II.15**, which therefore is required to be compensated.

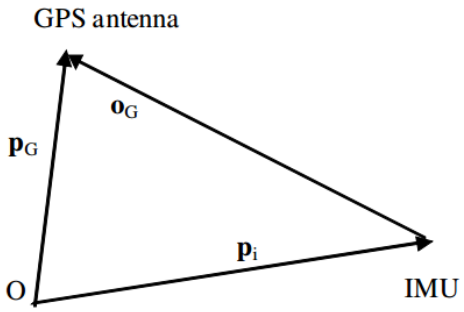

Figure II.15 GPS antenna offset.

Let us denote the vector from IMU to the GPS expressed in the body coordinate system as o_G^b, the positional vector of the antenna as p_G and the positional vector of the IMU as p_i. The offset o_G^b can be computed by

$$o_G^b = R_e^b o_G^e = R_e^b(p_G^e - p_i^e) \tag{II.104}$$

If vector y contains coordinates of the GPS antenna determined by GPS, then the GPS observation equation will be as follows

$$\tilde{y} = \hat{p}_G^e - \delta = \hat{p}_i^e + \hat{R}_b^e \hat{o}_G^b - \delta \tag{II.105}$$

where δ denotes the residual vector. Taking into account the approximation

$$\hat{R}_b^e = (I - E^e)\tilde{R}_b^e$$

We have

$$R_b^a = \begin{bmatrix} 1 & \theta_z & -\theta_y \\ -\theta_z & 1 & \theta_x \\ \theta_y & -\theta_x & 1 \end{bmatrix} = I - E$$

Where **E** is the skew-symmetric matrix of Euler angles

$$E = \begin{bmatrix} 0 & \theta_z & -\theta_y \\ -\theta_z & 0 & \theta_x \\ \theta_y & -\theta_x & 0 \end{bmatrix}$$

Two basic operations with skew-symmetric matrix are given as follows

$$\mathrm{A}^{\mathrm{T}} = -\mathrm{A}, \qquad \mathrm{a} \times \mathrm{b} = \mathrm{Ab} = -\mathrm{Ba} \tag{II.106}$$

Where $\boldsymbol{A}$ and $\boldsymbol{B}$ is the skew-symmetric matrices of vectors $\boldsymbol{a}$ and $\boldsymbol{b}$, respectively.

The observation vector which is used in the Kalman filter is

$$\tilde{\mathrm{y}} = \tilde{\mathrm{p}}_{\mathrm{i}}^{\mathrm{e}} + \delta\tilde{\mathrm{p}}_{\mathrm{i}}^{\mathrm{e}} + (\mathrm{I} - \mathrm{E}^{\mathrm{e}})\tilde{\mathrm{R}}_{\mathrm{b}}^{\mathrm{e}}\mathrm{o}_{\mathrm{G}}^{\mathrm{b}} - \delta \tag{II.107}$$

$$\mathrm{L} = \tilde{\mathrm{y}} - \tilde{\mathrm{p}}_{\mathrm{i}}^{\mathrm{e}} - \tilde{\mathrm{R}}_{\mathrm{b}}^{\mathrm{e}}\mathrm{o}_{\mathrm{G}}^{\mathrm{b}} = \delta\mathrm{p}_{\mathrm{i}}^{\mathrm{e}} + (\mathrm{o}_{\mathrm{G}}^{\mathrm{e}} \times)\varepsilon^{\mathrm{e}} \tag{II.108}$$

Where the misalignment angles in the e-frame $\varepsilon^{\mathrm{e}} = [\varepsilon_{\mathrm{X}}^{\mathrm{e}} \quad \varepsilon_{\mathrm{Y}}^{\mathrm{e}} \quad \varepsilon_{\mathrm{Z}}^{\mathrm{e}}]^{\mathrm{T}}$, the vector product can be transferred to the skew-symmetric operation by Eq. (II.106)

$$(\mathrm{o}_{\mathrm{G}}^{\mathrm{e}} \times) = \begin{bmatrix} 0 & -\mathrm{o}_{\mathrm{z}}^{\mathrm{e}} & \mathrm{o}_{\mathrm{y}}^{\mathrm{e}} \\ \mathrm{o}_{\mathrm{z}}^{\mathrm{e}} & 0 & -\mathrm{o}_{\mathrm{x}}^{\mathrm{e}} \\ -\mathrm{o}_{\mathrm{y}}^{\mathrm{e}} & \mathrm{o}_{\mathrm{x}}^{\mathrm{e}} & 0 \end{bmatrix}$$

With the observation equation in the Kalman filter, i.e. Eq. (II.108), we can get the design matrix for the loose integration.

$$H_{Loose} = \begin{bmatrix} 1 & 0 & 0 & 0 & 0 & 0 & 0 & -\mathrm{o}_{\mathrm{z}}^{\mathrm{e}} & \mathrm{o}_{\mathrm{y}}^{\mathrm{e}} \\ 0 & 1 & 0 & 0 & 0 & 0 & \mathrm{o}_{\mathrm{z}}^{\mathrm{e}} & 0 & -\mathrm{o}_{\mathrm{x}}^{\mathrm{e}} \\ 0 & 0 & 1 & 0 & 0 & 0 & -\mathrm{o}_{\mathrm{y}}^{\mathrm{e}} & \mathrm{o}_{\mathrm{x}}^{\mathrm{e}} & 0 \end{bmatrix} \tag{II.109}$$

To obtain the design matrix for the tight integration, we have

$$\rho_A^s(\tilde{t}_A) - \rho_{A0}^s(\tilde{t}_A) = AX \tag{II.110}$$

Where $A = \begin{bmatrix} a_x^s & a_y^s & a_z^s \end{bmatrix}$ and $X = [\Delta X \quad \Delta Y \quad \Delta Z \ ]$

The left side of Eq. (II.110) is the observation vector for the tight integration as that in Eq. (II.87) i.e. $L = \rho_A^s(\tilde{t}_A) - \rho_{A0}^s(\tilde{t}_A)$. Multiplying A matrix at both sides of Eq. (II.87), we get

$$\mathrm{AL} = \mathrm{A}\delta\mathrm{p}_{\mathrm{i}}^{\mathrm{e}} + \mathrm{A}(\mathrm{o}_{\mathrm{G}}^{\mathrm{e}} \times)\varepsilon^{\mathrm{e}} = \mathrm{AX} + \mathrm{A}(\mathrm{o}_{\mathrm{G}}^{\mathrm{e}} \times)\varepsilon^{\mathrm{e}} \tag{II.111}$$

We obtain the design matrix for the tight integration

$$\mathrm{H}_{\mathrm{Tight}} = [\mathrm{A} \quad 0 \quad \mathrm{A}(\mathrm{o}_{\mathrm{G}}^{\mathrm{e}} \times) \ ] \tag{II.112}$$

We note that each of the 3 sub matrices in Eq. (II.112) is a matrix with 3×3 elements.

II.4 Conclusion

This chapter describes different sensors which provide measurements in continuous time or at a sufficiently high frequency, with bounded measurement noise, also we mentioned in this chapter a different approach for attitude estimation and some known algorithms which are based on inertial sensors and based on IMU/GPS fusion measurements.

Chapter III

Study of states observers

III.1 Introduction

The ability to estimate the orientation (attitude) of a rigid body is an important feature in many engineering applications. As such, this problem has attracted the attention of many researchers and industrials for several decades.

The state observers have shown their effectiveness in different applications of many dynamical systems. The main drawback usually reported for most observers is their dependence on mathematical model of system. Therefore, the design of observers has faced critical challenges in practical applications due to the presence of nonlinearities, disturbances and dynamic uncertainties. Thus, obtaining high-performance robust observer design was the target of many researchers. In the last two decades, several advanced observer design techniques have been proposed like high gain observers, the invariant and the cascaded observers which are the main interest of this chapter.

III.2 The Complementary Filter

In this subsection we will discuss about two versions of the nonlinear complementary filter where we try to find better convergence rates, the first one is "smooth nonlinear complementary filter" proposed by Mr. Mahony, and the second one is "nonsmooth nonlinear complementary filter" proposed by Mr. Berkane which is a Mahony's filter modified. The goal of the attitude complementary filter, is to fuse the available gyro measurements together with the reconstructed attitude R_y (or directly the inertial vector measurements) to obtain a good (filtered) attitude estimate $\hat{R}$.

III.2.1 smooth nonlinear complementary filter

III.2.1.1 Conception

Let $R \in SO(3)$ denote a rotation matrix from the body fixed-frame to a given inertial reference frame. The rotation matrix R evolves according to the kinematic equation.

$$\dot{R} = R[\omega]_\times \tag{III.1}$$

Where $\omega \in R^3$ is the angular velocity expressed in the body fixed-frame. Let $\omega_y(t)$ denote the angular velocity measurement such that

$$\omega_y(t) = \omega(t) + n_\omega(t) \tag{III.2}$$

Where $n_\omega(t)$ is a priori bounded signal that captures the measurements noise and disturbances.

Consider the following nonlinear complementary attitude filter on $SO(3)$ proposed by Mahony [41]

$$\dot{\hat{R}} = \hat{R}[\omega_y]_\times - [\sigma]_\times \hat{R} \tag{III.3}$$

$$\sigma = -\psi(A\tilde{R}) \tag{III.4}$$

Where $\hat{R} \in SO(3)$ is an estimate of R with $\hat{R}(0) = \hat{R}_0 \in SO(3)$, σ the observer innovation term, $\tilde{R} = R\hat{R}^\top$ represents the attitude estimation error and A is a symmetric matrix such that $\bar{A} := tr(A)I - A$ is positive definite.

With the composition map $\psi \coloneqq vex \circ \mathbb{P}_a$, the projection map $\mathbb{P}_a(A) \coloneqq (A - A^T)/2$, $vex[\omega]_\times = \omega$ for all $\omega \in \mathbb{R}^3$, and $[vex(\Omega)]_\times = \Omega$ for all $\Omega \in \mathfrak{so}(3)$ such that, for

$A \coloneqq [a_{ij}] i, j = 1,2,3$. We have $\psi(A) \coloneqq vex\big(\mathbb{P}_a(A)\big) = \frac{1}{2}\begin{bmatrix} a_{32} - a_{23} \\ a_{13} - a_{31} \\ a_{21} - a_{12} \end{bmatrix}$.

The attitude estimator (III.3) falls under the category of gradient-based observers on Lie groups. In fact, the observer innovation term (III.4) can be directly obtained from the gradient of the following smooth attitude potential function $V_A(\tilde{R}) = tr\left(A\big(I - \tilde{R}\big)\right)$, Which is the well-known trace function on SO(3) that has been widely used in the literature for the design of attitude control systems.

Another explicit formulation of the observer input σ in (III.3)-(III.4) using directly inertial vector measurements is given as follows

$$\sigma = -\frac{1}{2}\hat{R}\sum_{i=1}^{n}\rho_i\big(b_i \times \hat{R}^T r_i\big) \tag{III.5}$$

Where $b_i = R^T r_i$ are body-frame vector measurements of know inertial vectors $r_i, i = 1,\cdots,n; n \geq 2$; thus, obviating the need for the rotation matrix reconstruction.

III.2.1.2 Analyze and Stability

Lemma: Let $R \in SO(3)$ and $A = A^{\mathsf{T}} \in R^{3\times3}$ such that $\bar{A} = tr(A)I - A$ is positive definite. Then, the following hold.

$$\|\psi(R)\|^2 = |R^2|_I^2 = 4|R|_I^2(1 - |R|_I^2) \tag{III.6}$$

$$2\lambda_{min}^{\bar{A}}|R|_I^2 \leq tr\big(A(I - R)\big) \leq 2\lambda_{max}^{\bar{A}}|R|_I^2 \tag{III.7}$$

$$\xi^2|R|_I^2(1 - |R|_I^2) \leq \frac{\|\psi(AR)\|^2}{(\lambda_{max}^{\bar{A}})^2} \leq |R|_I^2(1 - \xi^2|R|_I^2) \tag{III.8}$$

$$\psi(AR) = \frac{(I - [\mathcal{Z}(R)]_\times)}{1 + \|\mathcal{Z}(R)\|^2}\overline{A}\mathcal{Z}(R) \tag{III.9}$$

Where $\mathcal{Z}(R) = vex\big((R - I)(R + I)^{-1}\big) = \frac{\psi(R)}{2\left(1 - |R|_I^2\right)}$ defines the vector of Rodriguez parameters, usually use the unit quaternion or the angle axis representation, and in our

case we used directly rotation matrices on $SO(3)$, $\xi = \lambda_{min}^{\bar{A}}/\lambda_{max}^{\bar{A}}$ and $|R|_I \in [0,1]$ be the normalized Euclidean distance on $SO(3)$ which is given by $|R|_I^2 := \frac{1}{4}tr(I-R)$.

Proposition: Consider the attitude kinematics system (III.1) coupled with the attitude observer (III.3)-(III.4). Assume that $\omega_y \equiv \omega$. Then,

• The desired equilibrium point $\tilde{R} = I$ is almost globally asymptotically stable and locally exponentially stable.

• The undesired equilibria are characterized by $\tilde{R} \in \mathcal{R}_a(\pi, \mathcal{E}(A))$; where $\mathcal{E}(A)$ is the set of all unit eigenvectors of A, and $\mathcal{R}_a(\theta,u) = I + sin(\theta)[u]_\times + (1-\cos(\theta))[u]_\times^2$ is the representation of the attitude by the angle of rotation θ and the unit vector axis u.

The attitude estimator (III.3)-(III.4) proposed in [41] has been used in many applications due to its proven almost global asymptotic stability and its nice filtering properties.

Theorem 1: Consider the attitude kinematics system (III.1) coupled with the attitude observer (III.3)-(III.4). Assume that $\omega_y \equiv \omega$. Then, the set $\Pi = \{\tilde{R} \in SO(3)\ ;\ \left|\tilde{R}\right|_I = 1\}$ is forward invariant and non-attractive. Moreover, for any $\tilde{R}(0) \in SO(3)\backslash\Pi$ one has

$$\tilde{R}(t) = \mathcal{R}_r\left(e^{-\frac{\bar{A}}{2}t}\mathcal{Z}\left(\tilde{R}(0)\right)\right) \; for\ all\ t \geq 0. \tag{III.10}$$

With $\mathcal{R}_r(z) = (I+[z]_\times)(I-[z]_\times)^{-1} = \frac{1}{1+\|z\|^2}((1-\|z\|^2)I + 2zz^T + 2[z]_\times$ often known as Cayley's formula. In view of (III.1) and (III.3)-(III.4), one obtains

$$\begin{aligned}\dot{\tilde{R}} &= \dot{R}\hat{R}^T - R\hat{R}^T\dot{\hat{R}}\hat{R}^T \\ &= R[\omega]_\times\hat{R}^T - R\left[\omega_y\right]_\times\hat{R}^T + R\hat{R}^T[\sigma]_\times \\ &= \tilde{R}\left[\sigma - \hat{R}n_\omega\right]_\times\end{aligned} \tag{III.11}$$

This theorem provides an explicit solution for the attitude estimator of Mahony et al. [41] given by equations (III.3)-(III.4). Equation (III.10) shows that the Rodrigues vector associated to the attitude estimation error decays exponentially fast. The corresponding attitude error matrix is subsequently obtained via the Cayley's formula. It is worth

pointing out that, although the Rodrigues vector is converging exponentially to zero, the attitude estimation error does not necessary converge exponentially fast as well. And the attitude estimation error satisfies

$$\underline{\beta}\left(\left|\tilde{R}(t)\right|_I, t\right) \leq \left|\tilde{R}(t)\right|_I \leq \overline{\beta}\left(\left|\tilde{R}(t)\right|_I, t\right) \tag{III.12}$$

For all $t \geq 0$,such that $\underline{\beta}$ and $\overline{\beta}$ are given by

$$\overline{\beta}\,(\mathrm{s},\mathrm{t}) = \frac{se^{-\lambda_{min}^{\bar{A}} t/2}}{\sqrt{1-s^2\left(1-e^{-\lambda_{min}^{\bar{A}} t}\right)}} \tag{III.13}$$

$$\underline{\beta}\,(\mathrm{s},\mathrm{t}) = \frac{se^{-\lambda_{max}^{\bar{A}} t/2}}{\sqrt{1-s^2\left(1-e^{-\lambda_{max}^{\bar{A}} t}\right)}} \tag{III.14}$$

Consider the following Lyapunov function candidate

$$V\left(\mathcal{Z}(\tilde{R})\right) = \left\|\mathcal{Z}\left(\tilde{R}(t)\right)\right\|^2 \tag{III.15}$$

The time derivative of V is

$$\dot{V}\left(\mathcal{Z}(\tilde{R})\right) = -\mathcal{Z}(\tilde{R})^T \overline{A}\mathcal{Z}(\tilde{R}) + \left(1 + \left\|\mathcal{Z}(\tilde{R})\right\|^2\right)\mathcal{Z}(\tilde{R})^T \hat{R} n_\omega$$

$$\dot{V}\left(\mathcal{Z}(\tilde{R})\right) \leq -\lambda_{min}^{\bar{A}}(1-\varepsilon)\left\|\mathcal{Z}(\tilde{R})\right\|^2 \tag{III.16}$$

With $0 < \varepsilon < 1$

And this is shows that the attitude filter of [41] is locally input-to-state stable.

III.2.2 Non-smooth nonlinear complementary filter

III.2.2.1 Conception

In the previous section, we have shown that the attitude estimator (III.3)-(III.4) suffers from slow convergence for large attitude errors, so in a tentative to improve the convergence rate of this class of attitude observers, we introduce a state-dependent scalar gain function $k: SO(3) \rightarrow R_+$, into the observer innovation term, which is strictly positive on $SO(3)$. We consider, therefore, the following attitude estimation

$$\dot{\hat{R}} = \hat{R}\left[\omega_y\right]_\times - [\sigma]_\times \hat{R} \tag{III.17}$$

$$\sigma = -k(\tilde{R})\psi(A\tilde{R}) \tag{III.18}$$

Where $\hat{R} \in SO(3)$ is an estimate of R with $\hat{R}(0) = \hat{R}_0 \in SO(3)$, σ the observer innovation term, $\tilde{R} = R\hat{R}^\top$ represents the attitude estimation error and A is a symmetric matrix such that $\bar{A} := tr(A)I - A$ is positive definite. the attitude estimation scheme (III.17)-(III.18) has been proposed with the following gain function

$$k(\tilde{R}) = \frac{1}{\sqrt{1 - V_A(\tilde{R})/2\lambda_{min}^{\bar{A}}}} \tag{III.19}$$

Where V_A is given by $V_A(\tilde{R}) = tr\left(A(I - \tilde{R})\right)$.

In this work, we consider the following gain function

$$k(\tilde{R}) = \frac{1}{\sqrt{1 - |\tilde{R}|_I^2}} \tag{III.20}$$

The proposed attitude estimator, using solely vector measurements, is given by

$$\dot{\hat{R}} = \hat{R}\left[\omega_y\right]_\times - [\sigma]_\times \hat{R} \tag{III.21}$$

$$\sigma = -\frac{1}{2}\hat{R}\frac{\sum_{i=1}^{n}\rho_i(b_i \times \hat{R}^T r_i)}{\sqrt{1 - \frac{1}{8}\sum_{i=1}^{3}\left\|w_i - \hat{R}^T u_i\right\|^2}} \tag{III.22}$$

III.2.2.2 Analyze and Stability

In view of (III.7), one has $k(\tilde{R}) \geq \frac{1}{\sqrt{1-|\tilde{R}|_I^2}}$, which in view of (III.8), implies that

$$(\lambda_{min}^{\bar{A}})^2 \left|\tilde{R}\right|_I^2 \leq k(\tilde{R})^2 \left\|\psi(A\tilde{R})\right\|^2 \quad \text{(III.23)}$$

And therefore, the observer innovation term σ in (36) has a lower bound which increases as the attitude error increases. This guarantees a faster convergence of the attitude estimator (III.17)-(III.18) compared to the estimation proposed in [1].

Another advantage of considering $k(\cdot)$ as defined in (III.19) is that the overall observer innovation term σ in (III.18) can be directly written in terms of vector measurements, by considering $A = \sum_{i=1}^{n} \rho_i r_i r_i^T$ such that $\rho_i, i = 1, \cdots n$ are positive scalars, as follows

$$\sigma = -\frac{1}{2}\hat{R}\frac{\sum_{i=1}^{n} \rho_i (b_i \times \hat{R}^T r_i)}{\sqrt{1-\sum_{i=1}^{n} \rho_i \left\|b_i - \hat{R}^T r_i\right\|^2 / 4\lambda_{min}^{\bar{A}}}} \quad \text{(III.24)}$$

Where $b_i = R^T r_i$ are body-frame vector measurements of know inertial vectors $r_i, i = 1, \cdots, n; n \geq 2$; thus, obviating the need for the rotation matrix reconstruction.

With this choice of the gain function k in (III.20), the bound (III.23) is also satisfied thus guaranteeing the improvement of the convergence speed for large attitude errors. The drawback of our choice of $k(\cdot)$ in (III.20) is that an explicit expression of $k(\tilde{R})$ in terms of an arbitrary number of vector measurements b_i may not exist. Since the scalar function $k(\tilde{R})$ serves only as a gain to compensate for the decrease in the norm of $\psi(A\tilde{R})$ near large attitude errors, we can compute the term $|\tilde{R}|_I$ using directly any two vector measurements available without the need to reconstruct the whole attitude matrix as follows:

Let b_1 and b_2 be two (non-collinear) body-frame vector measurements corresponding to the inertial unit vectors r_1 and r_2 such that $b_1 = R^T r_1$ and $b_2 = R^T r_2$. Let us define the vectors $u_1 = \frac{r_1}{\|r_1\|}$, $u_2 = \frac{r_1 \times r_2}{\|r_1 \times r_2\|}$ and $u_3 = \frac{u_1 \times u_2}{\|u_1 \times u_2\|}$ along with their corresponding body frame vectors $\mathcal{w}_1 = b_1$, $\mathcal{w}_2 = (b_1 \times b_2)$ and $\mathcal{w}_3 = (b_1 \times b_2) \times b_1$. Then, one can verify that

$$\left|\tilde{R}\right|_I^2 = \frac{1}{8}\sum_{i=1}^{3}\left\|w_i - \hat{R}^T u_i\right\|^2 \quad \text{(III.25)}$$

Which is a quite convenient formula for the computation of $k(\tilde{R})$ in (III.20) without the need for the reconstruction of the rotation matrix.

Theorem 2: Consider the attitude kinematics system (III.1) coupled with the attitude observer (III.21)-(III.22). Assume that $\omega_y \equiv \omega$. for any $\tilde{R}(0) \in SO(3)\backslash\Pi$ one has

$$\underline{\beta}\left(\left|\tilde{R}(0)\right|_I, t\right) \leq \left|\tilde{R}(t)\right|_I \leq \overline{\beta}\left(\left|\tilde{R}(0)\right|_I, t\right) \quad \text{(III.26)}$$

For all $t \geq 0$,such that $\underline{\beta}$ and $\overline{\beta}$ are given by

$$\overline{\beta}\,(\mathrm{s},\mathrm{t}) = \frac{s}{\cosh\left(\lambda_{min}^{\bar{A}} t\right) + \sqrt{(1-s^2)}\sinh\left(\lambda_{min}^{\bar{A}} t\right)}$$

$$\underline{\beta}\,(\mathrm{s},\mathrm{t}) = \frac{s}{\cosh\left(\lambda_{max}^{\bar{A}} t\right) + \sqrt{(1-s^2)}\sinh\left(\lambda_{max}^{\bar{A}} t\right)} \quad \text{(III.27)}$$

it follows that the attitude error $|\tilde{R}(t)|^2$ satisfies

$$\begin{aligned}\left|\tilde{R}(t)\right|^2 &\leq f^{-1}\left(\lambda_{max}^{\bar{A}} t + f\left(\left|\tilde{R}(0)\right|_I^2\right)\right)\\ &\leq \frac{|\tilde{R}(0)|_I^2}{\left[\cosh\left(\lambda_{min}^{\bar{A}} t\right) + \sqrt{\left(1-|\tilde{R}(0)|_I^2\right)}\sinh\left(\lambda_{min}^{\bar{A}} t\right)\right]^2}\\ &= \left(\overline{\beta}\left(\left|\tilde{R}(0)\right|_I, t\right)\right)^2\end{aligned}$$

(III.28)

According to Theorem 2, it is straightforward to conclude almost global exponential stability of the equilibrium point $|\tilde{R}|_I = 0$. The convergence rate of the attitude estimator (III.21)-(III.22) is improved for large attitude errors as compared to the smooth attitude estimator (III.3)-(III.4). It is worth pointing out that the choice of the innovation term σ in (III.22), which corresponds to

$$\sigma = -\frac{\psi(A\tilde{R})}{\sqrt{1-|\tilde{R}|_I^2}} \quad \text{(III.29)}$$

Does not correspond, as far as we know, to any gradient of a potential function on $SO(3)$. In fact, this observer was designed by inspection of the dynamics of the attitude error and the desirable performance instead of the traditional systematic gradient-based method where the designer starts from a given potential function, which is typically

taken as a Lyapunov candidate, and then designs the observer based on the gradient of this potential function.

non-smooth attitude estimation schemes, evolving on $SO(3)$, exhibiting faster convergence rates, compared to the smooth observer of [41].

The non-smooth attitude observer guarantees Locally-Input-to-State-Stable (LISS) with a robustness region being independent from the attitude estimation error, i.e., starting from any initial condition and for all disturbances, the filter is robust to external gyro disturbances.

III.3 The invariant observer

In this subsection we will discuss about an observer ensures semi-global exponential convergence and stability and suggests that a high-gain observer is the price to pay for a large basin of attraction.

III.3.1 Conception

Consider the system

$$\begin{cases} \dot{V} = ge_3 + Ra_B \\ \dot{R} = RS(\omega) \end{cases} \quad \text{(III.30)}$$

where $V \in \mathbb{R}^3$ is the body's linear velocity expressed in the inertial frame I; $R \in SO(3)$ is the matrix of rotation representing the orientation of the body frame B with respect to (w.r.t.) the inertial frame I; ω is the angular velocity of the body frame B, a_B is the so-called "specific acceleration" representing the sum of all non-gravitational forces applied to the body divided by its mass, expressed in the body frame B; g is the gravitational acceleration expressed in the inertial frame I, with $e_3 = [0; 0; 1]$; and $S(\cdot)$ is the skew-symmetric matrix.

Supposing that the embedded GPS and IMU are well calibrated, and the following measurements are available:

• GPS-velocity: measures the linear velocity V.

• Gyroscopes: measure the angular velocity ω.

• Accelerometers: measure the specific acceleration a_B. By defining

$$a_I \triangleq \dot{V} - ge_3 \quad \text{(III.31)}$$

one has $a_B = R^T a_I$, with the T transpose operator.

• Magnetometers: whose measurements are normalized to obtain m_B, the normalized earth's magnetic field expressed in the body frame B. One has $m_B = R^T m_I$, with m_I the normalized earth's magnetic field expressed in the inertial frame I.

Let $\hat{V}$ and $\hat{R}$ denote estimates of V and R respectively. Define the error variables

$$\tilde{V} \triangleq V - \hat{V} \text{ and } \tilde{R} = R\hat{R}^T \quad \text{(III.32)}$$

Assumption 1: There exist four positive constants $\underline{C_a}$, $\overline{C}_a$, C_v and C_ω such that $\forall t \in \mathbb{R}_+ \triangleq [0, +\infty]$.

$$\underline{C_a} \leq |a_I(t)| \leq \overline{C}_a\,, \qquad |\ddot{v}(t)| \leq C_v, \qquad |\omega(t)| \leq C_\omega$$

Assumption 2: (Observability condition) There exists a constant $C_{obs} > 0$

Such that $\forall t \in \mathbb{R}_+$

$$\left| m_I(t) \times \frac{a_I(t)}{|a_I(t)|} \right| \geq C_{obs} \tag{III.33}$$

Assumption 1 indicates that the body's acceleration is bounded and different from ge3, and that the time-derivative of the body's acceleration is bounded. These properties are satisfied in "normal" flight conditions. As for Assumption 2, it indicates that the earth's magnetic field direction and the direction given by a_I are never collinear, to guarantee the system's observability.

Consider System (1) and the observer system

$$\dot{\hat{\mathrm{V}}} = \mathrm{k}_1\left(\mathrm{V} - \hat{\mathrm{V}}\right) + ge_3 + \hat{R}a_B$$

$$\dot{\hat{R}} = \hat{R}S(\omega + \sigma) \tag{III.34}$$

$$\sigma = k_2 m_B \times \hat{R}^T m_I + k_3 a_B \times \hat{R}^T (V - \hat{V})$$

With k_1, k_2, k_3 are positive constant gains.

Suppose that Assumptions 1 and 2 are satisfied. Then, for any $k_2, k_3 > 0$.

1.For any $k_1 > 0$, the equilibrium $(\tilde{v}, \tilde{R})$=(0,I_3) is locally exponentially stable.

2.For any closed neighborhood $\mathbb{V}\ of\ (0, I_3)\ \mathbb{R}^3$, with $\mathbb{V} \subset \mathbb{R}^3 \times SO(3) \setminus \mathbb{U}$, and $\mathbb{U}$ defined by

$$\mathbb{U} \triangleq \{R \in SO(3): tr(R) = -1\} \tag{III.35}$$

There exists a constant $\mathbb{K}_1 > 0$ such that for all $k_1 > \mathbb{K}_1$ and $(\tilde{V}(0), \tilde{R}(0)) \in \mathbb{V}$ the set point $(\tilde{V}(t), \tilde{R}(t))$exponentially converges to the equilibrium (0,I_3).

III.3.2 Analyze and stability

Let us first prove the second statement of Theorem 1. From Eqs. (III.31), (III.34), and (III.32) one obtains the error system:

$$\dot{\tilde{V}} = -k_1\tilde{v} + \left(I_3 - \tilde{R}^T\right)a_I$$

$$\dot{\tilde{R}} = -k_2 S\left(m_I \times \tilde{R}m_I\right)\tilde{R} - k_3 S(a_I \times \tilde{R}\tilde{V})\tilde{R} \qquad \text{(III.36)}$$

Consider the following candidate Lyapunov function

$$\mathcal{L} \triangleq \frac{1}{2}tr\left(I_3 - \tilde{R}\right) + \frac{l_1}{2}\left|\tilde{V}\right|^2 - \frac{k_3}{k_1}\tilde{V}^T P_a(\tilde{R})\tilde{R}^T a_I \qquad \text{(III.37)}$$

With l_1 some positive constant specified hereafter.

Denote $\tilde{q} \triangleq (\tilde{s}, \tilde{r})$ the quaternion associated with the matrix of rotation $\tilde{R}$, Where $\tilde{s}$ and $\tilde{r}$ are the real part pure part of the $\tilde{q}$ respectively [46,47 and 48] they verify

$$\tilde{s}^2 + |\tilde{r}|^2 = 1 \qquad \text{(III.38)}$$

Note that $\tilde{r} = 0$ dorresponds to $\tilde{R} = I_3$ And $\tilde{s} = 0$ correspends to

$$\text{tr}(\tilde{R}) = -1 \text{ (i.e } \tilde{R} \in \mathbb{U})$$

From Rodrigue's formula $\tilde{R} = I_3 + 2\tilde{s}S(\tilde{r}) + 2S(\tilde{r})^2$ one obtains

$$\text{tr}(I_3 - \tilde{R}) = 4|\tilde{r}|^2 \ , \ P_a(\tilde{R}) = 2\tilde{s}S(\tilde{r}) \ , \ I_3 - \tilde{R}^T = 2\tilde{s}S(\tilde{r}) - 2S(\tilde{r})^2 \qquad \text{(III.39)}$$

Then , one verifies that $\mathcal{L}$ defined by (eqt number) can be rewritten as

$$\mathcal{L} = 2|\tilde{r}|^2 + \frac{l_1}{2}\left|\tilde{V}\right|^2 + \frac{2k_3}{k_1}\tilde{s}\left(\tilde{R}^T a_I\right)^T\left(\tilde{r} \times \tilde{V}\right) \qquad \text{(III.40)}$$

Using eq (III.40) and the assumption 1 one deduces that

$$2|\tilde{r}|^2 + \frac{l_1}{2}|\tilde{v}|^2 + \frac{2\overline{C}_a k_3}{k_1}|\tilde{v}||\tilde{r}| \geq \mathcal{L} \geq 2|\tilde{r}|^2 + \frac{l_1}{2}|\tilde{v}|^2 - \frac{2\overline{C}_a k_3}{k_1}|\tilde{v}||\tilde{r}| \geq 2\left(1 - \frac{\overline{C}_a^2 k_3^2}{l_1 k_1^2}\right)|\tilde{r}|^2$$

(III.41)

The candidate Lyapunov function $\mathcal{L}$ is positive and proper with respect to $\tilde{v}$ and $\tilde{r}$ if $k_1 \geq \overline{C}_a k_3/\sqrt{l_1}$. Now, let us calculate the time-derivative of $\mathcal{L}$. To this purpose and the

clarity of the calculation, we first calculate the time derivative of intermediary terms using (III.36) one verifies that

$$\frac{d}{dt}tr(I-\tilde{R}) = -2k_2\left|P_a(\tilde{R})m_I\right|^2 - 2k_3\tilde{v}^T P_a(\tilde{R})\tilde{R}^T a_I \quad \text{(III.42)}$$

And $$\frac{d}{dt}|\tilde{v}|^2 = -2k_1|\tilde{v}|^2 + 2\tilde{v}^T\left(I_3 - \tilde{R}^T\right)a_I \quad \text{(III.43)}$$

And $$\tilde{v}^T P_a(\tilde{R})\tilde{R}^T\dot{a}_I = \tilde{v}^T P_a(\tilde{R})\tilde{R}^T\ddot{v}_I \quad \text{(III.44)}$$

$$\tilde{v}^T\frac{d}{dt}\left(P_a(\tilde{R})\tilde{R}^T\right)a_I = \frac{k_2}{2}a_I^T S\left(\left(\tilde{R}+I_3\right)\left(m_I\times\tilde{R}m_I\right)\right)\tilde{R}^2\tilde{v} + \frac{k_3}{2}a_I^T S\left(\left(\tilde{R}+I_3\right)\left(a_I\times\tilde{R}\tilde{v}\right)\right)\tilde{R}^2\tilde{v} \quad \text{(III.45)}$$

One has

$$\left(\tilde{R}+I_3\right)\left(m_I\times\tilde{R}m_I\right) = 2m_I\times P_a(\widetilde{R})m_I + 2P_a(\widetilde{R})(m_I\times\tilde{R}m_I) \quad \text{(III.46)}$$

Using Eqs. (III.45), (III.46) and the fact that $|m_I| = 1$ one deduces that

$$\left|\tilde{v}^T\frac{d}{dt}\left(P_a(\tilde{R})\tilde{R}^T\right)a_I\right| \le k_2|a_I||\tilde{v}|\left(\left|P_a(\widetilde{R})m_I\right| + \left|P_a(\widetilde{R})(m_I\times\tilde{R}m_I)\right|\right) + k_3|a_I|^2|\tilde{v}|^2 \quad \text{(III.47)}$$

From relations (III.38), (III.41), (III.42), (III.43), (III.45), (III.46), and (III.47) one verifies that

$$\dot{\mathcal{L}} \le -\left(k_1 l_1 - \frac{k_3^2|a_I|^2}{k_1}\right)|\tilde{v}|^2 - k_2\left|P_a(\tilde{R})m_I\right|^2 - \frac{k_3}{k_1}\left|P_a(\tilde{R})a_I\right|^2 + l_1\tilde{v}^T\left(I_3-\tilde{R}^T\right)a_I$$
$$+\frac{k_3}{k_1}|\tilde{v}|\left|P_a(\tilde{R})\tilde{R}^T\ddot{v}_I\right| + \frac{k_2k_3}{k_1}|a_I||\tilde{v}|\left(\left|P_a(\tilde{R})m_I\right| + \left|P_a(\widetilde{R})(m_I\times\tilde{R}m_I)\right|\right) \quad \text{(III.48)}$$

Using (III.48), the quaternion notation, Assumptions 1 and 2, and the last mathematical property in Section 2 one deduces

$$\dot{\mathcal{L}} \le -\left(k_1 l_1 - \frac{\overline{C}_a^2 k_3^2}{k_1}\right)|\tilde{v}|^2 - \frac{4\underline{C}_a^2 C_{obs}^2 k_2 k_3}{k_1k_2 + \underline{C}_a^2 k_3}\tilde{s}^2|\tilde{r}|^2 + 2\sqrt{2}\,\overline{C}_a\left(l_1 + \frac{k_3\left(C_v + 2k_2\overline{C}_a\right)}{\sqrt{2}\,\overline{C}_a k_2}\right)|\tilde{v}||\tilde{r}| \quad \text{(III.49)}$$

Define

$$\alpha_1 \triangleq \frac{k_3\left(C_v + 2k_2\overline{C}_a\right)}{\sqrt{2}\,\overline{C}_a}, \qquad \alpha_2 \triangleq \frac{2\underline{C}_a^2\, C_{obs}^2 k_3}{\overline{C}_a^2}, \qquad \alpha_3 \triangleq \frac{\underline{C}_a^2 k_3}{k_2}$$

Choosing $k_1 > \overline{C}_a k_3/\sqrt{l_1}$, and using inequality (III.49) one obtains

$$\dot{\mathcal{L}} \leq -2\sqrt{2}\,\overline{C}_a\left(\sqrt{\frac{\alpha_2\left(k_1^2\, l_1 - \overline{C}_a^2\, k_3^2\right)}{k_1(k_1+\alpha_3)}}|\tilde{s}| - \frac{k_1 l_1 + \alpha_1}{k_1}\right)|\tilde{v}||\tilde{r}| \tag{III.50}$$

Define

$$\varepsilon \triangleq \min\left(1 - |\tilde{r}(0)|, \frac{1}{2}\right) \tag{III.51}$$

Since $\tilde{R}(0) \notin \mathbb{U}$ with $\mathbb{U}$ defined by (III.35),$|\tilde{r}(0)| < 1$. Therefore, ε is strictly positive. One verifies that

$|\tilde{r}(0)| \leq 1 - \varepsilon$. Now let us choose $l_1$as follows

$$l_1 \triangleq min\left(\frac{4\varepsilon(1-\varepsilon)\left(\sqrt{\frac{3}{2}-\varepsilon}-\sqrt{1-\varepsilon}\right)^2}{|\tilde{v}(0)|^2}, \frac{\alpha_2\varepsilon}{2}\right) \tag{III.52}$$

Note that l_1 is well-defined and strictly positive even in the case$|\tilde{v}(0)| = 0$. It follows from Eq. (III.52) that $\alpha_2\varepsilon l_1 > l_1^2$, so that there exists $k_1(l_1,\varepsilon) > 0$ such that for all $K_1 > k_1(l_1,\varepsilon)$ the following inequality is satisfied:

$$(\alpha_2\varepsilon\, l_1 - l_1^2)k_1^3 - (2\alpha_1 l_1 + \alpha_3 l_1^2)k_1^2 - \left(\alpha_1^2 + 2\alpha_1\alpha_3 l_1 + \overline{C}_a^2\, k_3^2\alpha_2\varepsilon\right)k_1 - \alpha_1^2\alpha_3 > 0$$

which is equivalent to

$$\varepsilon\alpha_2 l_1\left(k_1^2\, l_1 - \overline{C}_a^2\, k_3^2\right) > (k_1 l_1 + \alpha_1)^2(k_1 + \alpha_3) \tag{III.53}$$

Therefore, with the choice of k_1 satisfying

$$k_1 > \mathbb{K}_1 \triangleq \max\left(\frac{\sqrt{2}\,\overline{C}_a k_3}{\sqrt{\varepsilon l_1}}, k_1(l_1,\varepsilon)\right) \tag{III.54}$$

Inequality (III.53) holds. Note that the choice of $k_1$in (III.54) verifies the inequality

$$k_1 > \overline{C}_a k_3 / \sqrt{l_1}$$

From (III.41) and (III.54) one verifies that

$$\mathcal{L}(0) \leq 2(1-\varepsilon)^2 + \frac{|\tilde{v}(0)|^2}{2} l_1 + 2\sqrt{\varepsilon}(1-\varepsilon)|\tilde{v}(0)|\sqrt{l_1} \quad \text{(III.55)}$$

Now consider the following equation (with s the variable)

$$\frac{|\tilde{v}(0)|^2}{2} s^2 + 2\sqrt{\varepsilon}(1-\varepsilon)|\tilde{v}(0)|s - \varepsilon(1-\varepsilon) = 0$$

Note that S_{max} tends to $+\infty$ when $\tilde{v}(0)$ tends to zero. Thus,$\forall s \in [0, S_{max}]$

$$\frac{|\tilde{v}(0)|^2}{2} s^2 + 2\sqrt{\varepsilon}(1-\varepsilon)|\tilde{v}(0)|s + 2(1-\varepsilon)^2 \leq 2\left(1-\frac{\varepsilon}{2}\right)(1-\varepsilon)$$

This relation and inequality (III.55) and the definition of l_1 in (III.52) imply that

$$\mathcal{L}(0) \leq 2\left(1-\frac{\varepsilon}{2}\right)(1-\varepsilon) \quad \text{(III.56)}$$

As a consequence of (III.53) and (III.54) one has

$$1 - \frac{(k_1 l_1 + \alpha_1)^2 (k_1 + \alpha_3)}{\alpha_2 k_1 \left(k_1^2 l_1 - \overline{C}_a^2 k_3^2\right)} > 1 - \varepsilon \quad \text{(III.57)}$$

And

$$1 - \frac{\overline{C}_a^2 k_3^2}{k_1^2 l_1} \geq 1 - \frac{\varepsilon}{2} \quad \text{(III.58)}$$

Then, one deduces from inequalities (III.58), (III.57), and (III.56) that

$$\mathcal{L}(0) \leq 2\left(1 - \frac{\overline{C}_a^2 k_3^2}{k_1^2 l_1}\right)\left(\frac{(k_1 l_1 + \alpha_1)^2 (k_1 + \alpha_3)}{\alpha_2 k_1 \left(k_1^2 l_1 - \overline{C}_a^2 k_3^2\right)}\right) \quad \text{(III.59)}$$

Using inequalities (III.59) and (III.41) one deduces that

$$\tilde{s}(0)^2 > \delta \triangleq \frac{(k_1 l_1 + \alpha_1)^2 (k_1 + \alpha_3)}{\alpha_2 k_1 \left(k_1^2 l_1 - \overline{C}_a^2 k_3^2\right)}$$

Let us prove (by contradiction that $\forall t \in \mathbb{R}_+, \tilde{s}(t)^2 > \delta$.Assume that there exists $T > 0$ such that $\tilde{s}(T)^2 \leq \delta$ and $\forall t \in [0, T]$, $\tilde{s}(t)^2 > \delta$. This supposition and inequality (III.41) imply that

$$\mathcal{L}(T) > 2\left(1 - \frac{\overline{C}_a^2\, k_3^2}{k_1^2\, l_1}\right)\left(\frac{(k_1 l_1 + \alpha_1)^2(k_1 + \alpha_3)}{\alpha_2 k_1\left(k_1^2 l_1 - \overline{C}_a^2\, k_3^2\right)}\right)$$

Then, this relation and inequality (III.59) imply that $\mathcal{L}(T) > \mathcal{L}(0)$ so that there exists a time-instant $\tau \in (0,T)$ such that $\dot{\mathcal{L}}(\tau) > 0$. But this contradicts inequality (III.50) since $\tilde{s}(\tau)^2 > \delta$. This result and inequality (III.50) imply the existence of a positive constant k_v, k_r, k such that $\dot{\mathcal{L}} \leq -k_v|\tilde{v}|^2 - k_r|\tilde{r}|^2 \leq -k\mathcal{L}$ (III.60)

From here the exponential convergence of $\mathcal{L}$ to zero follows. The exponential convergence of $(\tilde{v},\tilde{r})$ to zero, i.e., of $(\tilde{v},\tilde{R})$ to $(0,I_3)$, then directly follows. The stability of the equilibrium $(\tilde{v},\tilde{R}) = (0,I_3)$ is a direct consequence of relation (III.37) and (III.60). Now, to prove the first statement of the theorem let us consider the linearized system of System (III.36) about the equilibrium $(\tilde{v},\tilde{r}) = (0,0)$ which is given by (using (III.36) and the fact that $(\tilde{R} - I_3 \approx 2S(\tilde{r}) \approx I_3 - \tilde{R}^T)$

$$\dot{\tilde{V}} = -k_1\tilde{v} + 2\tilde{r} \times a_I$$

$$\dot{\tilde{r}} = -k_2 m_I \times S(\tilde{r})m_I - \frac{k_3}{2}a_I \times \tilde{v} \qquad \text{(III.61)}$$

Consider the candidate Lyapunov function

$$\mathcal{L}_1 \triangleq \frac{1}{2}|\tilde{r}|^2 + \frac{\gamma_1}{2}|\tilde{v}|^2 - \frac{k_3 - \gamma_1}{2k_1}\tilde{v}^T(\tilde{r} \times a_I) \qquad \text{(III.62)}$$

With $0 < \gamma_1 < k_3/4$, $k_1 > (k_3 - 4\gamma_1)\overline{C}_a/(2\sqrt{\gamma_1})$(to ensure that $\mathcal{L}_1$is positive and proper with respect to $\tilde{r}$ and $\tilde{v}$). The time derivative of $\mathcal{L}_1$ along the solution to (III.61) satisfies (proceeding majorations like in (III.48) and (III.49))

$$\dot{\mathcal{L}}_1 \leq -\frac{4k_1^2\gamma_1 - k_3(k_3 - 4\gamma_1)\overline{C}_a^2}{4k_1}|\tilde{v}|^2 - \frac{\underline{C}_a^2\, C_{obs}^2 k_2(k_3 - 4\gamma_1)}{k_1 k_2 + \underline{C}_a^2(k_3 - 4\gamma_1)}|\tilde{r}|^2 + \frac{(k_3 - 4\gamma_1)\left(C_v - k_2\overline{C}_a\right)}{2k_1}|\tilde{v}||\tilde{r}|$$

(III.63)

Denote $\kappa_0(\gamma_1) \in \mathbb{R}_+$ the largest positive solution to the equation

$$0 = f(\kappa) \triangleq \kappa^3 - \left(k_3\overline{C}_a^2 + \frac{\left(C_v + k_2\overline{C}_a\right)^2}{\underline{C}_a^2 C_{obs}^2}\right)\frac{k_3 - 4\gamma_1}{4\gamma_1}\kappa - \frac{\left(C_v + k_2\overline{C}_a\right)^2(k_3 - 4\gamma_1)^2}{16\, C_{obs}^2 k_2\gamma_1}$$

The existence of $\kappa_0(\gamma_1)$ is a direct consequence of $f(0) < 0$ and $\lim_{\kappa \to +\infty} f(\kappa) = +\infty$. From here choosing $k_1$satisfying $k_1 > \mathbb{K}_0(\gamma_1) \triangleq max\left(\frac{(k_3-4\gamma_1)\overline{C}_a}{2\sqrt{\gamma_1}}, \kappa_0(\gamma_1)\right)$ (III.64)

One ensures that $f(k_1) > 0$ or, equivalently

$$\sqrt{\frac{\left(4k_1^2\gamma_1 - k_3(k_3-4\gamma_1)\overline{C}_a^2\right)\overline{C}_a^2 C_{obs}^2 k_2(k_3-4\gamma_1)}{k_1\left(k_1k_2 + \underline{C}_a^2(k_3-4\gamma_1)\right)}} > \frac{(k_3-4\gamma_1)\left(C_v + k_2\overline{C}_a\right)}{2k_1}$$

This inequality, relations (III.62) and (III.63), and Young's inequality ensure the existence of three positive constants γ_r , γ_v , $\gamma_{\mathcal{L}}$ such that $\dot{\mathcal{L}}_1 \leq -\gamma_r|\tilde{r}|^2 - \gamma_v|\tilde{v}|^2 \leq \gamma_{\mathcal{L}}\mathcal{L}_1$.Then , the letter inequality and the definition of $\mathcal{L}_1$ imply the exponential stability of the equilibrium $(\tilde{v}, \tilde{r}) = (0,0)$, i.e. of $\left(\tilde{v}, \tilde{R}\right) = (0, I_3)$, Now, it's important to prove that for any $k_1(> 0)$there exists a positive constant $\gamma_1$such $k_1 > \mathbb{K}_0(\gamma_1)$. One verifies from (III.64) that $\gamma_1(< k_3/4)$ tends to $k_3/4$, $\kappa_0(\gamma_1)$ and $\mathbb{K}_0(\gamma_1)$ tend to zero. Therefore, by continuity of the function $\kappa_0(\gamma_1)$ and $\mathbb{K}_0(\gamma_1)$ one deduces that for any $k_1 > 0$ there exists a positive value of $\gamma_1(< k_3/4)$ such that $\kappa_0(\gamma_1) < k_1$ and $\mathbb{K}_0(\gamma_1) < k_1$. This concludes the proof.

A sufficient condition for the gain $k_1$is provided (i.e., inequality (III.53)) ensuring the convergence and stability results. In view of (III.51) and (III.52), one deduces that $k_1$must tend to $+\infty$ to guarantee the satisfaction of (III.53) when $|\tilde{r}(0)|$ tends to one (the value for which $\tilde{R}(0) \in \mathbb{U}$). One also remarks that the size of $k_1$is proportional to the size of the domain of initial estimation error for which (III.53) is satisfied.

The main interest of this section related to Observer (III.34) is to yield a semi-global exponential convergence proof which was not achieved before. In fact, Property 1 of Theorem 1 concerning the local exponential stability is similar to the stability property proved in [45], but the present assumptions upon the reference trajectory (Assumptions 1 and 2) are more explicit and less restrictive than those given [45]. As for Property 2, it ensures the semi-global stability property under a "high-gain"-like condition on k_1 This condition indicates that the size of the basin of attraction is proportional to the size of k_1, but k_1 tends to infinity only when the initial estimated rotation makes a π angle with the true rotation. In practice it should never happen as the initial guess of the body's attitude is never that bad.

III.4 The Cascaded observer

In this subsection we will discuss about an observer for which the associated convergence and stability analyses do not rely on “high-gain” conditions proposed by Minh-Duc Hua.

The design of this observer shows how a_I can be estimated from the measurements of V, ω, and a_B.

III.4.1 Conception

And the observer is given by

$$\dot{\hat{V}} = k_1\left(V - \hat{V}\right) + ge_3 + Qa_B$$
$$\dot{Q} = QS(\omega) + k_V\left(V - \hat{V}\right){a_B}^T \qquad \text{(III.65)}$$

With k_1, k_V positive constant gains, and $Q \in R^{3\times3}$ a virtual matrix.

Suppose that $\forall t \in R_+$, $\omega(t)$, $\dot{V}(t)$, $and\ \ddot{V}(t)$ are bounded. Then; the assumptions are:

1. $\forall(\hat{V}(0), Q(0)) \in \mathbb{R}^3 \times \mathbb{R}^{3\times3}, (\tilde{V}(t), (a_I - Qa_B)(t))$ converges to zero;

2. Furthermore, if the acceleration $\dot{V}(t)$ is constant and $|a_I(t)| > 0$, then the equilibrium $(\tilde{V}, a_I - Qa_B) = (0, 0)$ is globally exponentially stable.

Since $(\tilde{V}, Qa_B)$ converges to $(0, a_I)$, one can view either Qa_B or $\hat{V} - ge_3$ $(= k_1\tilde{V} + Qa_B)$ as the estimate of a_I.

Consider System (III.30) and the observer system (III.65) complemented with the following attitude estimator

$$\dot{R} = RS(\omega + \sigma)$$
$$\sigma = k_2 m_B \times Rm_I + k_3 a_B \times \hat{R}^T(Qa_B + k_1(V - \hat{V})) \qquad \text{(III.66)}$$

With k_2, k_3 some positive gains, and $Q, \hat{V}$ given by System (III.65).

Define $\xi = a_I - Qa_B$. Suppose that Assumptions 1 and 2 are satisfied. Then

1. For any initial condition $(\hat{V}(0), Q(0), \hat{R}(0)) \in \mathbb{R}^3 \times \mathbb{R}^{3\times3} \times SO(3), (\xi, \tilde{V}, \tilde{R})$ asymptotically converges to the set $E = E_1 \cup E_2$ with $E_1 = \{0\} \times \{0\} \times \mathbb{U},\ E_2 = (0, 0, I_3)$, and $\mathbb{U} \in SO(3)$ defined by

$$\mathbb{U} \triangleq \{R \in SO(3): tr(R) = -1\} \quad \text{(III.67)}$$

2. furthermore, if the acceleration $\dot{V}$ is constant, then E is an equilibrium set with the subset E_1 unstable and the subset E_2 stable.

III.4.2 Analyze and Stability

This observer uses an auxiliary matrix Q which (surprisingly) is not a rotation matrix. But this matrix is such that $Qa_B - Ra_B$ tends to zero. Thus, Q allows an estimation of the specific acceleration in the inertial frame I a_I.

Once this is done, the mathematical problem is very close to the case where the approximation $a_I \approx -ge_3$ is made. Indeed, the images by the rotation R of two distinct vectors of the body frame are now known. The form of the attitude observer (III.66) is close to the nonlinear observers already proposed in the literature (e.g. [41] [42]) for the attitude estimation problem under the approximation $a_I \approx -ge_3$. Note that (III.65) also defines an invariant observer [43] [44]. Note that there does not exist any smooth globally asymptotically stable observer due to the topology of the Lie group $SO(3)$. The simultaneous achievement of these stability and convergence properties in the case of constant accelerations is a new result. Additionally, let me remind that for observer [45] specifying the domain of attraction is not easy to achieve, even in the case of constant accelerations.

In view of the proof of the cascaded observer one ensures that $||Q||$ remains bounded in the case of perfect measurements. In practice, however, sensor noises and drifts and numerical errors can drive $||Q||$ arbitrarily large which possibly yields large estimation errors. This suggests to replace the expression of $\dot{Q}$ in (III.65) by the following

$$\dot{Q} = QS(\omega) + k_V\left(V - \hat{V}\right){a_B}^T - \rho Q$$
$$\rho = k_q \max\left(0, \|Q\| - \sqrt{3}\right), with\ k_q > 0 \quad \text{(III.68)}$$

Since $a_I = Ra_B$ can be estimated via the vector Qa_B, $||Q||$ can be theoretically bounded by $\sqrt{3}$ (i.e. the value of the Frobenius norm of any rotation matrix R). The term $-\rho Q$ in the expression of $\dot{Q}$ in (III.67) creates a dissipative effect when $||Q||$ becomes larger than $\sqrt{3}$, allowing it to be driven back to this threshold and thus avoiding numerical drifts of Q. This astute of robustification does not destroy the convergence properties.

Observer

From (III.30) and (III.65) one obtains

$$\dot{\tilde{V}} = -k_1\tilde{V} + (R - Q)a_B \tag{III.69}$$

Along the solutions of the closed-loop system, the time-derivative of the candidate Lyapunov function

$$\mathcal{W} \triangleq \frac{1}{2}\left|\tilde{V}\right|^2 + \frac{1}{2k_V}\|R - Q\|^2 \tag{III.70}$$

Satisfies

$$\dot{\mathcal{W}} = -k_1\left|\tilde{V}\right|^2 + \tilde{V}^T(R - Q)a_B - tr((R - Q)^T\tilde{V}a_B{}^T) + \frac{1}{k_V}tr((R - Q)^T(R - Q)S(\omega))$$

$$\dot{\mathcal{W}} = -k_1\left|\tilde{V}\right|^2 \tag{III.71}$$

The time-derivative of $\mathcal{W}$ is negative semi-definite, so that $\tilde{V}$ and Q are bounded. In view of (III.69) and the boundedness of $\tilde{V}, Q, a_B$ (since $\dot{V}$ is bounded from assumption), one deduces the boundedness of $\dot{\tilde{V}}$. Then, one deduces from (III.71) the boundedness of $\ddot{\mathcal{W}}$, i.e., $\dot{\mathcal{W}}$ is uniformly continuous along every system's solution. Then, the application of Barbalat's lemma ensures the convergence of $\dot{\mathcal{W}}$ to zero which implies the convergence of $\tilde{V}$ to zero. The boundedness of $\ddot{V}_I$ and ω from Assumption 1 implies the boundedness of $\dot{a}_B$ since $a_B = R^T(\dot{V} - g)$. This along with (III.69) and the properties obtained previously (i.e., the boundedness of $\tilde{V}, \dot{\tilde{V}}, Q, \dot{Q}, \dot{R}$) implies that $\ddot{\tilde{V}}$ is bounded, i.e., $\dot{\tilde{V}}$ is uniformly continuous. Since $\tilde{V}$ converges to zero and $\dot{\tilde{V}}$ is uniformly continuous, the application of Barbalat's lemma ensures the convergence of $\dot{\tilde{V}}$ to zero

which implies the convergence of Qa_B to a_I. It remains to show the last statement of the lemma. If $\dot{V}$ is constant, one has

$$\frac{d}{dt}\big((R-Q)a_B\big) = -k_V|a_I|^2\,\tilde{V} \qquad \text{(III.72)}$$

From (III.69) and (III.72), the exponential stability of ($\tilde{V}$, $a_I - Qa_B$) to zero is straightforward.

Estimator

One verifies that

$$\dot{\tilde{R}} = -S\big(k_2 m_I \times \tilde{R}m_I + k_3 a_I \times \tilde{R}a_I\big)\tilde{R} + E \qquad \text{(III.73)}$$

With

$$E \triangleq\ k_3 S\big(a_I \times \tilde{R}(a_I - Qa_B - k_1\tilde{V})\big)\tilde{R} \qquad \text{(III.74)}$$

Along the solutions to the closed-loop system, the time-derivative of the candidate Lyapunov function where $\tilde{R} \in \mathbb{U}$

$$\mathcal{V} \triangleq tr\big(I_3 - \tilde{R}\big) = 4sin^2\big(\frac{\tilde{\theta}}{2}\big) \qquad \text{(III.75)}$$

Satisfies

$$\dot{\mathcal{V}} = tr(k_2 S\big(m_I \times \tilde{R}m_I\big)\tilde{R} + k_3 S(a_I \times \tilde{R}a_I\big)\tilde{R} - E)$$

(III.76)

$$\dot{\mathcal{V}} \le -ksin^2\big(\tilde{\theta}\big) - tr(E) \qquad \text{(III.77)}$$

The boundedness of $\dot{\mathcal{V}}$ which implies the uniform continuity of $\mathcal{V}$ and therefore of $\tilde{\theta}$.

When the body's acceleration $\dot{V}_I$ is constant, as a consequence of (III.69) and (III.72) one has

$$\begin{aligned}\dot{\tilde{V}} &= -k_1\tilde{V} + \xi \\ \dot{\xi} &= -k_V|a_I|^2\tilde{V}\end{aligned} \qquad \text{(III.78)}$$

With $\xi = a_I - Qa_B$

Defines $y \triangleq 1 + \cos(\tilde{\theta})$; $z \triangleq 1 - \cos(\tilde{\theta})$ and verifies that $\tilde{\theta} = \pi$ and $\tilde{\theta} = 0$ corresponds to $y = 0$ and $z = 0$ respectively. Note that $y = 2 - \frac{v}{2}$ And $z = \frac{v}{2}$. Using (III.76) one obtains

$$\dot{y} = (k_2|\tilde{a} \times m_I|^2 + k_3|\tilde{a} \times a_I|^2)\left(1 - \frac{y}{2}\right)y + \frac{1}{2}tr(E)$$
$$\dot{z} = -(k_2|\tilde{a} \times m_I|^2 + k_3|\tilde{a} \times a_I|^2)\left(1 - \frac{z}{2}\right)z - \frac{1}{2}tr(E) \quad \text{(III.79)}$$

From (III.78), (III.79), it is straightforward to verify that $(\xi, \tilde{V}, y) = (0, 0, 0)$ and $(\xi, \tilde{V}, z) = (0, 0, 0)$ are equilibrium points. This implies that E is an equilibrium set of $(\xi, \tilde{V}, \tilde{R})$. From the definition of y and z, Therefore, the linearization of system (III.79) about the equilibriums $(\xi, \tilde{V}, y) = (0, 0, 0)$ and $(\xi, \tilde{V}, z) = (0, 0, 0)$ are

$$\dot{y} = (k_2|\tilde{a} \times m_I|^2 + k_3|\tilde{a} \times a_I|^2)y$$
$$\dot{z} = -(k_2|\tilde{a} \times m_I|^2 + k_3|\tilde{a} \times a_I|^2)z \quad \text{(III.80)}$$

From (III.80) one directly deduces that the equilibrium $(\xi, \tilde{V}, y) = (0, 0, 0)$ of the linearized system is unstable. This implies that the equilibrium set E_1 of $(\xi, \tilde{V}, \tilde{R})$ is unstable.

The stability property established in this observer is weaker than that of invariant observer but the convergence result, being independent of the gain values, is stronger. Furthermore, when $\dot{V}$ is constant, one obtains the strongest possible result, i.e., stability of the desired equilibrium $E_2 = (0, 0, I_3)$, instability of the “undesired” equilibrium set E_1, and convergence to $E_1 \cup E_2$.

III.5 Conclusion

In this chapter, four observers were discussed, for the two first are from a class of smooth nonlinear observers guarantees, in general, almost global asymptotic stability (AGAS), i.e., convergence to the actual attitude is guaranteed from any initial condition except from a set of Lebesgue measure zero, and two other attitude observers with associated Lyapunov-based convergence and stability analyses were discussed.

The first observer ensures semi-global exponential convergence and stability and suggests that a high-gain observer is the price to pay for a large basin of attraction. In turn, the second observer ensures almost global convergence without the “high-gain assumption”.

An inconvenience, however, is that its stability has yet to be derived for the case when the vehicle’s linear acceleration is non-constant. Which of these observers is best in practice may depend on sensor characteristics.

Chapter IV

Simulations and interpretations

IV.1 Introduction

In this chapter we will illustrate through simulation results the performance and robustness of each one from the four observers discussed in the previous chapter.

In order to compare between the four observers, we will decompose them into two pairs, the first pair is the smooth and non-smooth observers, while the second is the invariant and the cascaded observers, then three simulations will be done.

The first will be multiple simulations of the smooth and the non-smooth observers under a different initial conditions and disturbances in order to illustrate their effect on the attitude estimated values.

Then we will do the same kind of simulations for the second pair, to finally choose the ones that give a good performance and accuracy, to do a third simulation and compare between them.

IV.2 Simulation 1

This subsection presents numerical examples and comparisons between the smooth and non-smooth complimentary attitude observers introduced and discussed in the previous chapter.

IV.2.1 Initial data

The angular velocity is given by

$$\omega(t) = \begin{bmatrix} 0.5\sin(0.1t) \\ 0.2\sin(0.2t+\pi) \\ \sin(0.3t+\pi/3) \end{bmatrix} (rad/s)$$

And the initial condition $R(0) = I_3$, consider body-frame measurements b_1 and b_2 of two non-collinear inertial vectors given by

$$r_1 = \frac{1}{\sqrt{3}}[1,-1,1]^T \text{ and } r_2 = [0,0,1]^T$$

With the gains are given by

$$\rho_1 = 1 \text{ and } \rho_2 = 2$$

Therefore, the corresponding weighting matrix is given by

$$A = \rho_1 r_1 r_1^T + \rho_2 r_2 r_2^T = \frac{1}{3}\begin{bmatrix} 1 & -1 & 1 \\ -1 & 1 & -1 \\ 1 & -1 & 7 \end{bmatrix}$$

IV.2.2 Results

a- For the first simulation we chose the observer initial conditions so that we start from a large initial attitude error and the result is shown in **Figure IV.1**

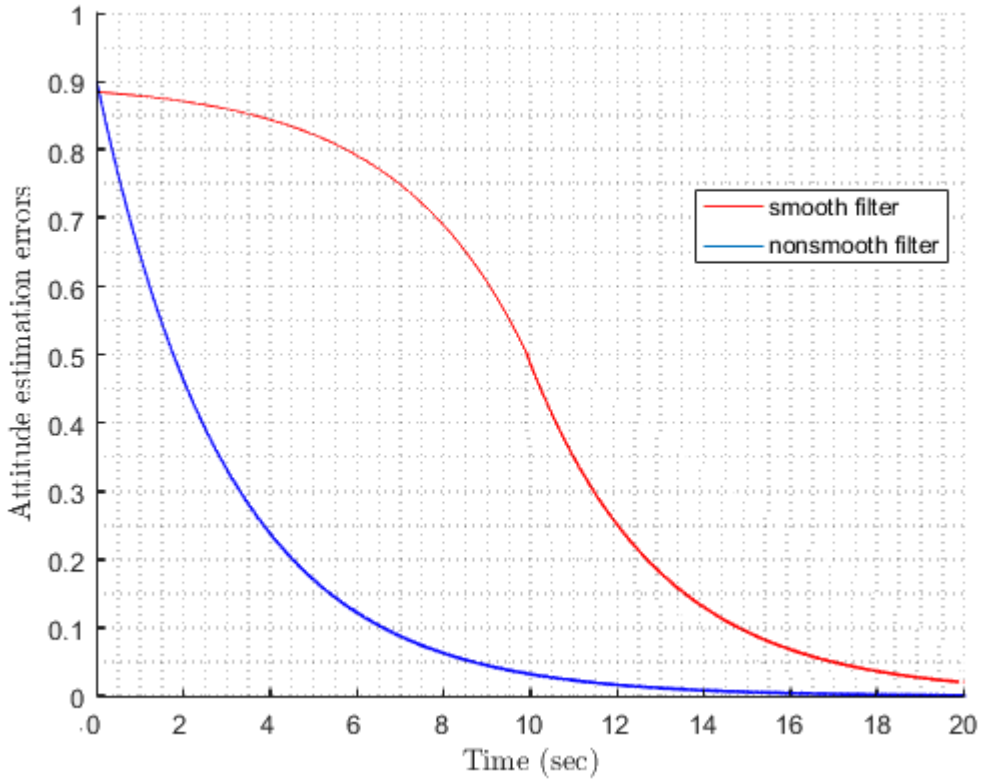

Figure IV.1 Comparison between the smooth and the non-smooth observers starting from a large attitude error.

The smooth attitude observer has a slow convergence rate for the large attitude estimation errors, where the non-smooth attitude observers exhibit faster convergence rate for large attitude errors as expected from the theoretical results obtained in the previous chapter.

b- For the second simulation, we will verify the convergence of the two observers with the presence of vanishing angular velocity disturbance.

$$\hat{R}n_{\omega}(t) = -3(3t+1)^{-\frac{1}{2}}[1,1,0]^{T}$$

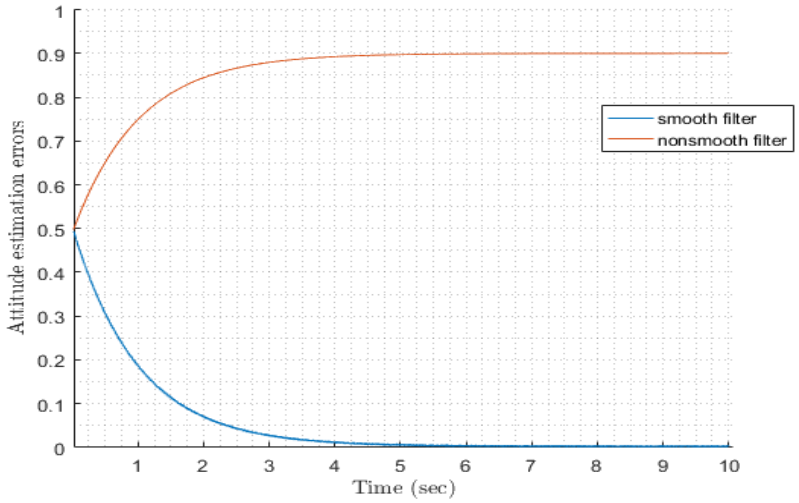

Figure IV.2 Comparison between the smooth and the non-smooth attitude observers in the presence of a vanishing disturbance.

The **Figure IV.2** shows the results of the second simulation in the presence of the vanishing disturbance, it can be seen that, as proved the smooth attitude observer has diverged to the undesired manifold angle even though the disturbance signal is vanishing as, t goes to infinity.

c- In the third simulation, we consider a sinusoidal-type disturbance of two different frequencies $n_\omega(t) = (2\sin(t) - 0.5\sin(10t))[1, -1, 0]^T$

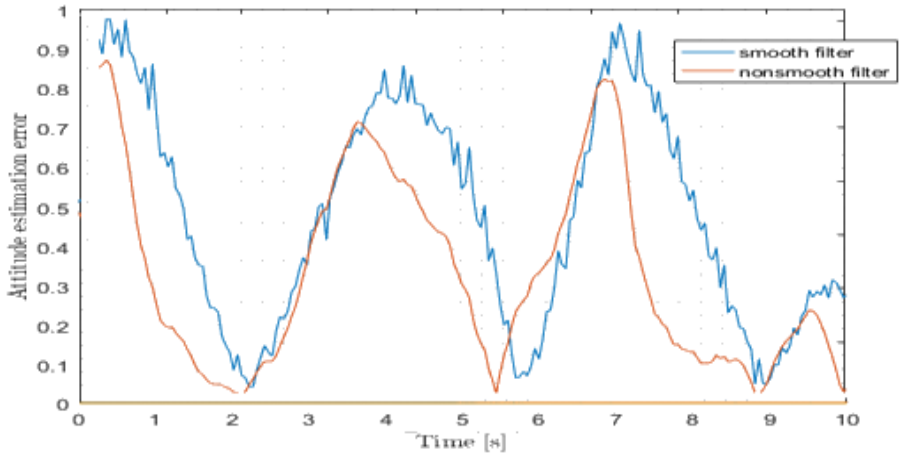

Figure IV.3 Comparison between the smooth and the non-smooth attitude observers in the presence of a bounded disturbance.

As it is shown, we used the sinusoidal signal to test the “attenuation” capacity of each one of the attitude observers. In the **Figure IV.3**, even though, both of the attitude observers have bounded states, it is seen that the non-smooth attitude observer allows to obtain a better disturbance attenuation level.

IV.3 Simulation 2

This subsection presents numerical examples and comparisons between the invariant and cascaded attitude observers introduced and discussed in the previous chapter.

IV.3.1 Initial data

The linear velocity of the vehicle in both observer's simulations is given by

$$v = [-15\alpha \sin(\alpha t)\,; 15\alpha \cos(\alpha t)\,; 0] \quad \text{with} \quad \alpha = 2\sqrt{30}/15$$

The normalized earth's magnetic field is taken as

$$m_I = [0.434; -0.0091; 0.9008]$$

Data for the invariant observer

The gains we have chosen as

$$k_1 = 3, \qquad k_2 = 3, \qquad k_3 = 0.03$$

The initial velocity estimate error is given as

$$\tilde{v}(0) = [-19.7;\ -14.1;\ -10](\mathrm{m/s})$$

The initial rotation matrix estimate error is given as

$$\tilde{R}(0) = diag([1; -1; -1])$$

Data for the cascaded observer

The gains have been chosen as

$$k_1 = 3, \qquad k_2 = 3, \qquad k_3 = 0.03, \qquad k_v = 0.12, \qquad k_q = 1$$

The initial conditions are given by $\tilde{Q}(0) = I_3$

The initial velocity estimate error is given as

$$\tilde{v}(0) = [-19.7;\ -14.1;\ -10](\mathrm{m/s})$$

The initial attitude estimate error is given as:

$$\tilde{R}(0) = diag([1; -1; -1])$$

IV.3.2 Results

For this simulation, the initial values of the invariant and cascaded observers are chosen very far from the real values, so as to test the extent of the associated domains of convergence.

Note that the gains $k_2,\ k_3$ of the invariant Observer and the cascaded are chosen so that they possess "similar performance" when $\dot{v} \approx 0$, in the case of perfect measurements:

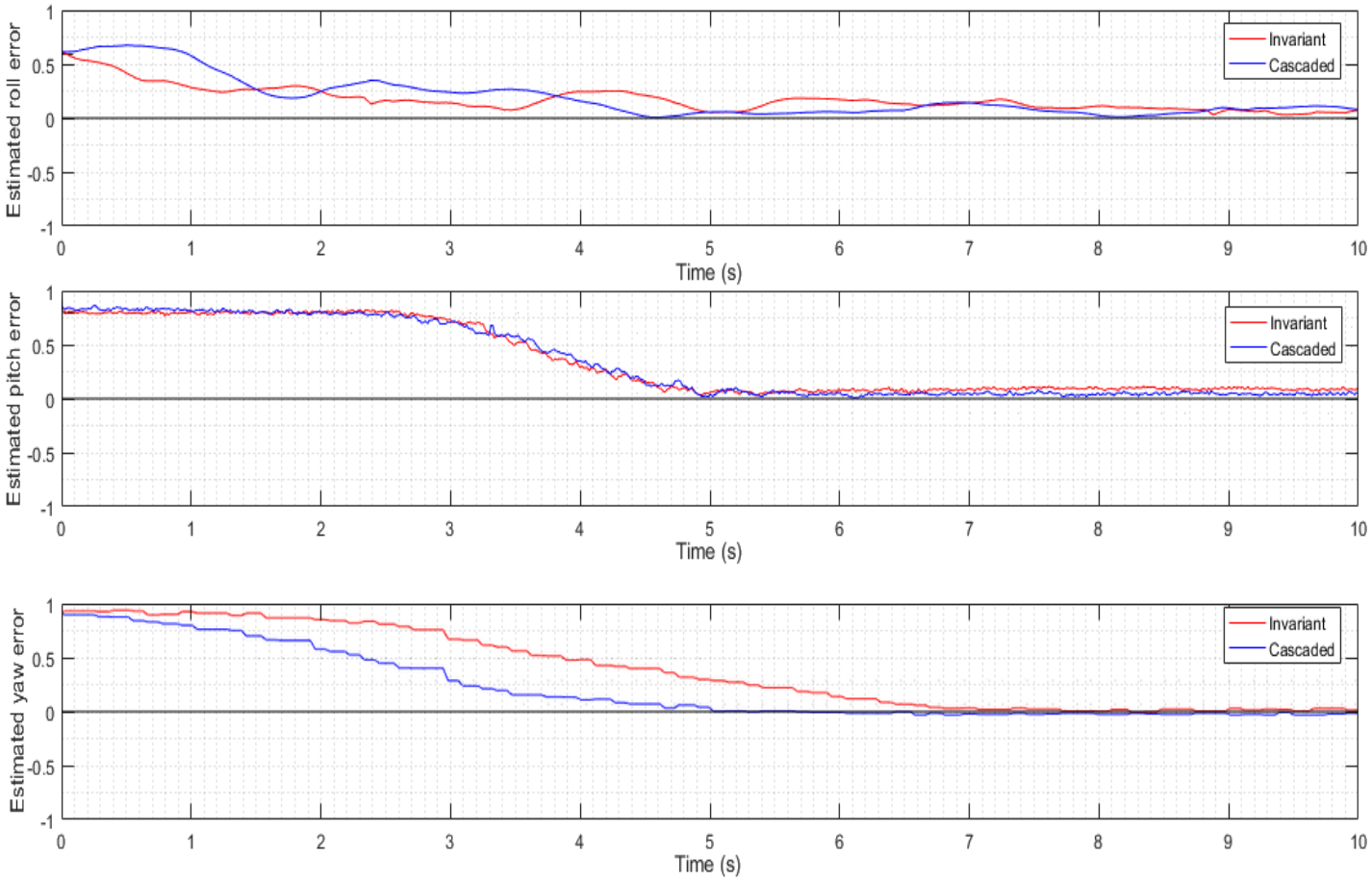

Figure IV.4 The estimated errors of the Euler angles ($k_1 = 3$).

The **Figure IV.4** shows the estimated errors of the Euler angles (roll, pitch, and yaw). Both the invariant and the cascaded observers ensure an asymptotic convergence of the estimated attitude to the real one despite the very large initial estimation errors.

Note that with the initial given conditions, the gain k_1 involved in the invariant observer does not correspond to the limit provided by the statement. Furthermore, the

simulations results tend to indicate that the domain of attraction is global for any positive value of the gain k_1.The closed-loop stability of invariant is quite sensitive and exhibit poor performance compared to cascaded.

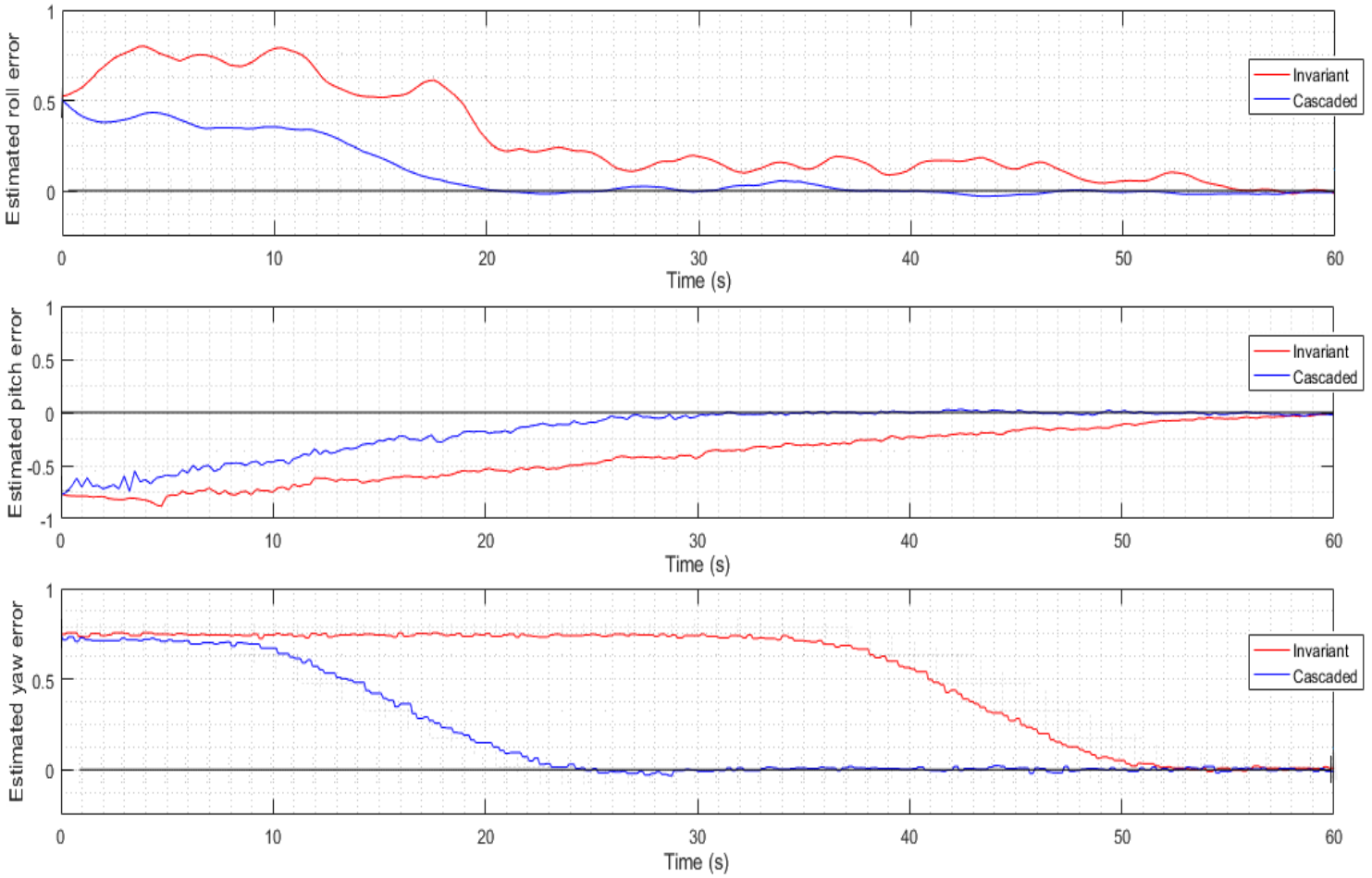

Figure IV.5 The estimated errors of the Euler angles ($k_1 = 0.03$).

An example case with $k_1 = 0.03$ (a very small value) is illustrated in the **Figure IV.5**. It shows that the convergence rate of the invariant observer is rather slow while the cascaded observer still provides a good performance it also implies that in the case where GPS velocity measurement is rather erroneous the cascaded observer can be more advantageous than the one in the invariant observer, because the small gain k_1 can be used to limit the influence of GPS velocity measurement noise.

IV.4 Simulation 3

This subsection presents comparison between the non-smooth and the cascaded attitude observers, which showed a better convergence rate in the previous simulations.

a- For the first simulation, we chose the observer initial conditions so that we start from a large initial attitude error to see which one will converge faster from the two observers, and the result is shown in **Figure IV.6.**

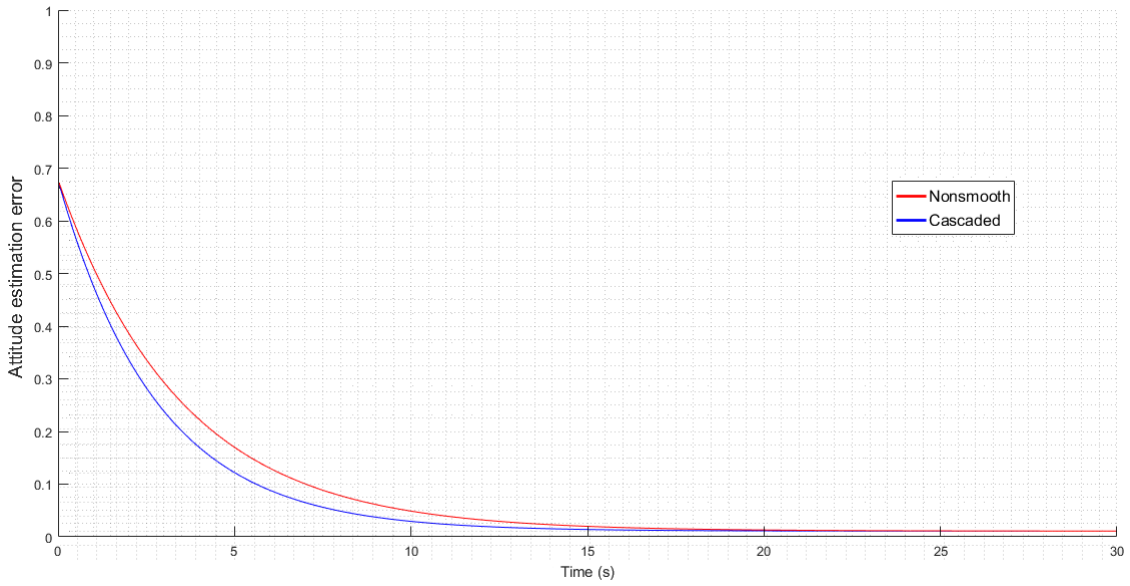

Figure IV.6 Comparison between the non-smooth and the cascaded attitude observers starting from a large attitude error.

the non-smooth attitude observer has a fast convergence rate for large attitude estimation errors, but the cascaded attitude observer exhibits faster convergence rate.

b- For the second simulation, we will verify the convergence of the two observers with the presence of vanishing angular velocity disturbance

$$\hat{R}n_{\omega}(t) = -9(3t+9)^{-\frac{1}{2}}[1,1,0]^{T}$$

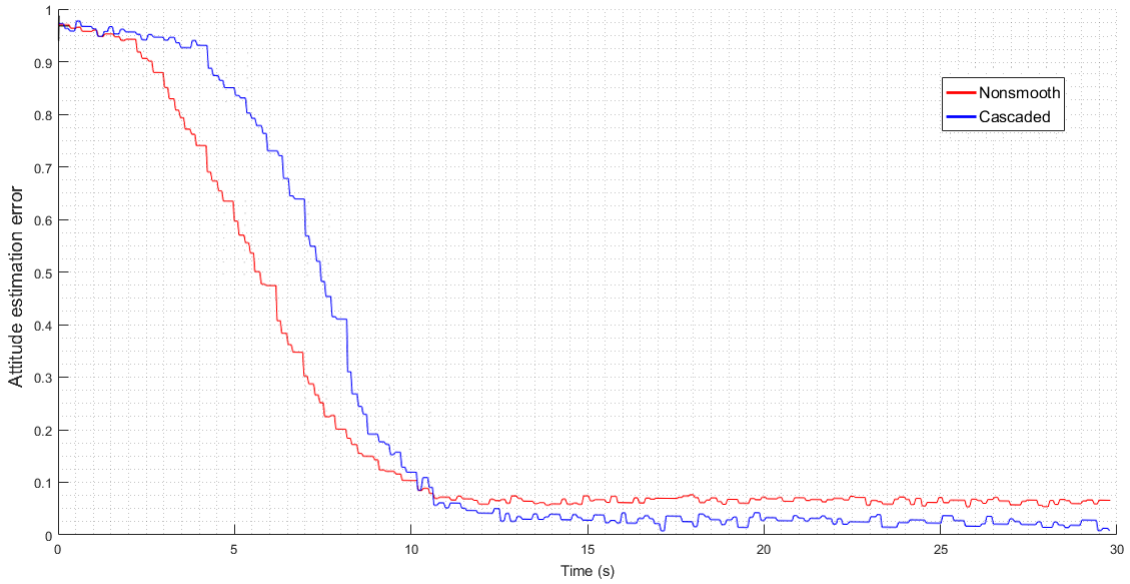

Figure IV.7 Comparison between the non-smooth and the cascaded attitude observers in the presence of a vanishing disturbance.

In the presence of the vanishing disturbance, the **Figure IV.7** illustrates that, the cascaded observer converges faster than the non-smooth attitude observer for the first 10 seconds, after that, the non-smooth observer shows a good convergence rate.

c- In the third simulation, we consider a sinusoidal-type for high disturbances of two different frequencies to test the “attenuation” capacity of each one of the attitude observers, the signal is given by

$$n_{\omega}(t) = (8\sin(5t) - \sin(10t))[1, -1, 0]^{T}$$

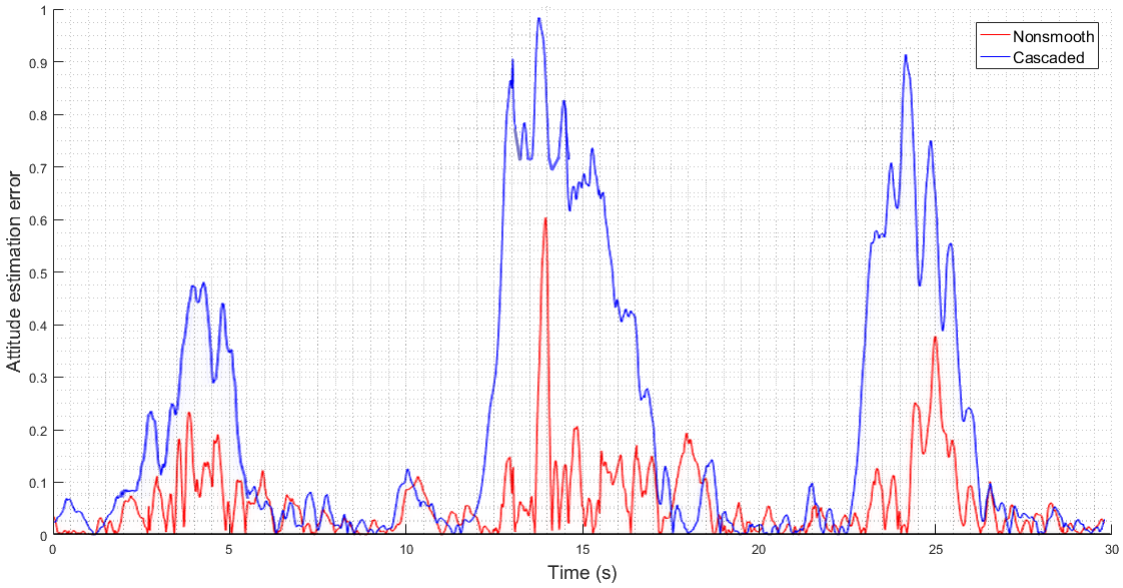

Figure IV.8 Comparison between the non-smooth and the cascaded attitude observers in the presence of a bounded disturbances.

In **Figure IV.8**, even though, both attitude observers have bounded states, it is seen that the cascaded observer shows a better disturbance attenuation level compared with the non-smooth attitude observer who suffer from high disturbances.

IV.5 Conclusion

As a result, and after doing these multiple simulations and comparisons between the observers.

We deduce from the comparison between the first pair, that the non-smooth observer converges faster than the smooth observer and gives more accuracy and stability against the low disturbances and gyro noises.

And from the comparison between the second pair, we deduce that the stability of invariant is quite sensitive and exhibit poor performance compared to cascaded, because it relies on high gain condition and that is a disadvantage compared to the cascaded observer that does not get affected from the gain.

At the end, and after comparing between the non-smooth and the cascaded observers which gave a good performance in the first simulations, we deduce that, the cascaded performs better and converges faster in the case of high disturbances.

General conclusion

The attitude estimation has been an interesting field of study for many researchers over the years. The Efficient control strategies for flying vehicles rely heavily on a good estimation of the attitude. Moreover, in many applications such as surveillance, infrastructure inspection, and aerial photography, the estimation of the aircraft position and velocity is important as well. Therefore, powerful and reliable estimation tools are required to generate good estimations under real time conditions such as noisy sensor measurements and unknown system parameters.

For many decades, conventional techniques such as Extended Kalman Filters were the work horses of the attitude estimation field. With the emergence of new methods, it is believed that new generations of estimation tools may be able to replace the existing methods due to their superior reliability, accuracy, and domain of convergence. Among these techniques, nonlinear attitude observers have gained huge attention among the scientific community during the last decade.

All the attitude estimation techniques require measurements provided by a range of sensors attached to the rigid body system. These provide information on the vehicle's angular velocity and vectorial measurements in the body frame and sometimes and for more accuracy they can be aided by another external systems such as the GPS.

A theoretical study of the different classes of attitude estimation techniques and algorithms was performed. The basics of static attitude determination and various methods of this kind are presented and discussed. Also, various dynamic methods were briefly introduced and discussed with detailed algorithms.

In this thesis, the objective was to look closely on the evolution and application of the nonlinear attitude observers, A deep studies on some of the latest developed observers were performed to provide readers with details on the design and convergence properties, these nonlinear attitude observers were followed with different types of simulations to show the performance of each observer under different kinds of disturbances. Then we finished the work with a comparison between these observers.

References

[1] [Christopher Jekeli Inertial Navigation Systems with Geodetic Applications]

[2] D.G. Luenberger. An introduction to observers. IEEE Transactions on Automatic Control, vol. 16, no. 6, pages 596–602, 1971

[3] R.E. Kalman. A new approach to linear filtering. Transactions of the ASME Journal of Basic Engineering, vol. 82, pages 35–45, 1960.

[4] D. Aubry. Contribution à la synthèse d'observateurs pour les systèmes non linéaires. Thèse, Université Henri Poincaré - Nancy I, 1999.

[5] Rodolfo Orjuela, Benoît Marx, José Ragot et Didier Maquin. « Conception d'observateurs robustes pour des systèmes non linéaires incertains : une stratégie multimodèle ». Thèse de Doctorat de l'Université Henri Poincaré, Nancy I, 2005.

[6] K. Reif, F. Sonnemann & R. Unbehauen. An EKF-based nonlinear observer with a prescribed degree of stability. Automatica, vol. 34, no. 9, pages 1119–1123, 1998.

[7] B.L. Walcott & S.H. Zak. State observation of nonlinear uncertain dynamical systems. IEEE Transactions on Automatic Control, vol. 32, no. 2, pages 166–170, 1987.

[8] David H. Titterton and John L. Weston. Strapdown Inertial Navigation Technology - 2nd Edition

[9] P. D. Groves, Principles of GNSS, Inertial, and Multisensor Integrated Navigation Systems

[10] Aboelmagd Noureddine, Tashfeen B.Karamat; Jacques Georgy < Fundamentals of inertial Navigation, Satellite-based positioning and their Integration > Springer-verlag Berlin Heidel berg.2013

[11] Spilker, J. J. Jr., Parkinson, B. W., "Overview of GPS operation and design," Chapter 2, and Spilker, J. J. Jr., "GPS navigation data," Chapter 4 in Parkinson, B.

[12] Cole, Gerald. (2004). Management Theory and Practice.

[13] Sohrab Mobasser and Carl Christian Liebe, Micro Sun Sensor for Spacecraft Attitude Control Pasadena; Jet Propulsion Laboratory, National Aeronautics and Space Administration, 2004.

[14] Handbook of Marine Craft Hydrodynamics and Motion Control

[15] Titterton, D. H., Weston, J. L., Strapdown Inertial Navigation Technology, American Institute of Aeronautics and Astronautics & Institution of Electrical Engineers, 2004

[16] Britting, Kenneth R. Inertial Navigation Systems Analysis. WileyInterscience, 1971.

[17] Salychev, O.S., Applied Inertial Navigation: Problems and Solutions, BMSTU Press Moscow, Russia, 2004.

[18] New Barbour N., Schmidt G. "Inertial sensor technology trends", Proc. of 1998 Workshop on Autonomous Underwater Vehicles, August 1998, pp. 55-62.

[19] Wahba, G. (1965). A least-squares estimate of satellite attitude. SIAM Review, 7(3):409

[20] M. D. Shuster. The QUEST for better attitudes. The Journal of the Astronautical Sciences, 54(3,4):657–683, 2006.

[21] Psiaki, M. L. (2010). Generalized Wahba problems for spinning spacecraft attitude and rate determination. Journal of the Astronautical Sciences, 57(1 and 2):73– 92.

[22] Farrell, J. L. et al. “A Least Squares Estimate of Satellite Attitude (Grace Wahba).” Siam Review 8 (1966): 384-386.

[23] Wessner, R. H. (1966). A least square estimate of spacecraft attitude. SIAM Review, 8(3):384–386.

[24] Velman, J. R. (1966). A least square estimate of spacecraft attitude. SIAM Review, 8(3):384–386.

[25] Brock, J. E. (1966). A least square estimate of spacecraft attitude. SIAM Review, 8(3) :384–386.

[26] KEAT, J. “Analysis of Least Squares Attitude Determination Routine, DOAOP,” Computer Sciences Corporation, CSC/TM-77/6034, February 1977.

[27] G. M. Lerner, “Three-axis attitude determination,” Spacecraft Attitude Determination and Control, vol. 73, pp. 420–428, 1978.

[28] Markley, F. Landis, “Attitude Determination Using Vector Observations and the Singular Value Decomposition,” Journal of the Astronautical Sciences, Vol. 36, No. 3, July-Sept. 1988

[29] Golub, G.H. and Van Loan, C.F. (1983) Matrix Computations. The Johns Hopkins University Press, Maryland.

[30] Markley, F.L., Mortari, D. Quaternion Attitude Estimation Using Vector Observations. J of Astronaut Sci 48, 359–380 (2000).

[31] Markley, F. Landis, “Attitude Determination Using Two Vector Measurements,” light Mechanics Symposium, Goddard Space Flight Center, Greenbelt, MD, May 1999.

[32] Graham, W. R., and Johnston, G. R., Integration Filter State Specification and Accuracy Predictions; Navigation, Vol. 33, No. 4, 1986-1987, pp. 295- 313.

[33] Cunningham, J., and Lewantowicz, Z. H., "Dynamic Integration of Separate INS/GPS Kalman Filters," Proceedings of the ION GPS '88 (Colorado Springs, CO), Institute of Navigation, Washington, DC, Sept. 19-23, 1988, pp. 273-282.

[34] Diesel, J. W, "Integration of GPS/INS for Maximum Velocity Accuracy," Navigation, Vol. 34, No. 3, 1987, pp. 190-211.

[35] R. Mahony, T. Hamel et J.M. Pflimlin: Complementary filter design on the special orthogonal group SO(3). In IEEE Conference on Decision and Control and the European Control Conference, 2005.

[36] J.M. Pflimlin, T. Hamel et P. Soueres: A nonlinear observer on SO(3) group for attitude and gyro bias estimation for a flying UAV. In IFAC World Congress, 2005.

[37] H. Rehbinder et B.K. Ghosh: Pose estimation using line-based dynamic vision and inertial sensors. IEEE Transactions on Automatic Control, 48(2):186–198, 2003.

[38] [the 44th IEEE Conference on Decision and Control - Seville, Spain (12-15 Dec. 2005)] Complementary filter design on the special orthogonal group SO(3).

[39] Martin Isler: An Ancient Method of Finding and Extending Direction

[40] S. Salcudean: A globally convergent velocity obsever for rigid body motion. IEEE Transactions on Automatic Control, 36(12):1493–1497, 1991.

[41] Mahony, R., Hamel, T., Pflimlin, J.-M., 2008. Nonlinear complementary filters on the special orthogonal group. IEEE Trans. on Automatic Control 53 (5), 1203–1218.

[42] Hamel, T., Mahony, R., 2006. Attitude estimation on SO(3) based on direct inertial measurements. In: IEEE Conf. on Robotics and Automation. pp.2170–2175.

[43] Bonnabel, S., Martin, P., Rouchon, P., 2008. Symmetry-preserving observers. IEEE Trans. on Automatic Control 53 (11), 2514–2526.

[44] Lageman, C., Trumpf, J., Mahony, R., 2009. Gradient-Like observers for invariant dynamics on a Lie group. IEEE Trans. On Automatic Control.

[45] Martin, P., Salaun, E., 2008. An invariant observer for Earth-Velocity-Aided attitude heading reference systems. In: IFAC World Congress. pp. 9857–9864.

[46] Robinson, A. C., 1958. On the use of quaternions in simulations of rigid-body motion. Tech. Rep. 58-17, Wright Air Development Center.

[47] Shuster, M. D., 1993. A survey of attitude representations. The Journal of the Astronautical Sciences 41 (4), 439–517. Shuster (1993)).

[48] Stuelpnagel, J., 1964. On the parametrization of the three-dimensional rotation group. SIAM Journal on Control and Optimization 6 (4), 422–430.